P-06-77

Oskarshamn site investigation

Borehole KLX03: Characterisation of pore water

Part 2: Rock properties and diffusion experiments

H N Waber
Rock Water Interaction, University of Bern

J A T Smellie, Conterra AB

April 2006

Svensk Kärnbränslehantering AB
Swedish Nuclear Fuel
and Waste Management Co
Box 5864
SE-102 40 Stockholm Sweden
Tel 08-459 84 00
+46 8 459 84 00
Fax 08-661 57 19
+46 8 661 57 19

ISSN 1651-4416
SKB P-06-77

Oskarshamn site investigation

Borehole KLX03: Characterisation of pore water

Part 2: Rock properties and diffusion experiments

H N Waber
Rock Water Interaction, University of Bern

J A T Smellie, Conterra AB

April 2006

Keywords: Site investigations, Matrix pore water, Diffusion, Chemistry, Isotopes, Fluid inclusions, Mineral chemistry .

Abstract

Accessible, interconnected pore water has been extracted successfully by laboratory out-diffusion methods from crystalline rocks using some 16 drillcore samples from borehole KLX03 as part of the Oskarshamn hydrogeochemical site investigation programme. With increasing depth these pore waters generally reflect hydrochemical trends already noted in adjacent formation groundwaters. In general, a different evolution seems to be established for pore water within the Ävrö granite compared to the underlying quartz monzodiorite. Insight into the palaeoevolution of the site has been obtained and there is the possibility to use the extraction method to derive rock matrix diffusion coefficients.

Interpretation of the extracted pore waters are supported by investigations of the rock mineralogy, mineral chemistry, whole rock chemistry, mineral fluid inclusions and crush-leach experiments.

Summary

Pore water that resides in the pore space between minerals and along grain boundaries in crystalline rocks of low permeability cannot be sampled by conventional groundwater sampling techniques and therefore has to be characterised by applying indirect methods based on drillcore material. Accessible, interconnected pore water has been extracted successfully by laboratory out-diffusion methods using 16 drillcore samples from borehole KLX03 as part of the Oskarshamn hydrogeochemical site investigation programme in the Laxemar subarea. Interpretation of the extracted pore waters are supported by detailed investigations on one rock sample which have included mineralogy, mineral chemistry, whole rock chemistry, mineral fluid inclusions and crush-leach experiments.

The objective was to characterise the pore water chemically and isotopically and relate these data to the present and past groundwater evolution of the site. In addition, the method of extraction, together with interfaced measurements of interconnected porosity, provides the opportunity to derive diffusion coefficient values of potential use in predicting future rates of solute transport.

The mineralogical composition of the rocks encountered in borehole KLX03 located in the Laxemar subarea compares well to those of the Simpevarp area as a whole, generally referred to as "quartz monzodiorite" although some samples classify more specifically as a monzo-granite to grano-diorite with quartz, plagioclase, K-feldspar, biotite and amphibole as major components and clinopyroxene and opaque phases (magnetite, illmenite, few pyrite) as minor components. Accessory minerals include among others prehnite, chlorite, vesuvianite, epidote, sphene, calcite and very few clay minerals. Plagioclase and K-feldspar are chemically zoned which contrasts to the amphibole and clinopyroxene phases.

Fluid inclusions in the quartz monzodiorite occur almost exclusively in quartz. All inclusions are secondary in origin and occur mainly along healed fissures. About 70% of all inclusions are single phase inclusions (liquid only) and 30% are multiphase inclusions (liquid-vapour-solid). The salinity of the fluids determined on about 100 inclusions show a bimodal distribution. A first group has a salinity mainly between about 2 and 8 eq-wt.% NaCl; these comprise around 60% of the total inclusions. The second group, comprising around 40% of the total inclusions, has a salinity mainly between about 16 and 18 eq-wt.% NaCl. In the highly saline (second group) inclusions $CaCl_2$ appears to be present in considerable amounts. On average, fluid inclusions constitute about 2–3 Vol.% of the total quartz volume of the quartz monzodiorite sample.

Aqueous leaching experiments of different grain-size fractions from the quartz monzodiorite reveal that the concentrations of Cl, together with Na, K and possibly SO_4, contain significant contributions from crushed fluid inclusions. The additional contribution from mineral dissolution during the experiments tends to increase with decreasing grain size of the extracted material. In combination with available mineralogical and fluid inclusion data, investigation of ion-ion ratios further helps to identify qualitatively the contribution of different proportions of ion concentrations to the experimental solution from the original pore water, fluid inclusions and mineral dissolution. In the quartz monzodiorite the aqueous extract experiments indicate that the in situ pore water has a Na/Cl ratio much higher than unity and Cl is not the dominating anion.

The water content of the rocks derived by different independent methods agrees well and shows a general decrease with increasing depth. Bearing this in mind, and considering that the density of the different rock types appears to be similar, the connected porosity displays the same general trend as the measured water content.

Chemistry of the out-diffusion solutions reveal essentially three pore water groups: 1) Samples in the Ävrö granite down to about 450 m depth are Na-HCO_3 in type and have a low total mineralisation of between about 300–500 mg/L. 2) Between 450–600 m depth, i.e. towards the lower end of the Ävrö granite, the chemical type changes to Ca-Na-SO_4 and the solutions are more strongly mineralised (600–960 mg/L), notably at identical water contents as the surrounding samples. 3) In the quartz monzodiorite (> 600 m depth) samples are generally Na-Ca-HCO_3-Cl in type with chloride increasing with depth. The total mineralisation varies little (250–300 mg/L) from 600–750 m and again below 850 m where low hydraulic transmssivity is indicated. However, between 750–850 m depth a higher mineralisation is encountered with Cl becoming also a major anion (sample KLX03-12, TDS = 552 mg/L). This sample originates from a strongly tectonised interval at around 800 m depth.

Using the isotope diffusive exchange method attempts were made to determine the stable water isotope composition of the pore water and compare these data with fracture groundwaters sampled and characterised from the same borehole. The δ^2H and $\delta^{18}O$ values of the shallow samples plot on or close to the GMWL only slightly below the present-day precipitation end-member, and show similarities with the fracture groundwaters. This suggests that steady-state conditions between pore and groundwater have been achieved. With increasing depth the samples plot to the left of the GMWL close to the reference brine water. At these depths steady-state conditions between pore water and fracture groundwater are not achieved and it appears that the pore water contains at least a component that is significantly older than the fracture groundwater. These conclusions are supported by comparing the chloride concentrations derived for the pore water with those of the fracture groundwater. The higher diffusivity of water compared to that of solutes indicates that steady-state conditions would be achieved earlier for the water isotopes than for chloride. The isotope data support the differences observed for the chloride concentrations between pore water and fracture groundwater when calculated using the measured water contents.

Compared to total chloride the chlorine isotopes differ in their behaviour with depth between pore water and fracture groundwater samples. In the Ävrö granite the $\delta^{37}Cl$ values of the pore water are strongly enriched in ^{37}Cl and differ significantly from those of the fracture groundwater. This is in contrast to the steady-state conditions between pore water and groundwater as indicated by total chloride. Exactly the contrary is observed in the levels of the quartz monzodiorite. Here the chlorine isotopes suggest steady-state conditions while total chloride is different in pore water and fracture groundwater. At present these relationships are difficult to explain.

Strontium isotope systematics essentially support the differences in total chloride and the general chemical types observed for the pore waters as outlined above.

The out-diffusion time-series data for chloride from the granitic sample KLX03-7 showed that the best fit of the measured data is obtained for a pore diffusion coefficient, D_P, for chloride of about 8.1×10^{-11} m^2/s at a water-content porosity of 0.77 ± 0.14 Vol.% and at a temperature of 45°C. This converts to an effective diffusion coefficient, D_e, at 20°C of about 3.1×10^{-13} m^2/s. This value is in good agreement with effective diffusion coefficients for dioritic rocks from the Laxemar area obtained from through-diffusion and through-electromigration experiments (e.g. $D_e = 3.9\times10^{-13}$ m^2/s).

An underlining concern is the possible modification of the in situ water content induced by stress release. Every rock sample recovered from depth is potentially subjected to some stress release mechanisms. Such release will result in an increase of the void volume of a rock sample and thus perturb bulk density measurements and, if drilled with a drilling fluid, also the water content because some drilling fluid might enter this newly created void volume. Furthermore, small-scale fracturing of the rock core may expose fresh faces containing ruptured quartz grains releasing fluids (potentially saline) normally trapped in inclusions. A final problem is that in rocks with such low water contents the measurements employed in this study might simply not be accurate enough to resolve the effects of stress release. While a fully quantitative argumentation is difficult with the data at hand, several semi-quantitative arguments have been put forward which appear to show that measurable effects of stress release are minimal. Calculations based on hypothetical changes in water content show that a change of 50% caused by stress release would essentially increase the pore water chloride by a factor of 2.

Sammanfattning

Porvatten som förekommer i utrymmet mellan mineral och längs korngränser I lågpermiabelt kristallint berg kan inte provtas med konventionell teknik utan måste karakteriseras genom indirekta metoder, såsom lakning av borrkärnsprover. 16 prover från borrhål KLX03 i Laxemar har extraherats med avseende på tillgängligt porvatten från konnekterade porer genom utdiffusion. Dessa försök är en del av det pågående hydrogeokemiska programmet inom platsvalsundersökningarna i Simpevarp. Tolkningarna av de extraherade porvattnens karaktär har stöttats av detaljerade undersökningar av bergartsprov där mineralogi, mineralkemi, bergartskemi, samt studier av vätskeinklusioner och lakningsexperiment ingått.

Syftet har varit att karakterisera porvattnet med avseende på kemi och isotopsammansättning och att relatera dessa data till nuvarande och tidigare grundvattenkemi inom platsen. Dessutom har diffusionskoefficientvärden varit möjliga att bestämma baserade på extraktion och mätningar av konnekterad porositet.

Den mineralogiska sammansättningen hos bergarter påträffade i borrhål KLX03 är representativa för Simpevarpsområdet. Med avseende på mineralogi är det s k ”kvarts-monzodioritprovet” närmast en monzogranit till granodiorit med kvarts, plagioklas, kalifältspat, biotit och amfibol som huvudmineral och klinopyroxen och opaka mineral (magnetit, ilmenit, någon pyrit) som underordnade mineral. Accessoriska mineral är bland annat prenit, klorit, vesuvianit, epidot, titanit, kalcit, och mycket små mängder av lermineral. Plagioklas och kalifältspat är kemiskt zonerade i motsats till amfibol och klinopyroxen.

Vätskeinklusionerna i kvarts-monzodioriten är nästan uteslutande begränsad till kvarts. Samtliga inklusioner är sekundära och uppträder huvudsakligen längs igenläkta sprickor.

Cirka 70 % av inklusionerna består av en enda fas (endast vätska) och 30 % består av flera faser (vätska-gas-fast fas). Resultaten från de cirka 100 inklusionerna som undersökts uppvisar en bimodal salthaltsfördelning. Den ena gruppen, som utgör ca 60 % av inklusionerna, har en salthalt mellan ca 2 och 8 eq-vikts% NaCl**.** Den andra gruppen, som utgör ca 40 % av inklusionerna, har en salinitet huvudsakligen mellan 16 och 18 eq-vikts % NaCl. I den senare gruppen uppträder $CaCl_2$ i avsevärda mängder. I medeltal utgör vätskeinklusioner ca 2–3% av den totala kvartsvolymen i provet.

Lakningförsök på olika kornstorleksfraktioner från kvarts-monzodioriten visar att koncentrationen av Cl samt Na, K och möjligen SO_4 till stor del härrör från vätskeinklusioner. Bidraget bara från upplösning av mineral verkar öka med minskad kornstorlek hos det extraherade materialet. I kombination med tillgänglig mineralogisk data och vätskeinklusionsdata kan jon-jon kvoter bidra till att kvalitativt identifiera bidragen till experimentlösningen från de olika jonkoncentrationerna i det ursprungliga porvattnet, vätske inklusionerna och mineralupplösning. Vattenextraheringsexperimentet visar att in situ porvattnet har en Na/Cl kvot som är mycket större än 1 och att Cl inte är den dominerande anjonen i kvarts-monzodioriten.

Det vatteninnehållet som beräknats i bergarterna med hjälp av olika oberoende metoder överensstämmer bra och visar en allmän minskning med tilltagande djup. På grund av att densiteten är lika för de olika bergarterna uppvisar den konnekterade porositeten samma generella trend som mätningarna av vatteninnehållet.

Kemin hos lakningslösningarna resulterar i tre huvudsakliga porvattengrupper: 1) Prover från Ävrögraniten ner till ett djup av 450 m är av Na-HCO_3 typ och har en låg total mineralisering på mellan 300 till 500 mg/l. 2) På ett djup mellan 450 och 600 m, dvs i nedre

delen av Ävrögraniten, ändrar sig porvattnet till att vara av Ca-Na-SO_4 typ och lösningarna är starkare mineraliserade (600–960 mg/l) vid samma vatteninnehåll som för omgivande prover. 3) Prover från kvarts-monzodioriten (> 600 m djup) are vanligen av Na-Ca-HCO_3-Cl typ med ökande Cl innehåll mot djupet. Den totala mineraliseringen varierar lite (250–300 mg/l) från 600 till 750 m samt under 850 m djup där låg hydraulisk konduktivitet är uppmätt. Mellan 750 och 850 m djup påträffas en högre grad av mineralisering där Cl utgör en huvudsaklig anjon (prov KLX03-12, TDS = 552/l). Detta prov är från en starkt tektoniserat sektion av borrhålet vid ca 800 m djup.

Genom att använda isotoputbytesmetoden gjordes försök att bestämma innehållet av stabila isotoper i porvattnet och jämföra dessa data med grundvattnet från sprickor som provtagits och karaktäriserats från samma borrhål. δ^2H and $\delta^{18}O$ värden från de ytnära proverna plotter på eller nära GMWL och endast något under dagens nederbörd och visar likheter med grundvatten från sprickorna. Detta visar att jämviktsförhållanden har nåtts mellan porvattnet och grundvattnet. Vid större djup plottar proverna till vänster om GMWL och när referenslinjen för ”brine”. På dessa djup har inte jämvikt uppnåtts mellan porvatten och grundvatten och det ser ut som om porvattnet åtminstone innehåller en komponent som är avsevärt äldre än grundvattnet från sprickorna. Dessa slutsatser är i överensstämmelse med jämförelsen mellan kloridkoncentrationerna i porvattnet och grundvattnet. På grund av den högre diffusiviteten hos vatten jämfört med lösningar bör jämvikt uppnås tidigare för δ^2H och $\delta^{18}O$ än för kloridisotoperna. Isotopdata stöder observerade skillnaderna för kloridkoncentrationerna mellan porvatten och grundvatten beräknade från de uppmätta vatteninnehållen.

Till skillnad från det totala kloridinnehållet skiljer sig klorisotopernas uppträdande mot djupet mellan porvatten och grundvatten från sprickor. $\delta^{37}Cl$ värdena i porvattnet från Ävrögraniten är påtagligt anrikade på ^{37}Cl och skiljer sig signifikant från porvattnet från sprickorna. Detta är i motsats till jämviktsförhållandena som indikerats från det totala kloridinnehållet mellan porvatten och grundvatten. I kvarts-monzodioriten däremot indikerar kloridisotoperna jämviktsförhållanden medan totala kloridinnehållet är olika i porvatten och grundvatten från sprickor. För närvarande är dessa relationer svårförklarliga.

Strontiumisotoperna stöder i huvudsak skillnaderna i totalt kloridinnehåll och de generella kemiska typerna i porvattnet som angetts ovan.

Data från lakningsförsöken av klorid från granitprovet KLX03-7 visade att den bästa anpassningen av mätdata erhålles för en pordiffusionskoefficient, $D_{P,}$ på 8.1×10^{-11} m^2/s vid en vatteninnehållporositet på 0.77 ± 0.14 Vol.% och vid en temperature på 45°C. Detta motsvarar en effektiv diffusionskoefficient, D_e, vid 20°C på ca 3.1×10^{-13} m^2/s. Detta värde överensstämmer väl med den effektiva diffusionskoefficienten för kvarts monzodioriter i Laxemarområdet erhållna genom diffusion och elektromigreringsexperiment (t ex $D_e = 3.9\times10^{-13}$ m^2/s).

Ett problem är huruvida vatteninnehållet in situ är modifierat genom tryckavlastning.

Varje bergartsprov taget på ett specifikt djup påverkas potentiellt av störningar relaterade till denna avlastning. Till exempel kan porvolymen öka i provet och sålunda störa bulkdensitetsmätningarna. I sådana fall skulle spolvattnet som använts vid borrningen eventuellt påverka vatteninnehållet då spolvattnet kan tränga in i det nyskapade porutrymmet. Vidare kan småskalig uppsprickning av kärnan exponera färska ytor av spruckna kvartskorn som kan öppna upp vätskeinklusioner (potentiellt salta). Ett annat problem är att våra mätmetoder kanske inte har den upplösning som krävs för att se effekterna av tryckavlastningen. Då en helt kvantitativ argumentering är svår att föra med tillgänglig data kan emellertid flera halvkvantitativa argument anföras vilka tycks visa att de mätbara effekterna från tryckavlastning är minimala. En hypotetisk ökning av vatteninnehållet med 50% orsakad av tryckavlastning skulle öka den beräknade kloridhalten i porvattnet med en faktor 2.

Contents

1 Introduction

This document reports performance and results based on the activity '*characterisation of pore water'* in drillcore samples within the site investigation programme at Oskarshamn. The drillcore samples were selected during drilling of borehole KLX03 in the Laxemar subarea; see controlling document AP PS 400-04-043.

Crystalline rocks are characterised in general by two hydraulic regimes. The first regime includes the water-conducting zones related to regional or local fracture networks. The second regime includes the bedrock mass of low permeability between the water-conducting zones. Depending on the residence time of formation groundwater in the water-conducting zones, interaction with water present in the pore space of the low permeable bedrock might become significant. In addition, since repository construction will be restricted largely to bedrock of low permeability, this pore water over time will interact with the repository barrier materials (e.g. bentonite; canister) potentially leading to a deterioration in their physical properties. For safety assessment considerations it is therefore important to know the composition of such pore water and its evolution over recent geological time, certainly during the last thousands to hundreds of thousands of years in accordance with the expected lifespan of a repository. Pore water compositions can be assessed by combining the information gained from pore water profiles within bedrock of low permeability and the chemical and isotopic data of formation groundwaters circulating in the adjacent fracture zones.

Pore water that resides in the pore space between minerals and along grain boundaries in crystalline rocks of low permeability cannot be sampled by conventional groundwater sampling techniques and therefore has to be characterised by applying indirect methods based on rock drillcore material. Such techniques have been tested during the Matrix Fluid Chemistry Experiment in the Äspö HRL /Smellie et al. 2003/ and borehole KSH02 from the Simpevarp subarea investigation /Waber and Smellie 2004/. One of these techniques, the laboratory out-diffusion method, has been applied successfully to borehole KFM06A at Forsmark to trace the pore water chemistry in low permeable bedrock to depths of around 1,000 m /Waber and Smellie 2005/.

A similar approach has been carried out for borehole KLX03 from the Laxemar subarea, as part of the site investigation programme at Oskarshamn. The present report describes the employed methodology, the investigations of rock properties necessary for the interpretation of the pore water data and the comparison of the obtained pore water composition with formation groundwater sampled from nearby fractures.

The methodology and analytical data have been published also as an independent P-Report /Waber and Smellie 2006/.

2 Materials and methods

From borehole KLX03 16 drillcore sections were received between June 7st and September 7th, 2004 for pore water characterisation. The sections measuring about 20–35 cm in length were taken at regular depth intervals following a previously established sampling protocol (Activity Plan AP PS 400-04-043). This protocol required the samples to be taken from homogeneous, non-fractured bedrock volumes at least 5 m away from any water-conducting fractures or fracture zones. To safeguard against the selection of unsuitable samples, which might not be obvious at the time, extra core lengths were taken along the borehole length when good rock properties occurred.

A full mineralogical, geochemical and fluid inclusions characterisation of quartz monzodiorite samples, including aqueous leaching tests, has already been performed during the pore water characterisation feasibility study performed on core material from borehole KSH02 /Waber and Smellie 2004/. Because borehole KLX03 essentially contains the same rock types as borehole KSH02, only one additional sample from borehole KLX03 was investigated to the same degree of detail.

An important requirement for pore water characterisation using rock samples is the preservation of the fully water-saturated state of the rock material immediately following drilling and sampling and during transportation from the site to the laboratory. This precaution is to inhibit possible water-rock interactions induced by exposure of the rock sample to air. To minimise these potential perturbing effects the samples were immediately wiped clean with a dry towel following drilling and selection, inserted into a heavy-duty PVC bag which was repeatedly flushed with nitrogen, evacuated and heat sealed. This procedure was repeated with a second PVC bag and finally sealed in a plastic coated Al-foil. The samples were then air freighted to the laboratory at the University of Bern, Switzerland, where they were immediately stored at 4°C in a cooling room and prepared for the various measurements and experiments within about 20 hours after arrival.

Once exposed to the air and/or stored over too long a time period, the drillcore samples lose their value for pore water characterisation. Therefore, all samples received had to be rapidly conditioned so that the different laboratory experimental procedures could be initiated. For the out-diffusion experiments this involved all the drillcore samples collected (some 16).

In January 2005 a final decision was made as to: a) which rock sample would be selected for the full analytical programme, i.e. pore water determination plus full mineralogical, geochemical and fluid inclusion characterisation, and b) which samples involved in the ongoing out-diffusion experiments were considered unsuitable (e.g. located within or close to areas of high fracture frequency) or at least potentially problematic for future interpretation. This selection initially was based on the use of available drillcore mapping information, BIPS logs and also hydraulic data from downhole differential flow measurements. Advice and guidance by the field personnel were invaluable.

2.1 Samples and sample preparation

Down to a depth of about 620 m borehole KLX03 penetrated the Ävrö granite; from this depth to the bottom of the borehole quartz monzodiorite dominates. The lithology of the samples collected, the distance to the closest alteration zone above and below the samples, and the fracture intensity within this interval, are given in Table 2-1.

For legibility reasons the sample labelling adopted in this report is a subsequent numbering of the samples with depth using the borehole name as prefix; similar labelling was used for the laboratory studies. The conversion of this sample description to the SKB sample number and the average vertical depth along borehole is given in Table 2-1. The analytical programme performed on the samples is given in Table 2-2 and details for the out-diffusion experiments in Table 2-3.

Following arrival at the laboratory the core sections were cut by dry sawing into full-diameter samples of about 19 cm length to be used specifically for the out-diffusion experiments. The remaining material from the top and bottom of the core section was used for the isotope diffusive-exchange method and the determination of the water content. For these methods the outer rim of the core (~ 0.5 cm) was first removed by chisel and hammer to minimise any small-scale sample effects resulting from de-saturation during initial perturbations by drilling activities and subsequent sample preparation. The wet weight of such material was determined immediately after preparation. The remaining rim material was further prepared for mineralogical and geochemical investigations.

2.2 Analytical methods

Most of the analytical work of this study has been conducted at the Institute of Geological Sciences, University of Bern, Switzerland. Thus, if not otherwise stated the analyses have been performed at this institution.

Mineralogical investigations were performed by optical microscopy of thin sections and X-ray diffractometry on pulped rock material from sample KLX03-11. Bulk chemical analyses were performed by X-ray fluorescence at the University of Fribourg on homogenised rock material of less than 60 µ grain size.

Mineral chemical analyses were performed with a Joel JXA-8200 electron microprobe using natural or synthetic silicate standards. The beam conditions used were 15 kV and 20 nA with peak and background analysis times of 20–30 seconds each. Estimated detection limits in µg/g are: Si 140; Ti 75; Cr 400; Al 120; Fe 450; Mn 400; Mg 75; Ca 120; Na 120; K 55; F 300; Cl 40.

Bulk density (ρ_{bulk}) was determined on sample cubes of about 1 cm^3 from the core centre of sample KLX03-11 by the Hg-displacement method. The sample cubes were then ground to < 60 µm and the grain density (ρ_{grain}) was measured by He-pycnometry.

The water content was determined by the gravimetric determination of the water loss by drying subsamples at 105°C until stable weight conditions (± 0.002 g). If the material received allowed it, then the weight of these samples was chosen to be more than about 200 g to minimise de-saturation effects and to account for grain-size variations in the rocks.

Table 2-1. KLX03 borehole: list of samples used for pore-water studies.

Sample no	SKB sample no	Av. vertical depth (m)	Lithology	Alteration / tectonisation[1)]	Fracture intensity
KLX03-1	SKB 007250	159.22	Ävrö granite	± 5 m	Moderate
KLX03-2	SKB 007251	202.66		± 5 m	Moderate
KLX03-3	SKB 007252	253.72		± 5 m	Moderate
KLX03-4	SKB 007423	303.10		± 10 m	Moderate
KLX03-5	SKB 007424	355.66		± 10 m	Moderate
KLX03-6	SKB 007425	411.70		± 10 m	Moderate
KLX03-7	SKB 007426	462.76		± 5 m	Moderate
KLX03-8	SKB 007427	524.63		± 20 m	Weak
KLX03-9	SKB 007428	590.12		± 20 m	Weak
KLX03-10	SKB 007429	643.14	Quartz monzodiorite	± 10 m	Moderate
KLX03-11	SKB 007430	695.95		± 1 m	High
KLX03-12	SKB 007431	803.21		± 1 m	Very high
KLX03-13	SKB 007432	841.15		± 15 m	Weak
KLX03-14	SKB 005349	894.53		± 5 m	Weak
KLX03-15	SKB 005351	942.47		± 20 m	Weak
KLX03-16	SKB 005352	979.78		± 15 m	Weak

[1)] Approximate distance to next major alteration zone above and below sample

The water content was also determined on the material used for the isotope diffusive-exchange method using the same technique. These samples remained saturated throughout the experiment because they were placed in a vapour-tight vessel at 100% humidity during the equilibration procedure (see also below). The water-content porosity was calculated from the water loss and the grain density measured by He-pycnometry.

A measure for the bulk density of the rocks investigated was also obtained from the volume and saturated mass of the core samples used for out-diffusion experiments. The volume was calculated from measurements of height and diameter of the core samples using a vernier calliper with an error of ± 0.01 mm. Variations in the core diameter over the lengths of the samples was found to be less than 0.05 mm for most samples and a constant diameter was used in the calculation of the volume. For the derived wet bulk density this results in an error of less than 3%.

Fluid inclusion petrography and microthermometry were conducted using a Linkham THMSG-600 heating-cooling stage with a Linkham TMS 91 temperature control on a Olympus BX51 microscope equipped with a 100/0.80 LM PlanFI objective lens. Laser Raman micro-spectroscopy was performed using a Jobin Yvon LabRam HR 800 confocal-laser Raman microprobe with a frequency-doubled Nd-YAG laser. The Raman microprobe is equipped with an Olympus BX41 microscope with an Olympus100/0.95 UM PlanFI objective lens and a Linkham MDS-600 heating-cooling stage with a Linkham TMS 94 temperature. Measurement conditions were a laser beam at 532.12 nm, a hole width of 400 µm, a slit of 100 µm, and an accumulation time of 3×40 secs. The relative abundance of fluid inclusions was carried out by image analysis of individual quartz grains.

Table 2-2. KLX03 borehole: experiments and measurements performed on drillcore samples.

Sample	Mineralogy, geochemistry, fluid inclusions	Aqueous leaching	Water-content porosity	Physical porosity	Isotope diffusive exchange	Out-diffusion experiment
KLX03-1			X		X	X
KLX03-2			X		X	X
KLX03-3			X		X	X
KLX03-4			X		O	X
KLX03-5			X		X	X
KLX03-6			X		X	X
KLX03-7			X		X	X
KLX03-8			X		X	X
KLX03-9			X		–	X
KLX03-10			X		–	X
KLX03-11	X	X	X	X	X	X
KLX03-12			X		X	X
KLX03-13			X		O	X
KLX03-14			X		X	X
KLX03-15			X		O	X
KLX03-16			X		X	X

X = Experiment performed; analyses available.

– = Not enough sample material to perform the experiment.

O = Experiment performed; analytical data not produced based on final sample selection.

Table 2-3. KLX03 borehole: measurements performed on solutions from out-diffusion experiments.

Sample	Chloride time-series	pH and alkalinity	Anions and cations	$\delta^{18}O$ and $\delta^{2}H$	$\delta^{37}Cl$	$^{87}Sr/^{86}Sr$
KLX03-1	X	X	X	–	X	X
KLX03-2	–	X	X	X	X	X
KLX03-3	X	X	X	X	X	X
KLX03-4	–	X	X	X	O	O
KLX03-5	X	X	X	X	X	X
KLX03-6	–	X	X	–	X	X
KLX03-7	X	X	X	–	O	O
KLX03-8	X	X	X	–	O	O
KLX03-9	X	X	X	–	X	X
KLX03-10	O	X	X	–	O	O
KLX03-11	X	X	X	–	X	X
KLX03-12	X	X	X	–	X	X
KLX03-13	O	X	O	–	O	O
KLX03-14	X	X	X	–	X	X
KLX03-15	O	X	O	–	O	O
KLX03-16	X	X	X	–	X	X

X = experiment performed; analyses available.

– = not performed.

O = experiment performed; analytical data not produced based on final sample selection.

Aqueous leaching tests were performed on different grain-size fractions prepared from the centre material of drillcore KLX03-11. Leaching was performed in double-distilled water by gently shaking the PE tubes end over end for 24 hours under ambient conditions. Measurements of pH and alkalinity (by titration) were determined immediately after termination of the experiment. Major cations and anions were determined using a Metrohm 861 Compact ion-chromatograph with a relative error of ± 5%.

The stable water isotope composition of the pore water was determined by the isotope diffusive-exchange method as originally described by /Rogge 1997/, /Rübel 2000/ and /Rübel et al. 2002/. In this method the isotope exchange occurs through the gaseous phase without any direct contact between the rock sample and the test water. Rock pieces of about 1 cm in diameter from the centre of the core and a small petri dish filled with a test water are stored together in a vapour-tight glass container. The mass and stable water isotope composition of the test water are known. In the test water about 0.3 mol NaCl are dissolved to lower the water vapour pressure above the test-water surface. This is to minimise loss of test water from the petri dish and condensation on the rock fragments and the glass container walls. The petri dish with the test water and the whole container are weighed before and after the exchange experiment to check that no water is lost from the container and there was no transfer of test water to the sample by possible swelling of the rock material. Equilibrium in the three reservoir system, i.e. rock sample, test water, and the air inside the container as diaphragm, is achieved in about 10 to 30 days at room temperature depending on the size and water content of the rock pieces. After complete equilibration the test water was removed and analysed by ion-ratio mass spectrometry.

The isotope diffusive-exchange method was originally designed for rocks with water contents in the order of several percent. To account for the much lower water content in the crystalline rocks of borehole KLX03, the method was modified in that an artificial test water strongly enriched in ^{2}H and depleted in ^{18}O was used ($\delta^{18}O = -109.84‰$ and $\delta^{2}H = +425.5‰$ V-SMOW). This modification was necessary in order to obtain a modified test water composition after equilibration that is outside the standard analytical error of the mass-spectrometer. Obviously, solutions so much enriched in ^{2}H are difficult to analyse for $\delta^{2}H$ and certain memory effects cannot be excluded for some of the samples. In contrast, the oxygen isotope data are more reliable.

Out-diffusion experiments were performed on complete core samples of about 190 mm in length by immersion in the same artificial test water as used for the isotope diffusive-exchange method. To accelerate the out-diffusion process the vapour-tight PVC containers were placed into a water bath at a constant temperature of 45°C. The weight of the core sample, the experiment container, and the artificial test water used were measured before and after the experiment to ensure that no loss of test water occurred during the entire experiment. Weighing of the core before and after the experiment in addition gives valuable information about the saturation state of the core at the beginning of the experiment.

At specific time intervals, initially a few days and later a few weeks, 0.5 mL of solution was sampled for the determination of the chloride concentration as a function of time. These small samples were analysed on a Metrohm 761 Compact ion-chromatograph. The analytical error of these determinations is about 5% based on multiple measurements of the standard solutions.

After steady-state with respect to chloride was achieved, the core was removed from the container and the solution was immediately analysed for pH and alkalinity (by titration). The remaining solution was split into different aliquots for chemical and isotopic analyses. Major cations and anions were analysed by ion-chromatography at Hydroisotop GmbH with a relative error of 5%

The isotopic compositions of oxygen and hydrogen in the various test solutions (diffusive-exchange method, and out-diffusion experiments) were determined by conventional ion-ratio mass spectrometry at Hydroisotop GmbH. The results are reported relative to the V-SMOW standard with a precision of ± 0.15‰ for $\delta^{18}O$ and ± 1.5‰ for $\delta^{2}H$.

The $^{87}Sr/^{86}Sr$ isotope ratio was measured using a modified VG Sector® thermal ionisation mass spectrometer (TIMS) in simple collector mode, using oxidised Ta filaments. The analytical uncertainty is given with 2 σ of multiple measurements of the same sample. Total Sr concentrations are given in ppm.

The $^{37}C1/^{35}C1$ isotopic ratio, expressed as $\delta^{37}C1$ relative to SMOC, was measured at the University of Waterloo Environmental Isotope Laboratory (EIL) in Canada using a VG SIRA 9 Mass Spectrometer. Measurements were made with a precision of ± 0.15% (1 σ) based on repeat analyses of SMOC.

3 Rock properties

Borehole KLX03 encountered essentially two major lithologies, the Ävrö Granite down to about 620 m of depth followed by Quartz monzodiorite down to 1000 m depth. To characterise the pore water it is essential to know the rock porosity for each individual sample, for example in order to calculate the salinity of the pore water. Other properties of the rocks, such as the rock and mineral chemistry and the fluid inclusion compositions, also have to be known. Fortunately, within the context of pore water characterisation the similarity of the encountered rock types allows the transfer of data from one sample to another without loosing significant accuracy. Therefore, a full mineralogical, geochemical and fluid inclusion characterisation, including aqueous leaching experiments (see Chapter 4), has been performed only on one quartz monzodiorite core sample from about 700 m of depth (sample KLX03-11). This complements existing data earlier derived from borehole KSH02 in the Simpevarp subarea /Waber and Smellie 2004/.

It should be noted that even though all mineralogical, geochemical and fluid inclusion investigations presented below have been performed from the point of view of their importance for the pore water characterisation and not for a petrogenetic interpretation, the data can be used also for such purposes.

3.1 Mineralogy of the “quartz monzodiorite”

Given a long enough residence time, the pore water will finally reach equilibrium with the minerals present in the rock. However, the residence time of the pore water is *a priori* unknown which therefore excludes the use of geochemical modelling of the pore water by an equilibrium approach. Also, the chemical composition has to be assessed by indirect methods which, in turn, induce water-rock interactions during the experiments (e.g. diffusion, leaching) and thus alter the in situ concentrations of reactive components in the pore water in the experimental solutions. To correct for such contributions of experimentally induced water-rock interactions the mineralogical composition of the rock and the mineral chemistry must be known.

Under favourable experimental conditions such contributions can be corrected for by applying reactive-transport modelling strategies. Within this context the reaction rates and abundances of the individual mineral phases are of greater importance than the sequence of their formation during the emplacement of the rock body and possible later hydrothermal and/or metamorphic alteration(s). To optimise such corrections the mineral chemistry needs to be known accurately.

3.1.1 Mineralogical composition

The KLX03-11 rock sample is bluish-grey in colour and comprises a fine-grained matrix ($\leq$ 0.5 mm) containing a few phenocrysts between about 1–3 mm in diameter. The rock has a well preserved magmatic texture with no obvious metamorphic overprint such as a preferential lineation and/or extensive deformation features in individual minerals. The contents of quartz, K-feldspar and plagioclase constitute about 70 wt.% making this sample slightly more felsic compared to the rocks from borehole KSH02 (Table 3-1). In the QAP-diagram the rock composition of KLX03-11 plots on the boundary between typical granodioritic and

monzogranite composition (Figure 3-1). With its higher quartz content it compares closer to the typical Äspö diorite than to the granodiorite and monzogranite samples from borehole KSH02. For consistency reasons with other reported geological descriptions, the field description of the main rock types of borehole KLX03 will be referred to as "Ävrö granite" and "quartz monzodiorite" in this present report.

The fine-grained matrix (0.1–0.5 mm) of sample KLX03-11 is mainly composed of hypidiomorphic to idiomorphic plagioclase and K-feldspar and of xenomorphic to hypidiomorphic quartz. Mafic phases include amphibole, biotite and finely dispersed clinopyroxene and opaque phases consist mainly of magnetite, illmenite and a few pyrite grains. In the matrix phenocrysts of plagioclase (0.8–1.2 mm), amphibole (1–2 mm), biotite (1–3 mm) and rarely K-feldspar (0.8–1.2 mm) occur also.

The plagioclase phenocrysts often display growth-zonation with andesine composition typifying the center and more oligoclase composition at the rim (see below). They often display sericitic and less frequent saussuritic alteration in the central parts of the crystals. K-feldspar phenocrysts quite frequently occur as perthite, exhibit twinning and a few display also a granophyric texture. Most of the K-feldspar displays sericitic alteration while haematite staining, possibly representing an old or more recent oxidising alteration, is completely absent. Green amphibole phenocrysts are hypidiomorphic and frequently have an optically dark green rim. Amphibole is commonly altered at the rims to biotite, chlorite, opaque mineral phases and some calcite. The xenomorphic clinopyroxenes in the matrix have become replaced by amphibole, biotite, chlorite, opaque phases and calcite. Biotite occurs as a deuteric alteration product and as irregular, large flakes. Generally it is partly replaced by chlorite and sphene, the latter forming sagenite wire textures. Altered biotite also hosts prehnite and some vesuvianite. Accessory minerals include sericite, epidote, chlorite, prehnite, vesuvianite, calcite, sphene, zircon, monazite, apatite and very few clay minerals.

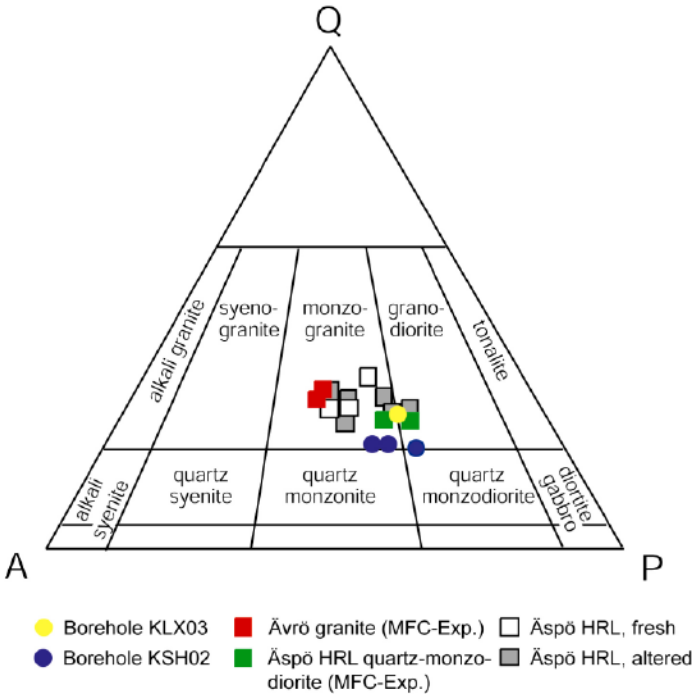

Figure 3-1. *Modal distribution of quartz, alkali feldspar and plagioclase (QAP) of sample KLX03-11 compared to samples from borehole KSH02 and crystalline rocks from the Äspö URL /data from Eliasson 1993, Smellie et al. 2003, Waber and Smellie 2004/.*

Table 3-1. Mineralogical composition of sample KLX03-11 compared to samples from borehole KSH02.

Borehole Sample Vertical depth (m)		KLX03 KLX03-11 695.80–696.10	KSH02 [1)] 785 G 785.30–785.52	KSH02 [1)] 879 G 879.28–879.53	KSH02 [1)] 997 G 997.01–997.26
Quartz	wt.% [2)]	18	12	16	14
K-feldspar	wt.%	16	20	19	14
Plagioclase	wt.%	34	28	34	32
Clinopyroxene	vol.%	1–5	1–5	5–10	5–10
Amphibole	vol.%	5–10	10–15	15–20	10–15
Biotite	vol.%	10–15	15–20	5–10	15–20
Opaque Phases	vol.%	1–5	5–10	1–5	1–5
Calcite	wt.%	0.5	0.6	0.9	< 0.5
Accessories		See text	Chlorite, sericite, clay minerals (very few), apatite, monazite, sphene, zircon.		

[1)] Data from /Waber and Smellie 2004/.

[2)] Wt.% from XRD analysis; vol.% from thin section analysis.

3.2.1 Mineral chemistry

The average chemical composition of the most abundant mineral phases in the quartz monzodiorite sample KLX03-11 are given in Table 3-2. The complete mineral chemical data including analyses of the secondary phases prehnite, vesuvianite and sphene, the normalised analyses for all minerals, and end-member percentages in the case of solid-solution phases, are given in the Appendix, Table A1. No analyses were performed on quartz and the secondary calcite due to their simple chemical composition.

Feldspar phases in crystalline rocks often display a pronounced chemical zonation from the centre to the rim of the crystals and such chemical differences influence the stability and the reaction rates of these mineral phases. This is important in the derivation of the pore water composition and the correction for mineral dissolution during the out-diffusion experiments. Therefore, average compositions specifically measured on the rim and in the centre of the feldspars are given in Table 3-2, while in the Appendix more randomly measured analyses are given also. For plagioclase and K-feldspar there is little difference between the crystal centre and rim. The centre is characterised by plagioclase of andesine composition ($An_{32–43}$); towards the rim there is a slight depletion in anorthite and a corresponding increase in oligoclase composition ($An_{23–34}$). In K-feldspar there appears to be a trend towards a more pure K-feldspar composition at the rim due to a small decrease in the albite component.

Clinopyroxene is of a diopside composition and is commonly rimmed or completely replaced by amphibole of hornblende composition. Both minerals show only small variations in their chemical composition.

Of further interest is the absence of measurable chloride (detection limit 40 µg/g) in biotite. Chloride in biotite (and amphibole) has earlier been suggested as a possible chloride source for pore water from some crystalline rocks /e.g. Edmunds et al. 1984, 1985/.

Table 3-2. Average chemical compositions of major mineral phases in quartz monzodiorite (sample KLX03-11).

	Plagio-clase centre	Plagio-clase rim	K-feldspar centre	K-feldspar rim	Diop side	Amphi-bole	Biotite	Magne-tite
SiO_2	58.80	60.05	65.06	64.91	52.51	54.67	37.01	0.02
TiO_2	0.10	0.01	0.02	0.01	0.14	0.31	3.05	0.04
Cr_2O_3	0.02	0.02	0.02	0.01	0.08	0.03	0.03	0.14
Al_2O_3	26.75	26.16	19.52	18.91	1.00	2.68	14.92	0.02
Fe_2O_3	0.00	0.00	0.00	0.02	0.54	0.00	0.00	0.00
FeO	0.10	0.16	0.05	0.00	9.75	13.31	19.89	93.08
MnO	0.02	0.01	0.05	0.03	0.68	0.46	0.21	0.02
MgO	0.00	0.00	0.00	0.00	12.38	13.76	10.96	0.01
CaO	8.19	7.23	0.89	0.00	22.72	11.98	0.01	0.04
Na_2O	6.68	7.23	1.83	0.75	0.36	0.33	0.10	0.03
K_2O	0.23	0.18	12.96	15.87	0.01	0.17	9.89	0.00
H_2O						2.06	3.86	
F							b.d.	
Cl							b.d.	
Total	100.89	101.04	100.40	100.52	99.99	99.74	99.92	93.39

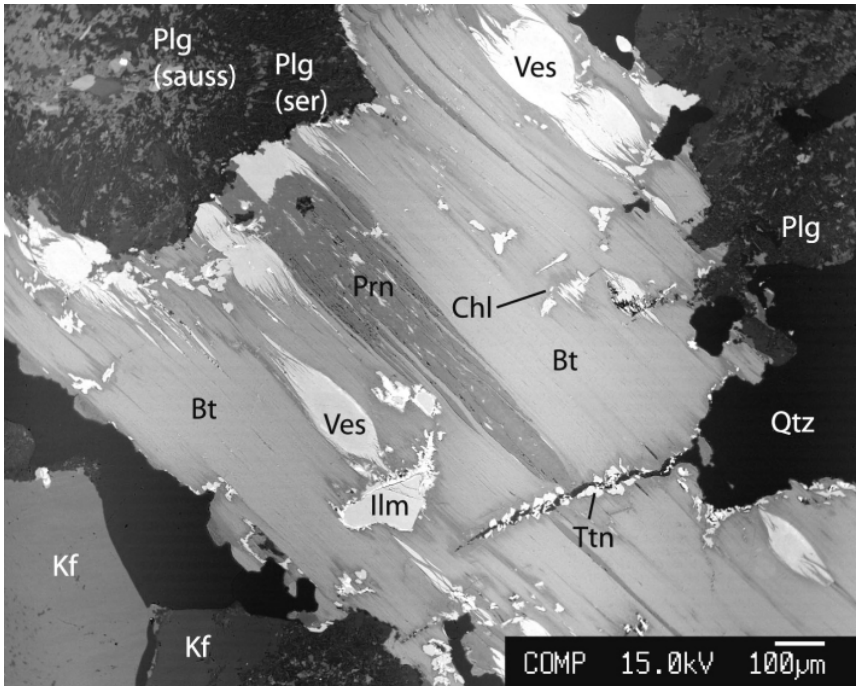

Figure 3-2. *Characteristic rock texture of sample KLX03-11 observed as an electron microprobe backscatter image. (Plg sauss: plagioclase with saussuritic alteration, Plg ser: plagioclase with sericitic alteration, Kf: K-feldspar, Qtz: quartz, Bt: biotite, Chl: chlorite, Prn: prehnite, Ves: vesuvianite, Ilm: ilmenite).*

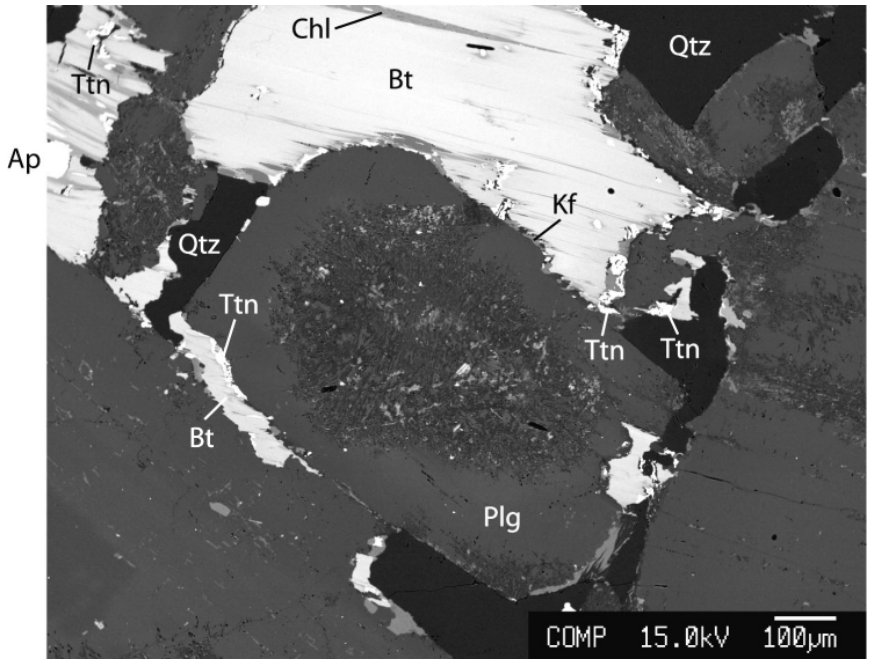

Figure 3-3. *Characteristic rock texture of sample KLX03-11 observed as an electron microprobe backscatter image. (Plg: plagioclase, Kf: K-feldspar, Qtz: quartz, Bt: biotite, Chl: chlorite, Ttn: sphene, Ap: apatite).*

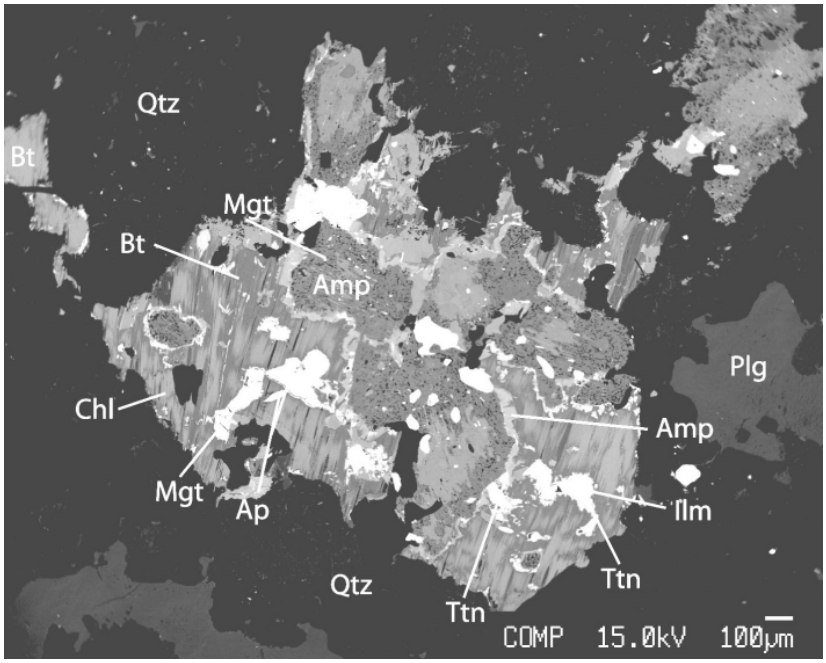

Figure 3-4. *Characteristic rock texture of sample KLX03-11 observed as an electron microprobe backscatter image. (Plg: plagioclase, Amph: amphibole, Qtz: quartz, Bt: biotite, Chl: chlorite, Mgt: magnetite, Ilm: ilmenite, Tit: sphene, Ap: apatite).*

3.2 Chemical Composition

The chemical composition of sample KLX03-11 is given in Table 3-3 and graphically represented in Figures 3-5 and 3-6. The KLX03-11 quartz monzodiorite sample compares well with the granodioritic samples of borehole KSH02. Lager differences are only observed for certain metallic trace elements that can be attributed to variations in the contents of opaque phases such as magnetite, illmenite and pyrite in these rocks. With an SiO_2 content of < 60 wt.%, the KLX03-11 quartz monzodiorite sample is more basic than most of the rocks of the Äspö URL area. It is further characterised by lower concentrations of Na, Rb, Sr, Nb, Ni, and Pb than the Äspö rocks. In contrast, the granodiorite has higher contents of K, Fe, Mg, Ca, Ti, and P.

X-ray diffraction and microscopic analysis did not reveal any Ba or Sr mineral phases; these elements appear to be associated mainly with feldspars and, for Sr, eventually with trace amounts of secondary calcite.

The chemical composition is consistent with the mineralogical analyses and normative calculations according to the CIPW-norm support the granodioritic to monzodioritic compositions obtained from the mineralogical investigations.

Table 3-3. Chemical compositions of quartz monzodiorite in sample KLX03-11 compared to samples from borehole KSH02.

Borehole sample vertical depth (m)		KLX03 KLX03-11 695.80–696.10	KSH02 [1)] 785 G 785.30–785.52	KSH02 [1)] 879 G 879.28–879.53	KSH02 [1)] 997 G 997.01–997.26
SiO_2	wt.%	58.09	58.90	57.46	58.06
TiO_2	wt.%	1.03	0.95	0.95	1.02
Al_2O_3	wt.%	16.77	15.53	15.73	16.24
Fe_2O_3	wt.%	7.25	7.20	6.60	7.53
MnO	wt.%	0.12	0.12	0.11	0.12
MgO	wt.%	3.05	3.38	2.45	2.70
CaO	wt.%	5.84	5.38	5.17	5.64
Na_2O	wt.%	3.33	2.91	3.22	3.02
K_2O	wt.%	3.02	3.71	3.68	3.04
P_2O_5	wt.%	0.42	0.27	0.29	0.30
LOI	wt.%	0.59	0.40	0.54	0.67
SUM	wt.%	99.70	99.05	96.49	98.64
Ba	ppm	789	915	868	782
Cr	ppm	68	81	19	8
Cu	ppm	20	< 2	26	8
Nb	ppm	14	14	13	14
Ni	ppm	14	25	11	13
Pb	ppm	15	30	20	36
Rb	ppm	84	98	102	77
Sr	ppm	666	593	597	594
V	ppm	25	< 5	< 5	< 5
Y	ppm	86	22	20	22
Zn	ppm	157	93	89	88
Zr	ppm	789	218	201	188

[1)] **D**ata from /Waber and Smellie 2004/.

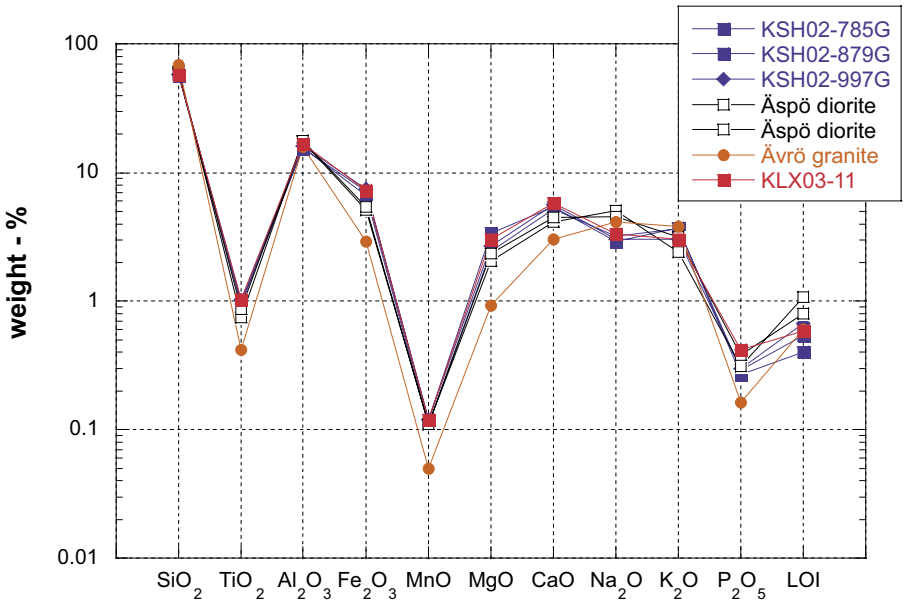

Figure 3-5. *Major element composition of sample KLX03-11 compared to samples from borehole KSH02 and of Äspö diorite and Ävrö granite from the MFC-Experiment (LOI: loss on ignition; data Äspö: /Smellie et al. 2003/, KSH02: /Waber and Smellie 2004/).*

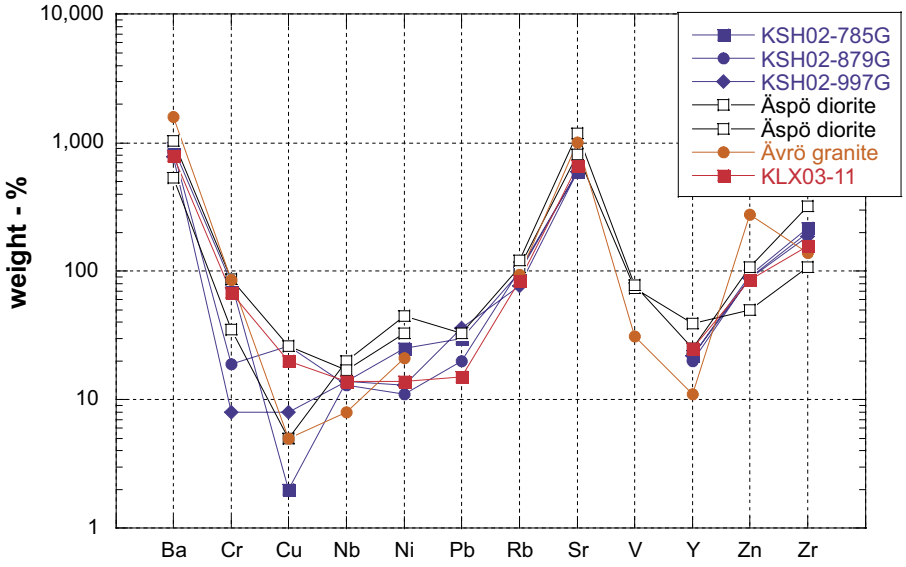

Figure 3-6. *Trace element composition of sample KLX03-11 compared to samples from borehole KSH02 and of Äspö diorite and Ävrö granite from the MFC-Experiment (data Äspö: /Smellie et al. 2003/, KSH02: /Waber and Smellie 2004/).*

3.3 Fluid inclusions in matrix minerals

The composition and abundance of fluid inclusions were investigated to evaluate the potential contribution of saline inclusion fluid to the pore water. In addition, such investigations are mandatory for a correct interpretation of indirect methods of pore water characterisation that involve disintegration of rock samples as shown by /Smellie et al. 2003/ and /Waber and Smellie 2004/. Core samples retrieved from great depth might also suffer from stress release, which could be an important perturbation factor for all pore water characterisation techniques; this is further discussed below from various points of view. If significant stress release takes place then it could induce rupture of fluid inclusions and thus potentially perturb experiments performed on intact core samples such as diffusion experiments.

In the quartz monzodiorite sample KLX03-11 fluid inclusions occur almost exclusively in quartz. Therefore, fluid inclusion investigations focussed on inclusions in quartz only. The full analytical dataset including photographic documentation and Raman spectra of inclusions is given in the Appendix (Table A2 and Figures A1 to A10).

3.3.1 Morphology, texture and abundance of quartz

Sample KLX03-11 displays a magmatic texture with only a weak indication of deformation. The recrystallisation of quartz as very fine-grained equigranular subcrystals around larger crystals, the occurrence of secondary fluid inclusions along healed fissures in quartz, the partial replacement of diopside by amphibole and that of biotite by chlorite and prehnite, are all indications for a deuteric and/or hydrothermal overprint of the rocks.

The fine-grained rock matrix mainly consists of quartz and feldspar (Figure 3-7) with quartz constituting about 18 wt.% of the total rock according to the XRD-analyses. Most of the quartz in this sample has a grain size of < 1 mm and zones with coarser grained quartz are rare. Three different types of quartz can be distinguished: a) xenomorphic to hypidiomorphic quartz grains with abundant solid inclusions of rutile and biotite, b) xenomorphic to hypidiomorphic grains free of solid inclusions, and c) fine-grained, recrystallised quartz around the first two types. Types (a) and (b) are generally somewhat coarser grained than (c). All types display weak undulous extinction under polarised light and there is no obvious anisotropy developed in the quartz texture.

Fluid inclusions occur in all three quartz types mainly as trails along healed fissures. As shown in Figure 3-8 fluid inclusions do not only occur in the central parts of quartz, but also occur near the grain boundary where they might be easily ruptured by stress release events.

3.3.2 Fluid inclusion populations

Following the fluid inclusion typology established for deep-seated granodiorite samples from borehole KSH02 /Waber and Smellie 2004/, all fluid inclusions observed in the quartz monzodiorite sample KLX03-11 can be categorised as ‘Type I’. This type includes single-phase liquid-only and multiphase liquid-vapour-solid inclusions. Type II inclusions (single-phase gas-only inclusions) documented in one sample from borehole KSH02 were not observed in the present KLX03 study. This does not, however, imply that such inclusions are absent.

Type I inclusions in the quartz monzodiorite sample KLX03-11 can be subdivided into single-phase liquid-only inclusions, which constitute about 70% of all inclusions, and multiphase liquid-vapour-solid inclusions which contribute about 30% of all inclusions. Both groups can be further subdivided into petrographic populations of different salinity (see Section 3.3.3).

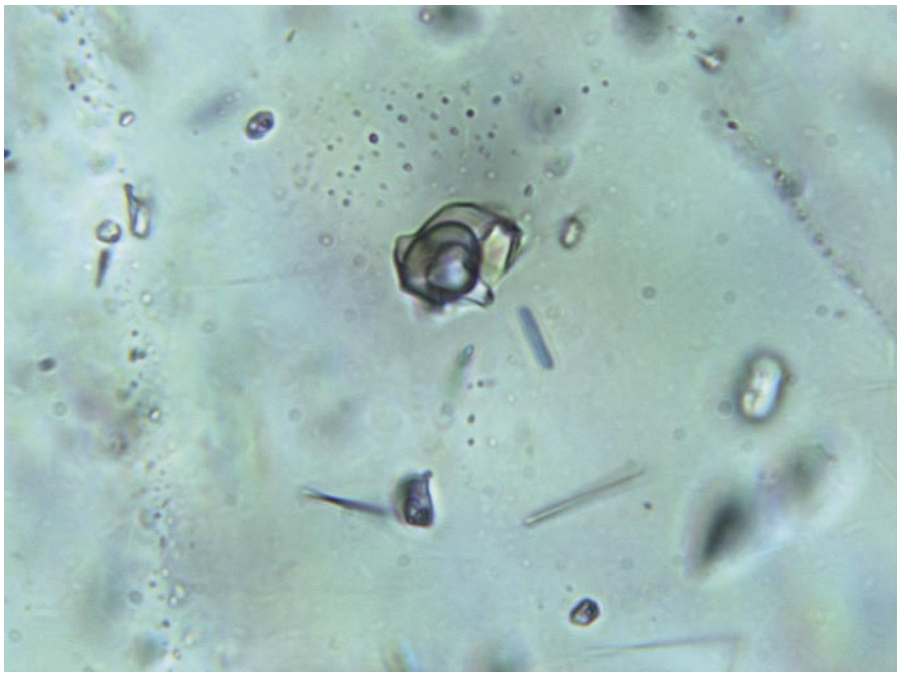

Figure 3-7. *Typical early crystallised (?) quartz with abundant solid inclusions of rutile and biotite and different fluid inclusion populations along healed fissures (sample KLX03-11 FI2).*

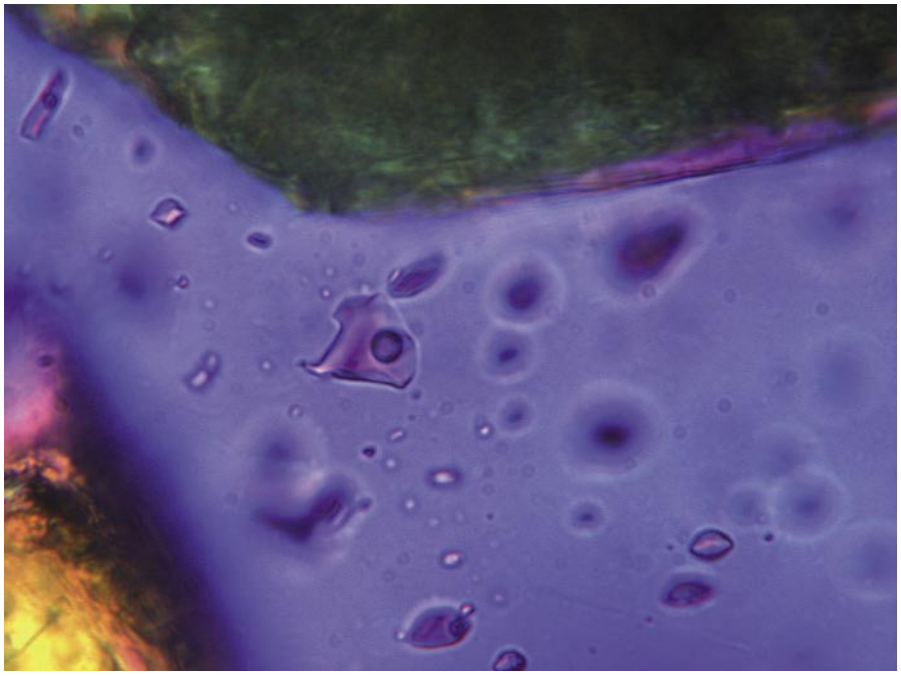

Figure 3-8. *Quartz free of solid inclusions, but with abundant fluid inclusions (1-phase and 2-phase) close to the grain boundary (sample KLX03-11 FI3 No 1).*

Single-phase, liquid-only inclusions of Type I are of secondary origin and occur mainly along healed fissures in quartz. The homogenisation temperature of these metastable inclusions appears to be below about 120°C because the gas/vapour bubble cannot nucleate below the solvus. Commonly, these inclusions occur in intimate association with multiphase inclusions forming one population. Based on this it can be assumed that the salinity of the single-phase, liquid-only inclusions is similar to that of the associated two-phase inclusions.

Multiphase, liquid-vapour inclusions of Type I are also of secondary origin occurring mainly along healed fissures in quartz. Most of these inclusions are two-phase liquid-gas inclusions with the gas/vapour bubble ranging from 0% (i.e. single-phase) to almost 100% within the same inclusion population along a healed fissure. The gas phase is predominantly CO_2 with traces of N_2 occuring in some inclusions (see Appendix, Figures A5 and A7). The salinity of these inclusions, however, is independent of the size of the gas/vapour bubble. This allows the above conclusion that the liquid-only inclusions have the same salinity as two-phase inclusions within the same inclusion association. The difference in the size of the gas/vapour bubble is most probably due to 'necking-down' features of the inclusions and not due to fluid separation. 'Necking-down' features inhibit the measurement of any petrologically meaningful homogenisation temperature and thus homogenisation temperatures were not measured.

In quartz grains with solid inclusions of rutile and biotite such multiphase fluid inclusions of Type I are often rich in CO_2 and have solid phase inclusions of calcite, biotite and rutile. This suggests a direct relation with the magmatic history of the rock.

3.3.3 Salinity

The two-phase Type I inclusions cover a salinity range from about 0.5 to > 24 eq.-wt.% NaCl based on the microthermometric measurements. This range coincides with that observed in some samples from borehole KSH02 /Waber and Smellie 2004/.

The salinity of the fluids determined on 100 inclusions shows a bimodal distribution. The first group has a salinity mainly from 2–8 eq-wt.% NaCl and the second group mostly from 16–18 eq-wt.% NaCl (Figure 3-9). Inclusions of the lower salinity range contribute to about 60% and those of the higher salinity range to about 40% of all inclusions measured (Figure 3-10).

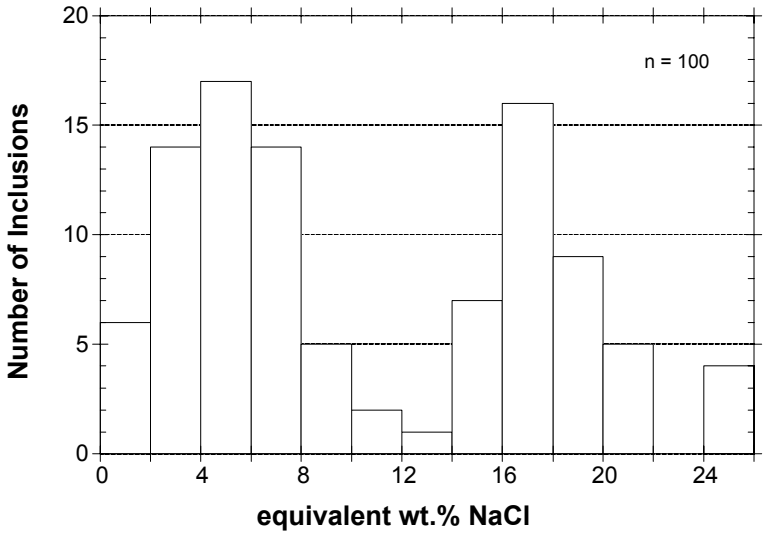

Figure 3-9. *Sample KLX03-11: Histogram of the fluid salinity in 100 fluid inclusions showing a bimodal distribution.*

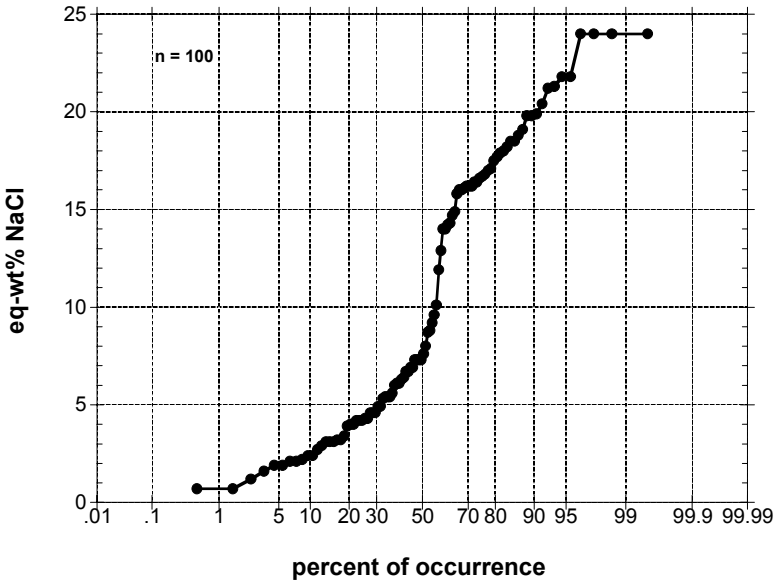

Figure 3-10. *Sample KLX03-11: Percent of occurrence of fluid inclusions with different fluid salinity showing that about 60% of all inclusions have a salinity of less than 12 eq-wt.% NaCl.*

Halite has not been observed as a solid phase in the fluid inclusions but hydrohalite ($NaCl \times 2H_2O$) occurs in the high-salinity inclusions of Type I. The occurrence of hydrohalite was also confirmed by Raman spectrometry (see Appendix, Figure A9). In many of these inclusions the decomposition temperature of hydrohalite is significantly decreased; this can be attributed to the presence of $CaCl_2$. Based on phase relationships the $CaCl_2$ present amounts to 7.4 wt.% at a total salinity of 16.4 wt.%. It should be noted, however, that the microthermometric investigations restrict the detection of KCl in the quaternary system H_2O-NaCl-$CaCl_2$-KCl. To confirm or otherwise the presence of KCl would require Laser-Ablation-ICPMS techniques.

3.3.4 Fluid inclusion abundance

To estimate the total abundance of fluid inclusions in quartz of the monzodiorite sample image analysing techniques were used. The inclusion density varies between about 0 and 5 Vol.% from quartz grain to quartz grain. On average fluid inclusions comprise about 2 to 3 Vol% of the total quartz volume in the quartz monzodiorite sample. This is higher than the estimate made for the granodioritic rocks of borehole KSH02 (0.5–1 Vol.%; /Waber and Smellie 2004/). It can be concluded that if rupturing of fluid inclusions were to occur (e.g. during stress release), then the availability of such fluids would be an additional significant salinity source in pore water experiments and possibly also for the extracted in situ pore water.

3.3.5 Potential influence of fluid inclusions on pore water experiments

To release fluid from inclusions in quartz requires a change in the physical conditions of the rock for rupturing individual quartz grains and allowing the fluid to migrate into the intergranular and possibly connected pore space. Such a change in the physical conditions includes essentially changes in the temperature and pressure (i.e. stress).

A change in temperature might lead to expansion of the enclosed fluid and finally to rupturing of the inclusions. This might happen if the temperature exceeds the homogenisation temperature of the fluid inclusion or during freezing of the fluid. The latter seems only important in the case of low salinity liquid inclusions because highly saline and/or single-phase gas inclusions have freezing temperatures that will not be reached in a natural environment. Inclusion homogenisation temperature have not been specifically measured on the present samples. However, the inclusion petrology indicates that all inclusions are of secondary origin and have to be related to the deuteric and/or later hydrothermal alteration. Such alteration and related inclusion of fluid into newly growing quartz commonly occurs at distinctly higher temperature than the 45°C used in the out-diffusion experiments (see Chapter 6). Therefore, it is not expected that fluid inclusions underwent rupturing during these experiments due to a temperature effect.

Regionally-induced stress release during crustal rebound might also potentially lead to rupturing of fluid inclusions and this has been proposed as a possible mechanism to explain the increasing salinity as a function of depth in intra-continental crystalline groundwater /e.g. Waber and Nordstrom 1992/. If this is the case, then even a fraction of inclusions opened mechanically and containing highly saline fluid might influence, for instance, a leach solution in measurable amounts (see Chapter 4). However, in the case of the out-diffusion experiments performed on entire drill cores (Chapter 6), the presence of such mechanical destruction is either absent or only very limited in the drilling disturbed zone. Furthermore, one would expect a homogeneous chloride distribution in the out-diffusion experimental solutions of the same rock type, which might possibly increase with the depth due to increasing stress on the samples, if stress release induced by the drilling activities would really have a significant effect. As will be shown below such a distribution of chloride is not developed for the present samples.

Ruptured fluid inclusions will also constitute new void space in the rock that is accessible for water and thus might potentially disturb water-content measurements. Comparing the estimated abundance of inclusions in quartz and the measured water contents (see Section 3.4) it can be shown, however, that all fluid inclusions in the rock would have to be opened to have a measurable influence on the water content determinations. This is not supported by present studies.

3.4 Petrophysical properties of the rock

The characterisation of pore water in rocks of very low permeability and low water content requires knowledge of the water-accessible porosity. This is simply because the pore water in such rocks cannot be sampled directly, but has to be accessed by indirect methods, all of which include a dilution of the in situ pore water present. Extensive reviews of this problem and of presently available techniques with their advantages and draw-backs are given in /Pearson 1999, Sacchi and Michelot 2000, Sacchi et al. 2001, Pearson et al. 2003, Smellie et al. 2003/.

However, the different porosity measurements available refer to different types of porosity that are not all appropriate for pore water characterisation, but necessary to evaluate possible deviations of the porosity in the rock sample at the surface from that in situ. Thus, the definitions and nomenclature of the different types of porosity follows those given in /Smellie et al. 2003/ in that the *physical porosity* describes the ratio of total void volume to the total volume of rock (calculated from bulk and grain density), the *connected porosity* is described by the water-content porosity obtained from gravimetric water-loss measurements and the *diffusion porosity* is determined by diffusion experiments.

Petrophysical measurements conducted on the core samples from borehole KLX03 include the determination of the water loss by drying at 105°C, bulk and grain density by Hg-displacement and He-pycnometry, respectively, the determination of the wet bulk density from volumetric and mass measurements, and the porosity determined by the isotope diffusive-exchange method. From the obtained values the different types of porosity are calculated.

Perturbation of porosity values measured in the laboratory from those present in situ have two major origins besides the analytical uncertainty. First, desaturation of the rock sample might occur during sample recovery and handling. This was investigated by comparing the mass of the rock samples before and after the out-diffusion experiments. Second, the rock sample might suffer stress release due to retrieval from great depth. This was investigated by the isotope diffusive-exchange method, which reveals a water-content porosity independent of stress release and, under favourable conditions, a diffusion porosity for water.

3.4.1 Bulk density, grain density and physical porosity

The physical porosity, Φ_{Phys}, of a rock can be calculated from measurements of bulk and grain density according to:

$$\Phi_{\Pi\eta\psi\sigma} = [1-(\rho_\beta/\rho_\gamma)] \quad (1)$$

where ρ_β is the bulk density and ρ_γ is the grain density.

For sample KLX03-11 a physical porosity of 0.93 Vol.% was derived from bulk and grain density measurements (Table 3-4). This value is considerably higher than those obtained for quartz-granodiorite samples from borehole KSH02 (0.07 ± 0.06 Vol.%; Waber and Smellie, 2004). While the bulk density of sample KLX03-11 is comparable to that derived from volume and mass measurements of the diffusion sample (see below) and those of the KSH02 samples, the grain density is considerably larger by about 0.25 g/cm^3. It is unknown if this difference is related to the heterogeneity of the rock samples (e.g. larger amount of magnetite/ilmenite in the KSH02 samples) or due to a low reproducibility and accuracy of the He-pycnometry method. In any case it highlights once again the low accuracy of such derived porosity data for crystalline rocks.

For the large-scale samples used for out-diffusion experiments a measure of their wet bulk density can be derived from their saturated mass and volume. The relative error of these measurements is estimated to be about ± 3%. The saturated mass of these samples is about 1,000 g and thus the wet bulk density values account for variations in mineralogical composition. The wet bulk density for the Ävrö granite samples is lower (average 2.73 ± 0.02 g/cm^3) compared to that of the quartz monzodiorite (average 2.79 ± 0.03 g/cm^3) consistent with the different mineralogy of these rocks types. For sample KLX03-11 the derived wet density is consistent with the dry density measured by Hg-displacement (Table 3-4).

The weight of the large-scale samples used for out-diffusion experiments was measured on two occasions: a) immediately after unpacking the sample, and b) after termination of the experiments, i.e. after approx 3 months of immersion in the test water. As shown in Figure 3-11, the two measurements agreed very well indicating that all samples were saturated at the time of their arrival in the laboratory.

Table 3-4. Bulk and grain density and physical porosity of samples from borehole KLX03.

Laboratory sample no	Lithology	Bulk density dry [1] (g/cm³)	Grain density [2] (g/cm³)	Physical porosity (Vol.-%)	Mass of sample (g)	Bulk Density wet [3] (g/cm³)
KLX03-1	Ävrö granite				1,015.640	2.72
KLX03-2					1,028.960	2.72
KLX03-3					1,227.891	2.71
KLX03-4					1,031.454	2.72
KLX03-5					1,028.396	2.75
KLX03-6					1,007.473	2.74
KLX03-7					1,027.610	2.76
KLX03-8					1,015.631	2.74
KLX03-9					1,002.790	2.73
KLX03-10	Quartz-monzo-diorite	2.800	2.825	0.93	982.509	2.73
KLX03-11					1,036.704	2.79
KLX03-12					1,050.850	2.78
KLX03-13					1,053.568	2.80
KLX03-14					1,044.860	2.80
KLX03-15					1,041.053	2.81
KLX03-16					1,047.565	2.80

[1] Determined by Hg-displacement on dry rock sample.

[2] Determined by He-pycnometry on dry rock sample.

[3] Determined from mass and volume of saturated (wet) drillcore sample used for out-diffusion experiments.

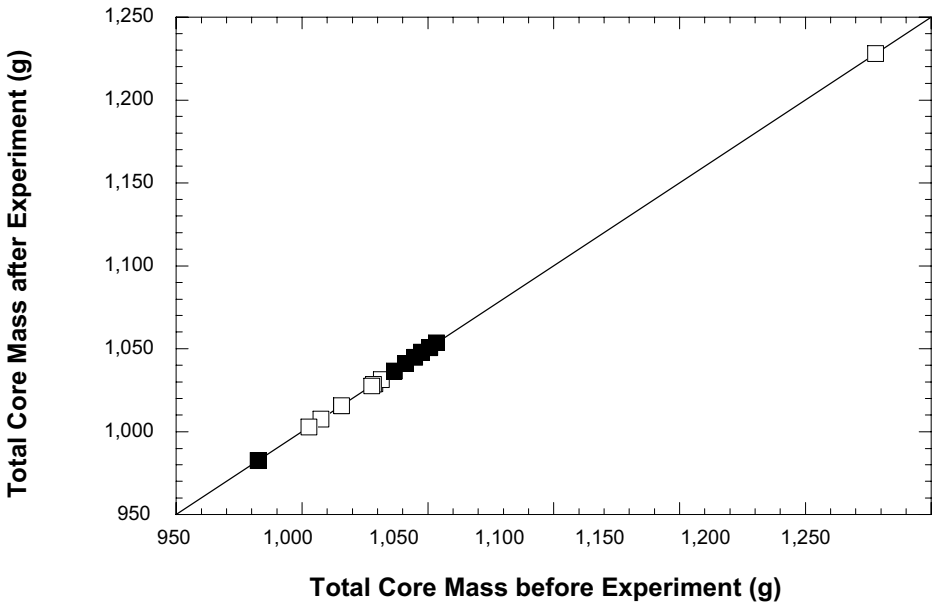

Figure 3-11. *Weight of samples from borehole KLX03 used for out-diffusion experiments measured before and after the experiment. The identical weights indicate saturation of the sample at the time of arrival in the laboratory (error ± 0.002 g; open symbols: Ävrö granite, closed symbols: quartz monzodiorite).*

3.4.2 Water content and connected porosity from gravimetric water-loss measurements

The water content, WC, was obtained by gravimetric measurement of the weight loss, WL, by drying the samples at 105°C until stable weight conditions. Where possible, the water content was determined for each core sample on three subsamples to account for effects of textural heterogeneity of the rocks and artefacts induced by drilling and possible stress release. The weight loss determinations included a large sample specifically assigned to such measurements (masses of 259.91 ± 112.51 g) and the two samples used for the isotope diffusive-exchange method (masses of 139.03 ± 32.16 g). Due to textural heterogeneity the standard deviation of the water content is larger for groups of subsamples with lower masses.

As will be shown in Chapter 6, the dominant fluid transport mechanism in the undisturbed rock matrix is diffusion. To a certain degree this also applies for the solvent H_2O of the pore water during drying although the drying process cannot be compared directly to the out-diffusion of a solute. This is because during drying a potential gradient is established, which will lead to a certain advective component in the movement of H_2O out of the rock. This makes the movement of H_2O during drying of the rock sample directly dependent on the hydraulic conductivity. The fact that for solutes diffusion is the dominant transport mechanism suggests that the pore apertures are small and thus the hydraulic conductivity is low. Therefore one has to expect that complete drying (as well as re-saturation) of a rock sample will last a considerable period of time depending on the sample size, certainly longer than the often used and arbitrarily chosen 24 or 48 hours.

This becomes obvious when looking at the periods of time required for drying the rock samples to stable weight conditions (± 0.002 g). The samples used for the isotope diffusive-exchange method invilved several pieces of about 1–2 cm^3 in size, while those used for water-content measurements alone were intact core pieces with a diameter of 51 mm and lengths of 30–60 mm. As a consequence the drying time varied from about 30 days to more about 170 days for individual samples. The loss of weight with time of the non-fractured samples describes a diffusion-type curve suggesting that the loss of the pore water occurs mainly by diffusion. This is exemplified in Figure 3-12 for sample KLX03-11.

The water-content porosity or connected porosity, Φ_{WC}, was calculated in two different ways based on the wet weight of the sample. For samples with a known grain density Φ_{WC} is calculated according to:

$$\Phi_{WC} = \frac{WC_{wet} \cdot \rho_{grain}}{WC_{wet} \cdot \rho_{grain} + (1 - WC_{wet}) \cdot \rho_{water}} \quad (2)$$

where WC_{wet} is the water content based on the wet weight, ρ_{grain} is the grain density and ρ_{water} is the density of the pore water (assumed to be 1).

Alternatively, for samples with no grain density value available, Φ_{WC} is calculated using the wet bulk density, $\rho_{bulk,\,wet}$, obtained from the samples used for out-diffusion experiments according to:

$$\Phi_{WC} = WC_{wet} \cdot \frac{\rho_{bulk,wet}}{\rho_{water}} \quad (3)$$

The water content determined by drying (WC_{drying}) and water-content (connected) porosity values determined on samples from borehole KLX03 are given in Table 3-5. The most remarkable change in water content and water-content (connected) porosity occurs with the change in lithology from Ävrö granite to quartz monzodiorite (Figure 3-13). In the Ävrö

granite above 620 m depth the WC_{drying} and water-content porosity show rather large variations with average values of 0.252 ± 0.074 wt.% and 0.71 ± 0.20 Vo.%, respectively. In contrast a more homogeneous distribution with depth is observed for the quartz monzodiorite with the exception of one sample from a strongly tectonised interval (sample KLX03-12 at 803 m depth). WC_{drying} and water-content porosity are less than half of those of the Ävrö granite with average values of 0.117 ± 0.065 wt.% and 0.32 ± 0.18 Vo.%, respectively.

Table 3-5. Average water content by drying at 105°C and water-content (connected) porosity of rock samples from borehole KLX03.

Laboratory sample no	Lithology	Number of samples	Water content average (wt.-%)	Water content 1 σ (wt.-%)	WC-Porosity average (Vol.-%)	WC-Porosity 1 σ (Vol.-%)
KLX03-1	Ävrö granite	3	0.217	0.014	0.588	0.038
KLX03-2		3	0.214	0.004	0.581	0.012
KLX03-3		3	0.242	0.019	0.661	0.051
KLX03-4		3	0.369	0.040	0.997	0.108
KLX03-5		3	0.212	0.016	0.582	0.044
KLX03-6		3	0.173	0.005	0.471	0.014
KLX03-7		3	0.276	0.051	0.757	0.139
KLX03-8		3	0.375	0.073	1.019	0.198
KLX03-9		1	0.190	–	0.51	–
KLX03-10	Quartz-monzo-diorite	1	0.068	–	0.186	–
KLX03-11		3	0.122	0.006	0.339	0.018
KLX03-12		3	0.258	0.010	0.715	0.027
KLX03-13		3	0.103	0.012	0.287	0.032
KLX03-14		3	0.083	0.010	0.232	0.027
KLX03-15		3	0.089	0.022	0.249	0.063
KLX03-16		3	0.094	0.023	0.263	0.064

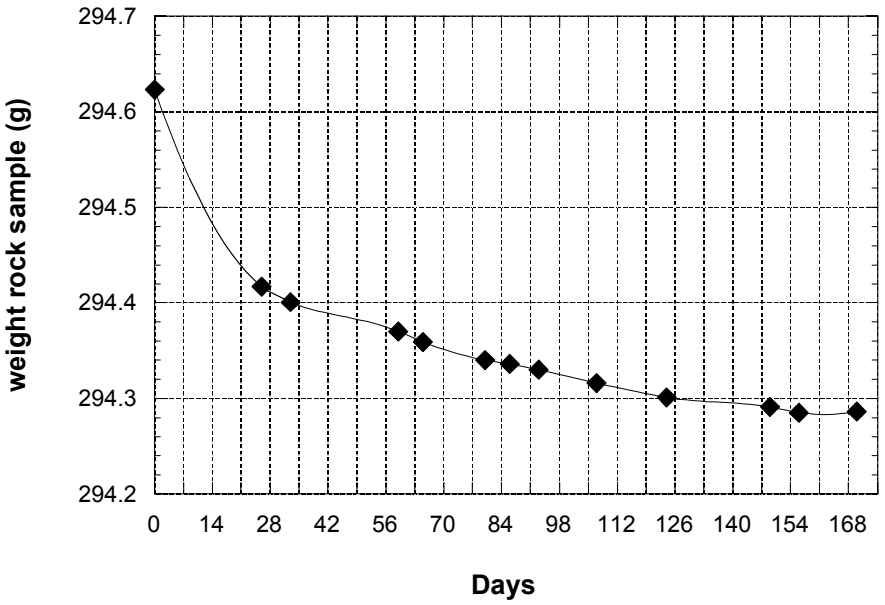

Figure 3-12. *Weight loss of sample KLX03-11 as a function of time. Initial saturated weight of the sample was 294.623 g; stable weight conditions were achieved after 170 days of drying at 105°C at 294.286 g (error ± 0.002 g).*

3.4.3 Water content from isotope diffusive-exchange

The water content of the rocks was also determined by the isotope diffusive-exchange method (WC_{isoex}). Details of this method are given in /Rübel et al. 2002/ and summarised in Section 5.1. Important at this stage is the fact that in the method used the water content is derived by equilibrating the oxygen and deuterium isotopes of the pore water with those of two test solutions of known isotopic composition over the vapour phase in a closed system. By applying isotope mass balance calculations the water content and the isotopic composition (see Section 5.1) of the pore water can be calculated.

As for gravimetric water content measurements fully saturated samples are required for this method. There are two main advantages to this method:

1. The rock sample does not have to be immersed in a test solution, as required for re-saturation techniques for gravimetric water-content measurements or for many other diffusive-exchange experiments. This excludes any experimental artefacts that are induced by immersion of a rock sample in a solution which is chemically and/or isotopically different from that of the pore water.
2. The method is independent from disturbances of the rock texture by stress release and/or drilling activities as long as the amount of induced drilling fluid is small compared to the amount of pore water. Because contact between drilling fluid and drillcore is commonly limited only to a few hours or less, and diffusion is the dominant solute transport mechanism in the rock matrix (see Chapter 6), it is unlikely in the present borehole that such contaminating effects have played a significant role.

The water content data derived by the two methods are given in Tables 3-5 and 5-1 and compiled in Figure 3-13. As can be seen from Figure 3-13 the water content derived by the isotope diffusive-exchange method (WC_{isoex}) agrees well with that derived by drying (WC_{drying}) for most samples and it reflects the same variations between the different lithologies. Only for sample KLX03-12 (depth of 803.21 m) is a larger discrepancy observed. From the analytical protocols there is no clear evidence indicating an analytical artefact. As mentioned above, sample KLX03-12 comes from a heavily tectonised zone (Table 2-1) which may have influenced the results from both methods to a certain degree.

The general agreement between the two independent methods supports: a) the fully saturated state of the sample upon arrival in the laboratory, and b) no detectable influence of drilling fluid with the present precision of the applied methods because desaturation and drilling fluid contamination would each affect the two methods in opposite ways.

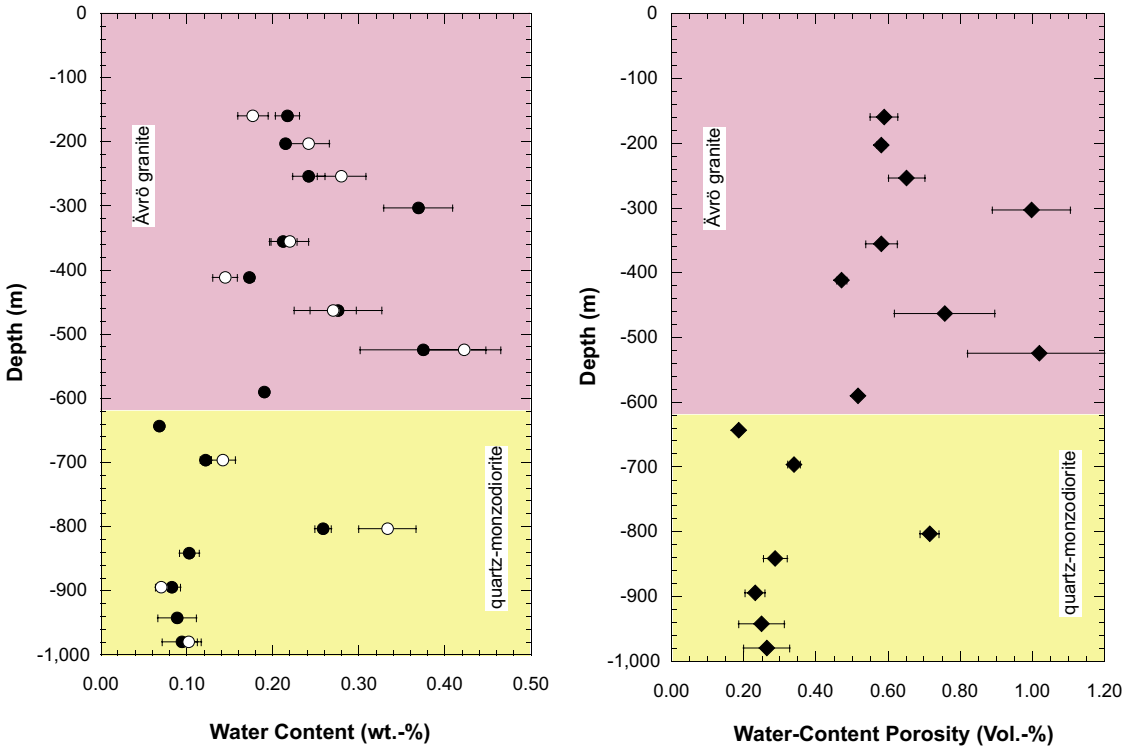

Figure 3-13. *Borehole KLX03: Water content (left) derived by drying (closed symbols) and by isotope diffusive exchange (open symbols) and water-content porosity (right) of drillcore samples as a function of depth. Note the change with changing lithology at about 620 m depth from Ävrö granite to quartz monzodiorite.*

4 Aqueous leaching experiments

Aqueous leaching is commonly performed on rock material dried under ambient conditions. During drying dissolved constituents in the pore water will precipitate as highly soluble salts following complex evaporation cycles. Crushing and grinding of the rock material will additionally liberate fluid trapped in mineral fluid inclusions. The mineralisation of a leachate solution is thus the sum of: 1) the constituents originally dissolved in the pore water, 2) the constituents present in inclusion fluids, and 3) water-rock interaction during the leaching process. Therefore, aqueous leach solutions represent a complex composition in rocks with abundant fluid inclusions and/or rapidly reacting mineral phases such as carbonates and sulphides. Nevertheless, some insight into the rock/pore water system can be gained.

The aim of the present experiment was: (a) to explore the impact of inclusion fluid on the leach solution, (b) to explore the impact of water-rock interaction during leaching in the coarse-grained fraction for comparison with the diffusion experiment, and (c) to derive a statement about potential changes of pore water composition in the near-vicinity of a future rupture zone without (coarser-grained fractions) and with (fine-grained fractions) the development of a fault gouge.

Aqueous leaching experiments were conducted only on the quartz monzodiorite sample KLX03-11 (695.95 m depth). The current study focussed on aqueous leaching of five different grain-size fractions. The two largest grain-size fractions (> 4 mm and 2–4 mm) were chosen to be slightly above and within the range of the average grain size of the KLX03-11 quartz monzodiorite sample. Fractions 0.83–2 mm and 0.14–0.83 mm are representative for the grain size of the fine-grained rock matrix, while in the most fine-grained fraction (< 63 μm) essentially all minerals are destroyed.

4.1 Composition of leach solution from different grain-size fractions

The complete chemical and isotopic data of the aqueous leaching experiments including the data calculated for the carbonate system are given in the Appendix in Table A3. Note that for the two most coarse-grained fractions the data given correspond to a solid: liquid ratio of 2:1 used in the experiment. For comparison with the other extract solutions these concentrations have to be divided by a factor of 2, which is, however, strictly only applicable to chemically conservative elements.

All dissolved anion and cation concentrations increase with decreasing grain size (Figures 4-1 and 4-2). The increase is particularly large for Cl, SO_4, Na and K. Besides the pore water, sources for these dissolved compounds in the aqueous extract solutions include fluid trapped in fluid inclusions for the conservative ion Cl. For Na, K, and SO_4 mineral dissolution reactions give rise to increased concentrations. In Chapter 3 it was shown that quartz in the fine- to medium-grained matrix contains abundant fluid inclusions with about 40% characterised by highly saline compositions ranging from 16–20 eq-wt.% NaCl. In the aqueous extract solutions the almost ten-fold increase in Cl with decreasing grain size therefore indicates an increasing salt contribution from crushed fluid inclusions to the

fine-grained fractions. The Na concentrations in the aqueous extract solution increase only by about a factor of 3 with decreasing grain size, but are significantly higher in the most coarse-grained fraction compared to Cl. As a consequence the Na/Cl ratio decreases from 6.6 in the extract solution of the most coarse-grained fraction to about 2 in that of the most fine-grained fraction. In the NaCl-dominated inclusion fluid the Na/Cl can be expected to be close to 1. Therefore, the higher ratios obtained in the aqueous extract solutions indicate that additional sources contribute to the Na concentrations. The increase in the Na/Cl ratio from fine-grained to the coarse-grained size fractions is, however, contrary to what one would expect if the inevitable mineral dissolution reactions would be a major source for Na in the extract solution. This is because such reactions are most pronounced in the fine-grained size fractions due to the largest available reactive mineral surface area.

Much more significant is the increase in the Na/Cl ratio from fine-grained to coarse-grained size fractions which indicates that the pore water itself has a Na/Cl ratio far above 2. This hypothesis is supported by the solution composition of the out-diffusion experiment of the same sample, which has Na/Cl ratio of about 9 (cf Chapter 6).

A similarly strong but more irregular increase in concentration with decreasing grain size is obtained for K and SO_4 (Figures 4-1 and 4-2). In the extract solution of the most fine-grained fraction (i.e. KLX03-11A) the concentrations of K are more than six times those of SO_4 and more than three times higher than the corresponding concentrations in the other extract solutions. This strong concentration increase in the most fine-grained fraction suggests that substantial amounts of K and SO_4 are derived from the dissolution of K-feldspar and biotite and of pyrite, respectively, during extraction. However, the concentrations of K and SO_4 in the most fine-grained fractions are also larger by a factor of 8 and 3, respectively, than those obtained in the out-diffusion experiments (see Chapter 6). In contrast to the 24-hour aqueous extraction at ambient temperature the out-diffusion experiment lasted over 90 days at 45°C and mineral dissolution can be expected to be at least similar in spite of the differences in the reactive surface area between the two experiments. Therefore, a significant contribution of K and SO_4 from crushed fluid inclusions to the aqueous extract solutions can not be excluded. Here it should be noted that a quantification of K and SO_4 based on the performed microthermometric fluid inclusion data and phase relationships can not be made (see Section 3.3.3)

The concentration of Ca also increases with decreasing grain size, while that of Mg remains always around the detection limit. All rock samples contain small amounts of calcite as a saussuritisation alteration product (Table 3-1) and the extract solutions are at equilibrium with calcite or even supersaturated with respect to calcite (Appendix, Table A3). The comparison of the molar concentrations of Ca and TIC (total inorganic carbon) reveals that in the extract solution the TIC is about 10 to 30 times higher than the Ca concentration and thus a carbon source other than calcite must be present. The distilled water used in the experiments was initially in equilibrium with the atmosphere and had a TIC concentration of about 1.3×10^{-5} mol and possible continuous equilibration with the atmosphere during the experiment would result in a log pCO_2 of about –3.5. The log pCO_2 calculated for all extract solutions is –4.6 or less. Therefore, neither the initial distilled water nor continuous air-equilibration during the experiment can account for the analysed TIC. Other carbon sources in the rock such as CO_2 in the original pore water and in fluid inclusions must contribute significantly to the measured TIC besides mineral dissolution.

To summarise, the aqueous extract solutions of different grain-size fractions reveal that not only the concentrations of Cl, but also that of Na, K and possibly SO_4 contain significant contributions from crushed fluid inclusions. The contribution from mineral dissolution during the experiments increases with decreasing grain size of the extracted material.

In combination with available mineralogical and fluid inclusion data, investigation of ion-ion ratios further helps to identify in a qualitative way the different proportions of ion concentrations which have contributed to the experimental solution from the original pore water, fluid inclusions and mineral dissolution. For sample KLX03-11 the aqueous extract experiments indicate that the in situ pore water has a Na/Cl ratio much higher than unity and Cl is not the dominating anion.

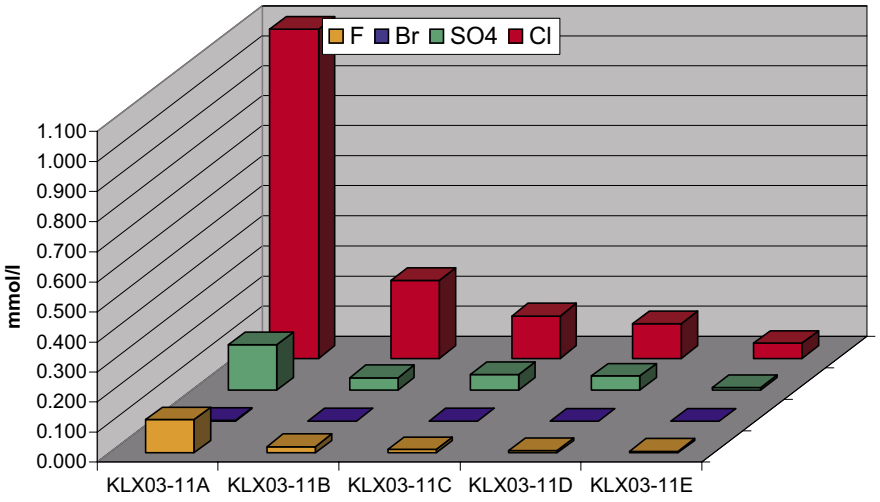

Figure 4-1. *Anion concentrations in aqueous leach solutions of different grain-size fractions from sample KLX03-11 (solid:liquid ratio 1:1; grain size: A < 63 µm, B = 0.14–0.83 mm, C = 0.83–2 mm, D = 2–4 mm, E = > 4 mm).*

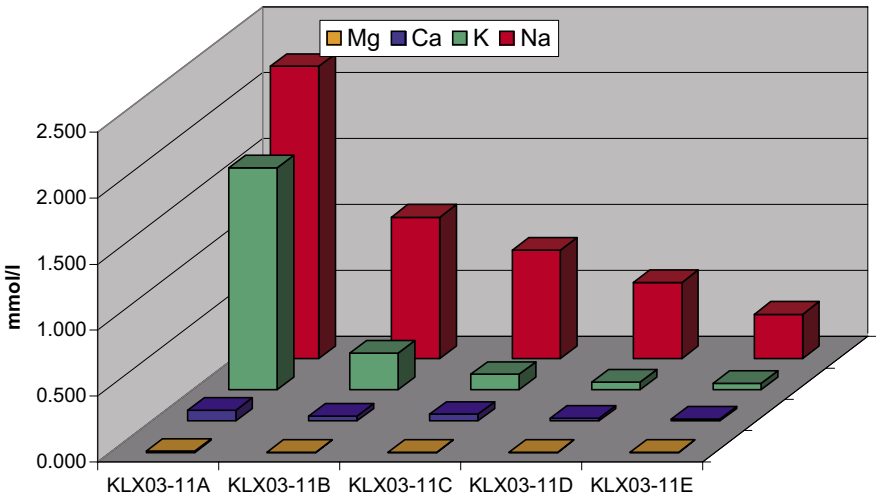

Figure 4-2. *Cation concentrations in aqueous leach solutions of different grain-size fractions from sample KLX03-11 (solid:liquid ratio 1:1;grain size: A < 63 µm, B = 0.14–0.83 mm, C = 0.83–2 mm, D = 2–4 mm, E = > 4 mm).*

5 $\delta^{18}O$ and $\delta^{2}H$ of pore water

5.1 Background of the isotope diffusive exchange method

The diffusive-exchange method for the determination of the stable water isotope composition and the water content of low-permeability rocks was developed by /Rogge 1997/ and /Rübel 2000/. It is based on the concept that the known water isotope composition of a test water will equilibrate with the unknown pore water composition using the gas phase as a diaphragm in a vapour-tight container. The response time τ of the system to completely equilibrate the test water and the pore water is most favourably done from the temporal evolution of either the $\delta^{2}H$ or $\delta^{18}O$ values of the test water by equilibrating several subsamples over different periods of time (time-series). Alternatively, the response time τ can be estimated from the relationship:

$$\tau_{\tau o \tau \alpha \lambda} = \mu / P_{\tau o \tau \alpha \lambda} \qquad (4)$$

where μ is the characteristic mass derived from ratio of mass of test water to mass of pore water and R_{total} denotes the total exchange rate according to:

$$P_{\tau o \tau \alpha \lambda} = [\delta^{2}{}_{\tau \varepsilon \sigma \tau} / (\Delta_{\omega \alpha \tau \varepsilon \rho} \infty \mu_{\tau \omega}) + \delta^{2}{}_{\pi \omega} / (\Delta_{\omega \alpha \tau \varepsilon \rho} \infty \mu_{\pi \omega}) + 1_{\alpha \iota \rho}] / (\Delta_{\alpha \iota \rho} \infty \rho_{\alpha \iota \rho} \infty A_{\alpha \iota \rho}) \qquad (5)$$

where d = distance between the surface of the test water and the surface of the most distant rock piece, D = diffusion coefficient of water, m = mass, r = density, A = cross-section area, tw = test water, and pw = pore water. This latter approach had to be chosen in the present study because the available mass of rock material was limited.

Condensation of the test water on the rock pieces and/or the container walls is minimised by adding NaCl to the test water. As a consequence, one has to consider a difference in the salinity between test water and the (unknown) pore water which results in a slight difference in isotope content of both reservoirs. While there is almost no effect on ^{18}O, the liquid-vapour equilibrium fractionation factor of Deuterium depends on salinity /Horita et. al., 1993/. The systematic effect on the result at room temperature is about 2.7‰×ΔM in $\delta^{2}H$, where ΔM denotes the difference in salinity in mol/kg_{H2O} between solutions. For the KLX03 core samples the difference in salinity is less than about 0.25 mol/kg_{H2O} (for most samples less than 0.1 mol/kg_{H2O}, see below) and the absolute error from this salinity effect on the $\delta^{2}H$ value is thus lower than 1‰.

The stable isotope composition of the pore water and the water content of the sample is calculated from mass balance relationship of the experiments according to:

$$m_{pw} \times c_{pw}\big|_{t=0} + m_{tw} \times c_{tw}\big|_{t=0} = (m_{pw} + m_{tw}) \times c_{tw}\big|_{t=\infty}, \qquad (6)$$

where m = mass, c = isotope concentration, pw = pore water, tw = test water and the concentrations on the left side of the equation are prior to equilibration (t = 0), while the concentration on the right side is after equilibration is achieved (t = ∞) in the experiment. Each equilibration experiment reveals two independent equations of the type (6) for $\delta^{18}O$ and $\delta^{2}H$. To enable the calculation of the three unknowns, i.e. the $\delta^{18}O$ and $\delta^{2}H$ of the pore water and the pore water mass (i.e. the water content), two different exchange experiments have to be performed for each sample to obtain the necessary four equations. It should be noted that at complete equilibration the mass balances remain correct even if a small amount of test water is transferred to the sample during the experiment.

By applying Gauss' law of error propagation, /Rogge 1997/ and /Rübel 2000/ showed that the error of the equilibration experiment for the determination of the isotope composition of the pore water grows with the difference in isotopic composition between test water and pore water. On the other hand, the error of the equilibration experiment for the determination of the water content decreases with the difference in isotopic composition between test water and pore water. Therefore, to minimise the analytical error a test water with $\delta^{18}O$ and $\delta^{2}H$ values close to those expected for the pore water were used for the determination of the isotopic composition and a test water with $\delta^{18}O$ and $\delta^{2}H$ values far from that expected for the pore water was used for the determination of the water content. In the present experiment this was achieved by using laboratory supply water and a synthetic distilled water enriched in ^{2}H and depleted in ^{18}O. The isotopic composition of the standard solutions are given in the Appendix in Table A4.

5.2 Pore water isotopic composition ($\delta^{18}O$ and $\delta^{2}H$)

This is the first time the isotope diffusive-exchange method has been applied to crystalline rocks with very low water content. Therefore it is no surprise that not all experiments revealed the expected accuracy and reasonability of results. Future experiments will, however, benefit from the experience gained.

The analytical results of 36 test solutions out of a total of 42 equilibrated solutions could be used for interpretation. For two samples the experiments with laboratory test water appear to have suffered from evaporation effects as indicated by a consistent enrichment of the heavy isotope according to a Rayleigh distillation process. The experiments are sensitive to an evaporation effect of more than about 3%, which is quite easily achieved at a total test solution volume of 3 mL. Evaporation could have occurred either during the experiment and/or storage of the 3 mL solutions. The $\delta^{2}H$ values of four solutions with traced test water are also likely to be erroneous. The analysed $\delta^{2}H$ values of these test solutions seem to be excessively enriched in ^{2}H; this can be mainly attributed to memory effects during the mass-spectrometric measurement of these test solutions initially enriched in ^{2}H by around 425‰. All other experimental solutions are not affected by any obvious analytical and experimental artefacts. The water content and pore water $\delta^{18}O$ and $\delta^{2}H$ values calculated from the individual test solutions according to Equation (6) are given in Table 5-1.

In Figure 5-1 the obtained pore-water isotopic compositions are shown in the conventional $\delta^{2}H$–$\delta^{18}O$ diagram and compared to the Global Meteoric Water Line (GMWL) and proposed end-member compositions of various groundwater types /Laaksoharju et al. 1999/. The $\delta^{2}H$ and $\delta^{18}O$ values of the shallow samples plot on or close to the GMWL only slightly below the present-day precipitation end-member. Except for the unreliable $\delta^{2}H$ signature of sample KLX03-6 there is no indication of a pronounced glacial component present in any sample. The reliable $\delta^{18}O$ value of sample KLX03-6 is, however, far too less negative for a glacial water and thus the derived composition is suspect. With increasing sample depth the samples have water isotope compositions that plot to the left of the GMWL close to the reference brine water. Such types of isotope compositions are known, for example, from very old crystalline groundwaters in the Canadian Shield /Frape and Fritz 1987/.

Table 5-1. $\delta^{18}O$ and $\delta^{2}H$ of pore water and water content derived from the isotope diffusive-exchange method.

Laboratory sample no	Average vertical depth (m)	$\delta^{18}O$ [1)] pore water (‰ V-SMOW)	$\delta^{2}H$ [1)] pore water (‰ V-SMOW)	Water Content [1)] (wt.-%)
KLX03-1	159.22	–12.26	–90.1	0.1767
KLX03-2	202.66	–11.44	–92.5	0.2417
KLX03-3	253.72	–11.43	–116.8	0.2799
KLX03-4	303.10	– [2)]	–	–
KLX03-5	355.66	–13.12	–78.2	0.2197
KLX03-6	411.70	–11.58	*–161.2*	0.1445
KLX03-7	462.76	–7.51	–83.9	0.2702
KLX03-8	524.63	–13.64	*–54.9*	*0.4226*
KLX03-9	590.12	--- [2)]	---	---
KLX03-10	643.14	---	---	---
KLX03-11	695.95	–9.38	*–28.3*	*0.1420*
KLX03-12	803.21	–10.94	–58.6	0.3333
KLX03-13	841.15	–	–	–
KLX03-14	894.53	–5.14	*–1.9*	*0.0704*
KLX03-15	942.47	–	–	–
KLX03-16	979.78	–6.56	–28.7	0.1020

[1)] Light shaded areas: Indications for slight evaporation during experiment with laboratory water, true calculated $\delta^{18}O$ and $\delta^{2}H$ values might be more negative.
Dark shaded areas with data in italics: Analysis of traced test water with larger than standard error (possibly memory effect during ^{2}H measurement) and calculated values are less reliable.

[2)] – : experimental solutions not analysed; --- : Not enough material to perform experiment

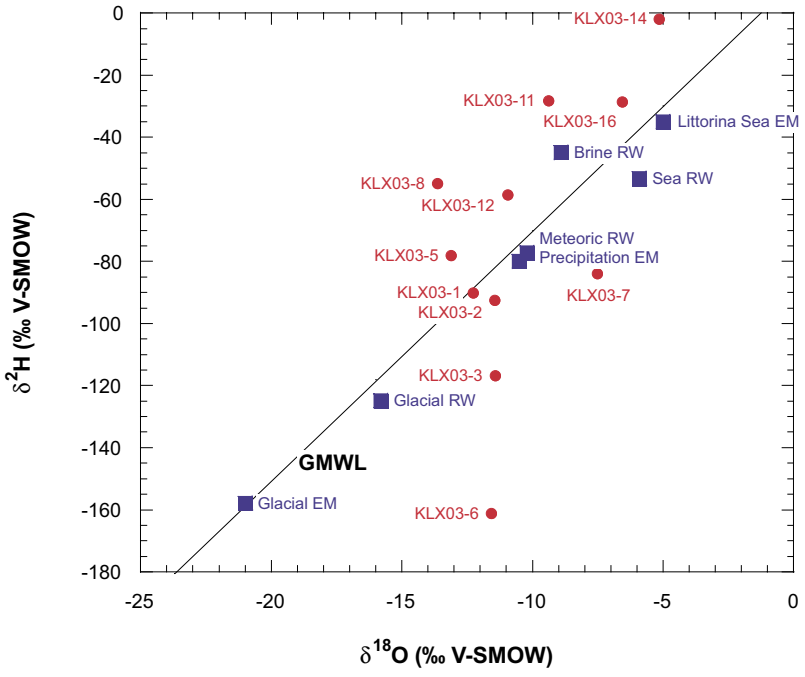

Figure 5-1. *Borehole KLX03: $\delta^{18}O$ and $\delta^{2}H$ values of pore water compared to the GWML and the isotopic compositions of proposed end-member (EM) and reference water (RW) compositions of various Swedish groundwaters /data from Laaksoharju et al. 1999/. Numbers refer to the laboratory samples.*

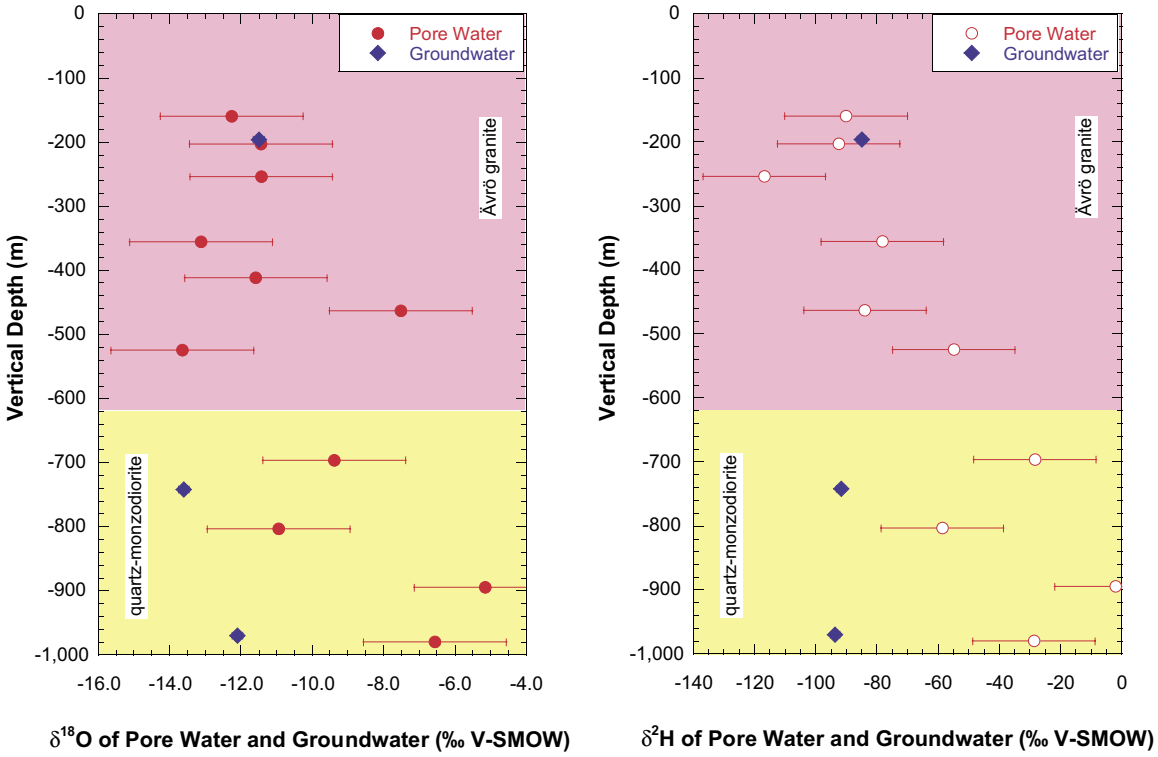

Figure 5-2. *Borehole KLX03: Vertical depth variation of $\delta^{18}O$ and $\delta^{2}H$ values in pore compared to fracture groundwater from the same borehole (error bars indicate the cumulated error).*

The stable isotope composition of the pore water shows no clear stratification with depth although a trend towards less negative δ-values is indicated in the quartz monzodiorite compared to the Ävrö granite (Figure 5-2) at about the same location where an increase in the chloride concentration occurs also (see Chapter 6). However, more samples would be required to support this trend. In the very shallow levels in the Ävrö granite, pore water and groundwater from nearby fractures intercepted by the same borehole have identical stable isotope compositions (Figure 5-2). This indicates steady-state conditions between pore and groundwater. At greater depth in the quartz monzodiorite the pore water isotope composition is strongly enriched in the heavy isotopes compared to the fracture groundwater. Pore water isotope compositions from these depths fall to the left of the meteoric water line (Figure 5-1) and thus suggest to be more of brine-type composition. At these depths steady-state conditions between pore water and fracture groundwater are not achieved and it appears that the pore water contains at least a component that is significantly older than the fracture groundwater.

6 Chemical composition of pore water

Pore water of the low-permeability crystalline rocks of the Laxemar area cannot be sampled by conventional groundwater techniques and have to be characterised by indirect methods. Obviously, such indirect methods are possibly subjected to artefacts induced during the drilling and sampling procedures and also during the experiments themselves. Such artefacts might influence the various experiments in different ways eventually affecting the obtained experimental solution compositions so that they no longer reflect the in situ pore water composition. This chapter describes the results of the performed out-diffusion experiments, their implication for the in situ pore water and the derivation of in situ concentrations of chemically conservative compounds.

6.1 Out-diffusion experiments

The crystalline rocks at Laxemar typically have a low water-accessible porosity and thus a low pore water content. This initially requires the use of relatively large rock samples for out-diffusion experiments in order to obtain: a) a reasonable amount of pore water and thus detectable chemical and isotopic signals, b) an optimised ratio of pore water to experimental solution in order to minimise the analytical uncertainties, and c) to account for the heterogeneity of the rock texture. The second important requirement is the preservation of complete saturation of the rock sample until commencement of the experiment. This demands a concerted logistic effort because the drillcore samples have to be packed vapour-tight immediately following recovery, and shipped to the laboratory and processed as quick as possible to minimise possible evaporation and thus loss of pore water and perturbation by chemical reactions.

Strictly speaking, out-diffusion experiments only deliver direct information about chemically conservative elements of the pore water due to the inevitable interactions between rock and test water during the experiment. For the reactive components geochemical modelling strategies have to be applied to correct for the interaction. The more mineralised a pore water is, however, the more the observed elemental concentrations in the final experiment solution will be dominated by those prevailing in the pore water compared to the contributions of mineral dissolution reactions. Thus, the chemical composition of the experimental solution can also reveal certain indications about general chemical trends in the pore water before applying geochemical modelling.

6.1.1 Experimental set-up

The set-up of the out-diffusion experiments consists of a PE-vessel with a vapour tight cap which is equipped with two swagelock™ valves and PEEK™ sampling lines. The diameter of the vessel is designed to keep the ratio of experiment solution to rock sample as low as possible, while full immersion of the rock is guaranteed throughout the experiment. Furthermore, the rock sample is placed into the vessel on two small-sized PE-rods to ensure contact with the experiment solution at the lower end of the core. The vessel containing the rock sample and test solution is placed into a water bath and held at a constant temperature of 45°C to accelerate out-diffusion. To avoid chemical stratification of the experiment solution and thus uncontrollable retardation of the diffusion process, the vessels are gently rotated in the water bath throughout the experiment. Two of the total 16 experiments were run at ambient temperature (20°C) for comparison.

The diameter of the conditioned rock samples varied between 50.1 mm and 50.4 mm with a length of the cylinders between 181.9 mm and 190.8 mm. The corresponding volume varied between 360.023 cm^3 and 379.456 cm^3 with a saturated mass between 982.509 g and 1053.568 g. The ratio of experimental solution to rock sample was between 0.086 and 0.118.

The experimental solution consisted of distilled water traced with ^{16}O and ^{2}H and prepared at Hydroisotop GmbH. The chemical composition of the blank solution is given in Table A5 and that of the isotopes in Table A4 (samples STD-TEW 1 to 6).

Steady-state conditions of the out-diffusion experiments were controlled by taking small-sized samples (0.5 mL) of the experimental solution at regular intervals (cf Section 6.2). The experiments were terminated and the supernatant solution removed for chemical and isotope analyses when the chloride concentrations had reached a plateau as a function of time, i.e. when steady-state conditions were reached. The experiments run at 45°C were terminated after about 90 days and those run at 20°C after about 190 days.

6.1.2 Composition of experimental solutions

The chemical and isotope compositions of the supernatant solution after termination of the out-diffusion experiments are given in Table A5 (Appendix) and Table 6-1, respectively.

The dominant lithologies encountered in borehole KLX03 are Ävrö granite down to about 620 m depth and quartz monzodiorite down to 1000 m depth. The general mineralogical composition of these lithologies is very similar except for the absolute contents of the individual mineral phases and the mineral grain size. The distilled water used as the experimental solution is expected to act rather aggressively on the minerals exposed at the drillcore surfaces inducing some mineral dissolution. Mineral dissolution obviously affects the concentrations of reactive compounds, pH and total mineralisation, so that these will not be representative for the in situ pore water. Major reactions that affect measured element concentrations in the experimental solutions involve the dissolution of diopside and amphibole (both Mg, Ca, Fe), plagioclase (Ca, Na), K-feldspar (K), biotite (K, Mg, Fe), prehnite (Ca), and possibly fluorite (F), pyrite (SO_4), magnetite (Fe) and calcite (Ca). Because of the similar mineralogy of all the rock samples, however, mineral dissolution during the experiments is expected to be similarly uniform, at least for samples within each of the two major lithologies present (i.e. Ävrö granite and quartz monzodiorite). Thus, observed differences in the chemical type and the degree of mineralisation of the experimental solutions will also indicate in a qualitative way differences in the in situ pore water between the two rock types.

The pH of the experimental solutions varied between 7.26 and 8.15 and the total mineralisation ranged from 243–968 mg/L. The chemistry of the experimental solutions reveal essentially three groups (Figure 6-1): 1) Samples down to about 450 m of depth are Na-HCO_3 in type and have a low total mineralisation of between about 300–500 mg/L. 2) Between 450 m and 600 m of depth, i.e. towards the lower end of the Ävrö granite, the chemical type changes to Ca-Na-SO_4 and the solutions are more strongly mineralised (600–960 mg/L) notably at identical water contents as the surrounding samples. In addition, there are no indications that the mineral sulphide content in the granite varies strongly with depth and it appears that this trend reflects actual differences in the pore water composition. 3) In the quartz monzodiorite (> 600 m depth) samples are generally Na-Ca-HCO_3-Cl in type with chloride increasing with depth. The total mineralisation varies little (250–300 mg/L) from 600–750 m and again below 850 m. However, between 750–850 m depth a higher mineralisation is encountered with Cl becoming also a major anion in the experimental solution (sample KLX03-12, TDS = 552 mg/L). This sample originates from a strongly tectonised interval at around 800 m depth.

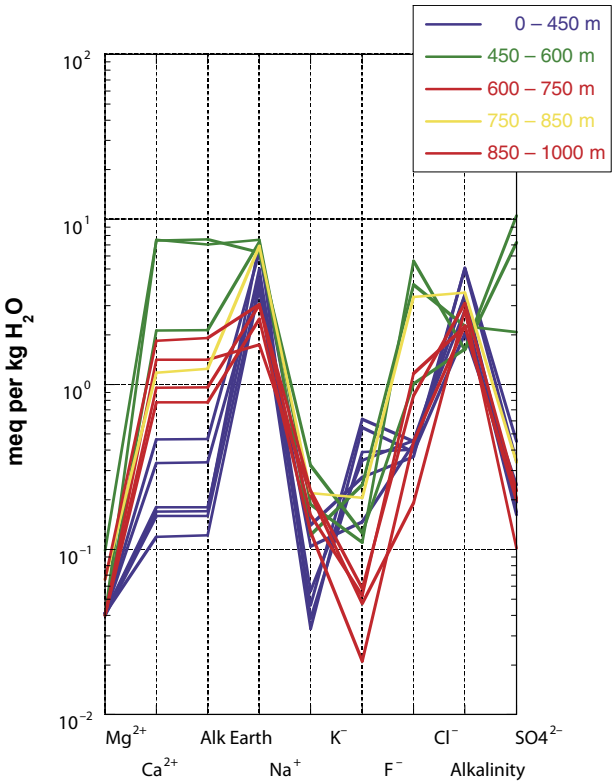

Figure 6-1. *Schoeller diagram of experimental solutions from the KLX03-drillcore samples showing the change in chemical type and degree of mineralisation as a function of depth. Note the distinct changes in solution composition as a function of depth. The boundary Ävrö granite – quartz monzodiorite is at about 620 m depth.*

Chemically conservative elements such as Cl and Br are not affected by mineral dissolution because there are no Cl- and Br-bearing minerals present in the rock. The only halide source in the rocks are mineral fluid inclusions, which indeed contain partly highly saline brines (cf Section 3.3). To release fluid from mineral inclusions to the experimental solution, however, requires a mechanism to open such inclusions. Hypothetically, mechanical stress (e.g. stress release), and/or physical stress (e.g. experiment temperature) during the out-diffusion experiment, could induce cracking of quartz grains which contain by far the largest fluid inclusion volume. However, the comparison with the aqueous leaching tests (cf Chapter 4) and the fluid inclusion investigations (cf Section 3.3) argue against such a contribution of halides from fluid inclusion leakage during the out-diffusion experiments. For example, in sample KLX03-11 the aqueous leach solution from the most coarse-grained fraction showed the least contribution from fluid inclusion leakage. In addition, the leach solution still had a Cl concentration higher by more than a factor of 2 compared to the out-diffusion experimental solution and calculated for the same mass of rock (15.4 mg/l versus 6.8 mg/L at 1036 g of rock). Similarly, since all fluid inclusions have formed at higher temperatures than the experiment temperature, no experimentally-induced physical stress on the inclusions is expected. Therefore, the concentrations of these compounds in the out-diffusion experimental solutions can be converted suitably to in situ pore water concentrations using mass balance calculations as is shown below in Section 6.2

Summarising, the chemistry of the experimental solutions in combination with the geological occurrence of the samples suggest for the pore water: a) a possible stratification of the pore waters as a function of depth, and b) a dependence on rock type lithology and fracture intensity.

6.1.3 Isotope composition of experimental solutions

By using a solution traced in ^{16}O and ^{2}H for the out-diffusion experiments it was initially attempted to obtain information about the water isotope composition of the pore water in an alternative way to the isotope diffusive-exchange method described in Chapter 5. The difference in $\delta^{18}O$ and $\delta^{2}H$ of the experimental solutions before and after out-diffusion of the pore water are well outside the analytical error of the isotope measurements indicating that the traced solution was well designed. However, the calculation of the measured isotope ratios to the in situ pore water ratios requires knowledge of an accurate water content of the rock sample. In addition, the traced experiment solution had initial isotope concentrations that varied greatly from zero. This contrasts with the determination of chloride where the concentration was essentially zero in the initial experimental solution (cf Table A5). Taking these factors together it can be shown that an absolute error in the isotope determination of 1‰, or a relative error in the water content of 1%, results in several tens of per mill difference in the final calculated isotope composition. *Therefore, the results given in Table 6-1 are irrelevant and have been included only for completeness. Such analyses subsequently were abandoned after the first batch of samples were analysed.*

The composition of the stable chlorine isotopes, expressed as $\delta^{37}Cl$, has also been measured on the experimental solutions. As can be seen from Figure 6-2 the $\delta^{37}Cl$-values cover a rather large range from about 0.6 to 2.5‰ SMOC and there is no trend established between the $\delta^{37}Cl$-values and the Cl concentration of the experimental solutions.

It is known that the chlorine isotopes fractionate during the diffusive transport of chloride /Desaulniers et al. 1986, Eggenkamp et al. 1994/. In contrast to other isotope pairs, this fractionation is measurable mainly due to the large difference in the natural abundance of the two isotopes ^{35}Cl and ^{37}Cl. Generic calculations of two-sided diffusion show that the $\delta^{37}Cl$ values in the initial reservoir (in this case the rock pore water) and the bounding reservoir (in this case the experimental solution) will become equal after steady state with total chloride is attained between the two reservoirs /Gimmi and Waber 2004/. The same accounts for the radial sample core geometry used in the present experiments. As will be

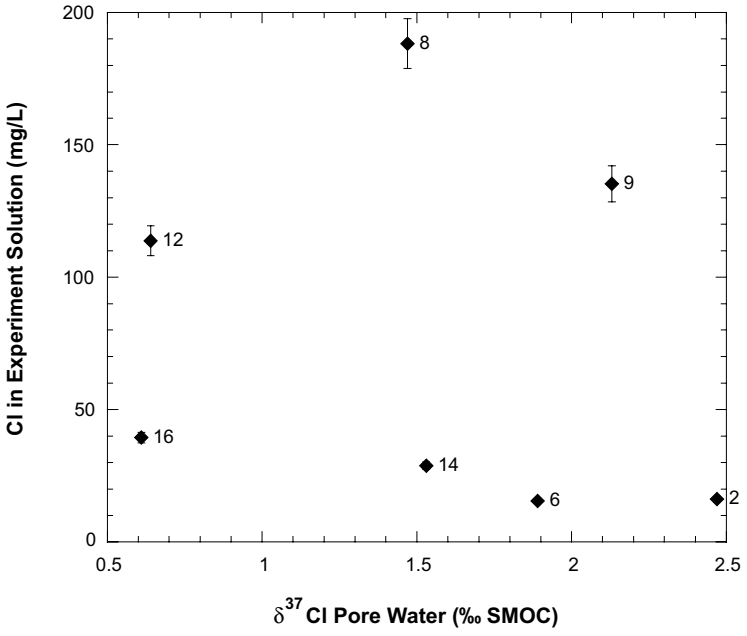

Figure 6-2. *Borehole KLX03: $\delta^{37}Cl$ vs Cl concentration of the out-diffusion experimental solutions of drillcores from borehole KLX03. No trend is established between the $\delta^{37}Cl$-values and the Cl concentrations (numbers refer to sample numbers).*

shown below steady state was attained for chloride in the experimental solutions, and the $\delta^{37}Cl$ values measured in these solutions appear to be representative for the in situ pore water.

In contrast to chloride, strontium is a reactive element and will be involved in mineral dissolution reactions. Depending on the total mineralisation of the in situ pore water the effect of such reactions on the total Sr concentration in the experimental solution will be small. This is due to the occurrence of Sr as a trace element in the minerals and the limited mineral dissolution over the experimental time. In contrast, the effect on the Sr-isotope ratio, $^{87}Sr/^{86}Sr$, is expected to be much greater. This is because Sr released from the Sr-bearing mineral phases (e.g feldspars, biotite, amphibole) contains most probably much more radiogenic Sr and thus a higher $^{87}Sr/^{86}Sr$ ratio compared to that of the pore water.

Total Sr concentrations, Sr_{tot}, are lowest in the Na-HCO_3 type experimental solutions of drillcore samples down to about 450 m depth (0.024–0.088 mg/L; Table 6-1). Experimental solutions of Na-Ca-HCO_3-Cl type from the quartz monzodiorite have higher Sr_{tot} (0.139–0.272 mg/L), while the overall highest Sr_{tot} concentrations are found in Ca-Na-SO_4 type solutions from cores between 450–600 m depth close to the Ävrö granite – quartz monzodiorite boundary. The same three groups are reflected by the corresponding $^{87}Sr/^{86}Sr$-ratios with the Na-HCO_3 type solutions characterised by intermediate ratios (0.7144–0.7155), the Na-Ca-HCO_3-Cl type solutions of samples by the highest ratios (0.7170–0.7211), and the Ca-Na-SO_4 type solutions by the lowest ratios (0.7083–0.7100; Figure 6-3). Although only a weak positive correlation is established between the concentrations of Sr_{tot} and those of Cl (Figure 6-4), it appears also that the Sr-isotope signature of the in situ pore water is different, at least as indicated by the experimental solutions representing samples from the Ävrö granite at shallow and intermediate depth levels along the borehole. To what degree the in situ pore water at the deeper levels also differs in its Sr-isotope composition would have to be confirmed by Sr-isotope analyses on minerals that potentially would undergo dissolution during the out-diffusion experiment.

Table 6-1. Isotopic composition of solutions from out-diffusion experiments at steady-state conditions.

Laboratory sample no	Vertical depth (m)	$\delta^{18}O$ [1] ‰ V-SMOW	$\delta^{2}H$ [1] ‰ V-SMOW	$\delta^{37}Cl$ ‰ V-SMOC	Sr [3] ppm	$^{87}Sr/^{86}Sr$	$^{87}Sr/^{86}Sr$ 1 σ
KLX03-1	159.22			b.d. [2]	0.024	0.715469	0.000029
KLX03-2	202.66	*69*	*–205*	2.47[2]	0.034	0.714463	0.00002
KLX03-3	253.72	*157*	*–858*	b.d. [2]	0.034	0.714416	0.000024
KLX03-4	303.10	*–12*	*60*				
KLX03-5	355.66	*–589*	*87*	b.d. [2]	0.068	0.714817	0.000032
KLX03-6	411.70			1.89	0.088	0.714955	0.000021
KLX03-7	462.76						
KLX03-8	524.63			1.47	1.851	0.708281	0.00002
KLX03-9	590.12			2.13	0.74	0.709984	0.000027
KLX03-10	643.14						
KLX03-11	695.95			b.d. [2]	0.139	0.71908	0.000027
KLX03-12	803.21			0.64	0.272	0.717795	0.000037
KLX03-13	841.15			b.d. [2]			
KLX03-14	894.53			1.53[3]	0.203	0.721149	0.000023
KLX03-15	942.47						
KLX03-16	979.78			0.61	0.166	0.717054	0.000034

[1] Dalculated data in italics are meaningless and not used for further interpretation (see text).

[2] b.d. = below detection or very small signal and not used for further interpretation.

[3] Analyses by mass spectrometry.

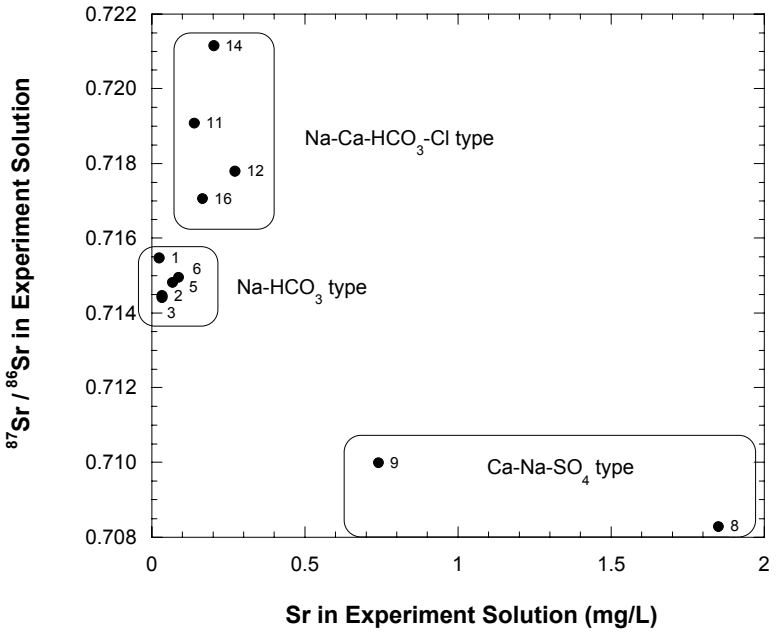

Figure 6-3. *Borehole KLX03: Strontium isotope ratios ($^{87}Sr/^{86}Sr$) plotted against the strontium concentrations of the drillcore out-diffusion experimental solutions. The different chemical types also have different isotope ratios (numbers refer to sample numbers).*

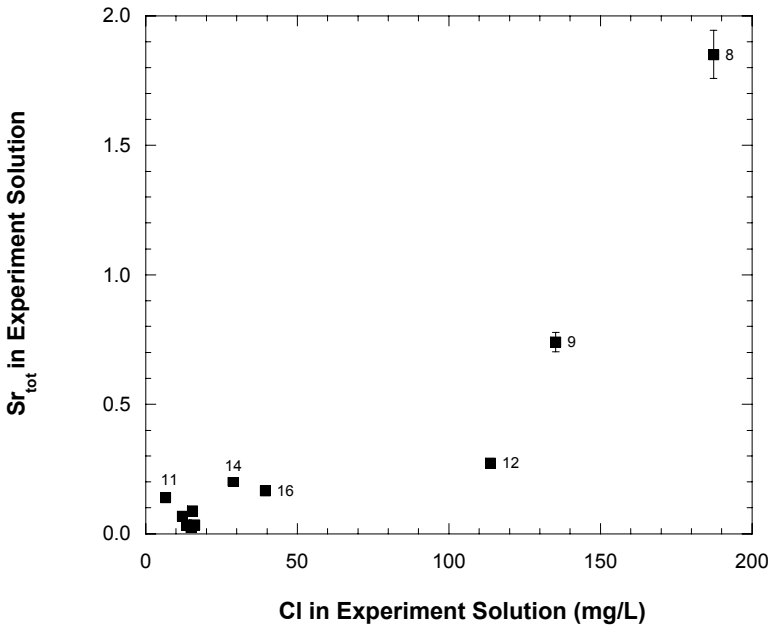

Figure 6-4. *Borehole KLX03: Correlation trend of total strontium concentration, Sr_{tot}, against chloride for the drillcore out-diffusion experimental solutions (numbers refer to sample numbers).*

6.2 Pore water chloride

The non-reactive behaviour of chloride and the non-destructive nature of the out-diffusion experiments, for example which contrast with crush/leach aqueous extraction techniques, make the pore water the only source for dissolved chloride in the experimental solution. Therefore, the chloride concentration of the experimental solution can be converted to pore water concentrations using mass balance calculations given that steady-state conditions in the out-diffusion experiment are achieved.

6.2.1 Control on steady state: chloride time-series

The monitoring of steady-state conditions in the out-diffusion experiments was performed with small-sized samples (0.5 mL) that were taken at regular time intervals and analysed for chloride. Steady-state conditions with respect to chloride diffusion is attained when the concentrations reach a plateau, i.e. when they remain constant. To account for the removal of experimental solutions for the analysis of time-series, the analysed Cl concentrations in the time-series samples have to be corrected for the volumes and concentrations of the experimental solution that have been systematically removed during the experiment. The calculation procedure for this correction is outlined below in Section 6.2.2.

The analysis of such small-sized samples is not straight forward. In addition, sample treatment and storage has to be thoughtfully done because the slightest evaporation of the sample will have a strong effect on the attempted final results. Figure 6-5 shows the results of chloride analyses of the 0.5 mL samples taken some 7 days before the termination of the experiment, compared with the larger 40 mL samples taken at the end of the experiment. The analyses were performed in two different laboratories for a quality check. As can be seen from this figure there is good agreement between the analyses, which gives confidence in the chloride time-series measurements.

In Figure 6-6 an example of chloride time-series is given to illustrate that steady-state conditions with respect to the out-diffusion of chloride were achieved in the experiments. In all experiments conducted at 45°C steady-state conditions with respect to Cl out-diffusion were achieved in about 60–70 days independent of rock type. In the experiment conducted at 20 °C steady-state conditions were achieved after about 120 days.

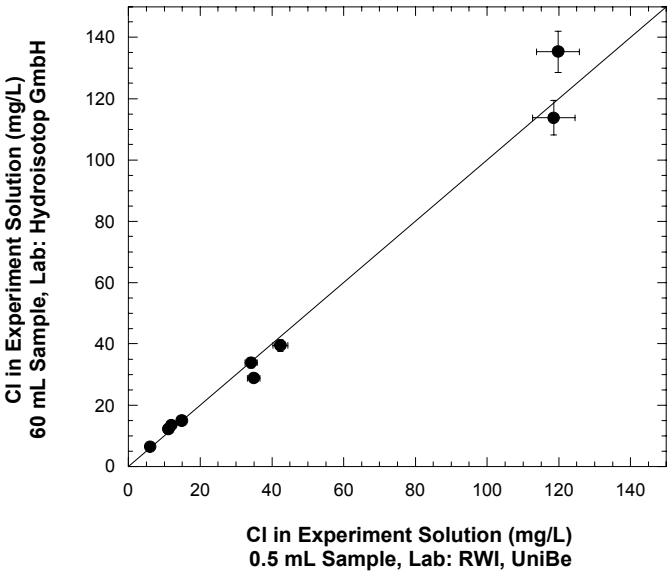

Figure 6-5. *Borehole KLX03: Chloride concentrations of experimental solutions analysed on small-sized 0.5 mL samples and larger 40 mL samples. The analytical error is ± 5%.*

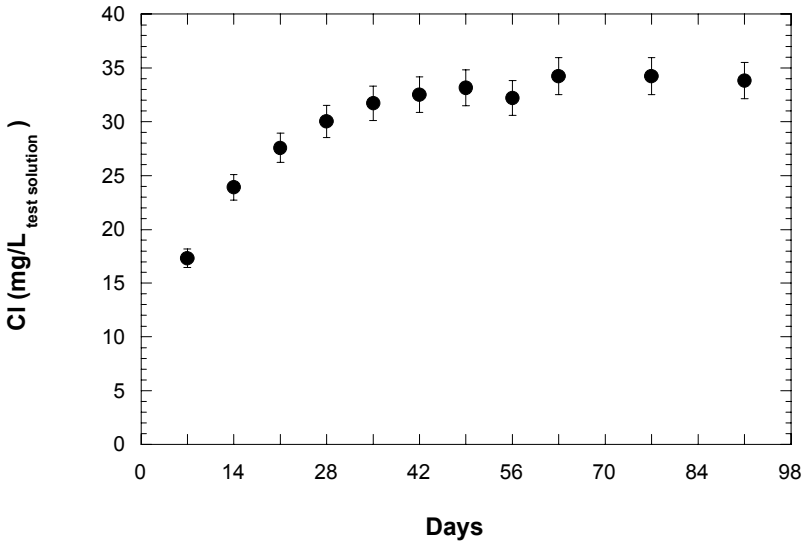

Figure 6-6. *Sample KLX03-7: Chloride concentrations of the experimental solution as a function of diffusion time (chloride time-series). The achieved plateau indicates steady-state conditions for chloride diffusion at 45°C after about 70 days.*

6.2.2 Derivation of pore-water chloride content

Out-diffusion of the pore water from the drillcore into the surrounding experimental solution has occurred from each surface face of the core as schematically shown in Figure 6-7. As for the time-series samples, the analysed Cl concentrations in the final solution have to be corrected for the volumes and concentrations of experimental solution that have been systematically removed during the experiment.

At steady-state conditions the chloride concentration in the connected porosity of the rock sample will be equal to that of the experimental solution. With knowledge of the mass of pore water in the rock sample from gravimetric water-content and/or isotope diffusive-

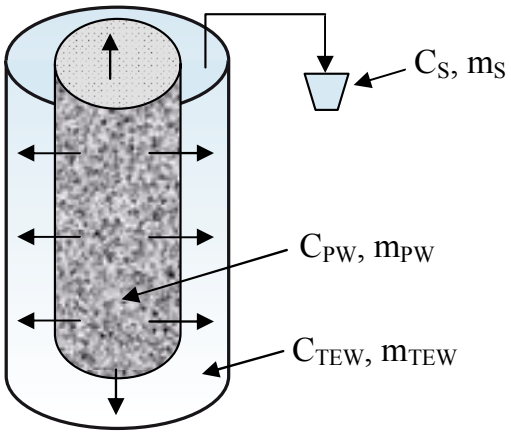

Figure 6-7. *Schematic picture of out-diffusion experiments performed (see Equation 7 for abbreviations).*

exchange experiments (cf Chapters 3 and 5), the chloride concentration of the pore water can be calculated according to:

$$C_{PW} = \frac{\left(m_{PW} + m_{TEWi} - \sum^{n} m_S\right) \cdot C_{equil,corrected} - (m_{TEWi} \cdot C_{TEWi}) + \sum^{n} m_S \cdot C_S}{m_{PW}} \quad (7)$$

with:

$$C_{equil.corrected} = \frac{C_{TEW\infty} \cdot \left(M_{TEWi} - \sum^{n} m_S\right)}{m_{TEWi}} \quad (8)$$

where C = concentration, m = mass, n = number of samples and the subscripts PW = pore water, TEW = experimental solution, S = small-sized sample taken for chloride time-series, i = at beginning of experiment, and ∞ = at end of experiment.

The last term in Equation (7), $\Sigma m_S \times C_S$, describes the amount of chloride removed from the initial experimental solution by the chloride time-series samples. The final measured concentration of chloride in the experimental solution, $C_{TEW\infty}$, is corrected for the the mass of solution removed by the chloride time-series samples from the initial mass of experimental solution, m_{TEWi}, to get the Cl concentration in the experimental solution at steady state, $C_{equil.corrected}$ (Equation 8). The correction for chloride in the initial experimental solution is necessary because this solution was not entirely free of chloride as shown in Table A5.

From Equation (7) it can be seen that the calculated pore water chloride concentration is inversely proportional to the mass of pore water. The mass of pore water is derived from the water content, which can be subjected to various perturbations that can deviate it from in situ conditions. The effect of possible perturbation on the calculated pore-water chloride content is discussed in Section 6.2.3.

The calculated pore water chloride compositions are given in Table 6-2 and shown in Figure 6-8 as a function of sample depth. The unit for the pore water concentration is given as mg/kg H_2O (and not mg/L) because it is derived on a mass basis rather than a volumetric basis. This is because the density of the pore water is not known beforehand. In reality the difference between mg/kg H_2O and mg/L is negligible at the expected ionic strength and total mineralisation, respectively, of the pore water.

The chloride concentration in the pore water of the Ävrö granite is below 1 g/kgH_2O down to about 450 m of depth and increases then to about 9 g/kgH_2O towards the base of the granite. Pore water chloride concentrations in the quartz monzodiorite show that the pore waters are variable at the top (~ 620 m) and become rather constant between 4 to 5 g/kgH_2O at greatest depth. The concentration pattern of pore water chloride shown with depth corresponds well to the hydraulic transmissivity measured in the borehole (Figure 6-8). Low concentrations occur in the depth intervals with elevated transmissivity whereas high concentrations are observed in the intervals with very low transmissivity, independent of rock type. Within this context it should be noted that between 450 m and 600 m a change towards a highly mineralised Ca-Na-SO_4 type pore-water composition is suggested by the experiment solutions (cf Figure 6-1). Because sulphate and not chloride seems to be the dominant anion in these pore waters the correspondence between highly mineralised pore water from this interval (samples KLX03-7, KLX03-8, KLX03-9) and transmissivity values below detection will become even better (Figure 6-8).

Table 6-2. Chloride concentration of pore water calculated from out-diffusion solutions and the water content of the samples.

Laboratory sample no	Average vertical depth (m)	Pore water Cl mg/kg H_2O	Pore water Cl + error [1] mg/kg H_2O	Pore water Cl - error [1] mg/kg H_2O
KLX03-1	159.22	806	55	48
KLX03-2	202.66	765	16	15
KLX03-3	253.72	503	41	35
KLX03-4	303.10	374	44	35
KLX03-5	355.66	613	49	42
KLX03-6	411.70	730	22	21
KLX03-7	462.76	1,377	305	210
KLX03-8	524.63	5,674	1,334	897
KLX03-9	590.12	8,578	938	767
KLX03-10	643.14	2,260	249	204
KLX03-11	695.95	513	28	25
KLX03-12	803.21	4,691	177	164
KLX03-13	841.15	–	–	–
KLX03-14	894.53	3,828	510	402
KLX03-15	942.47	–	–	–
KLX03-16	979.78	4,739	1,498	915

[1] Error based on the standard deviation of multiple water-content measurements except for samples KLX03-9 and KLX03-10 where an error of ± 10% for the single water-content measurement was assumed.

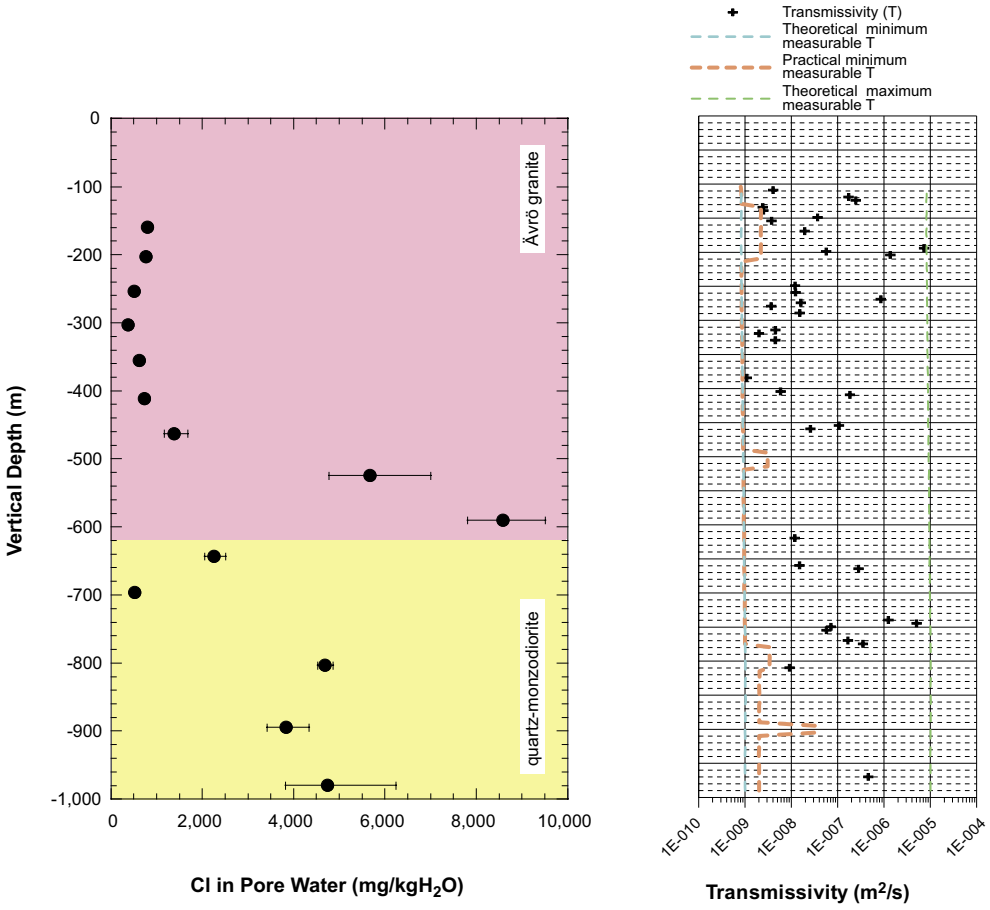

Figure 6-8. *Borehole KLX03: Chloride concentration in pore water as a function of sampling depth (left) compared to the measured borehole hydraulic transmissivity (right).*

6.2.3 Sensitivity of pore water chloride content

As shown above the calculated pore water chloride concentration is inversely proportional to the mass of pore water, i.e. the water content of the rock sample. Measurements of the water content can be subjected to various perturbations that can cause deviations from in situ conditions. These include desaturation of the rock samples, incomplete drying of the samples over a too short period of time before stable-weight conditions are achieved (note that this depends on sample size as well as rock type), and stress release of the rock sample during drilling and subsequent recovery from depth.

Desaturation of the samples would result in a too low water content and consequently in a too high calculated pore water concentration. The effect of desaturation would be greatly different for the water content determined by drying and that determined by the isotope diffusive-exchange method. This is because desaturation of the original pore water would result in a Rayleigh distillation of the pore water isotopes. After isotopic equilibration this would result in a deviation of the in situ water content that is greatly incompatible with that obtained for the water content determined by drying and to unrealistic isotope composition of the pore water. As shown in Figure 3-13 this is not the case. In addition, the large scale samples used for the out-diffusion experiment showed no difference in mass before and after the experiment (i.e. after approximately 3 months of immersion in the test water, cf Figure 3-11), which indicates full saturation of the samples upon arrival in the laboratory. Therefore, desaturation can be excluded as a perturbation based on the independent methods applied to determine the water content.

Incomplete drying of the rock samples would also result in a too low water content and consequently in a too high calculated pore water concentration. Incomplete drying can be excluded because all samples have been dried until stable weight conditions (± 0.002 g) were achieved. Depending on sample size and texture this process could last up to three months (cf Figure 3-12).

The last possible modification of the in situ water content is that induced by stress release. Every rock sample recovered from depth is potentially subjected to some stress release mechanisms. Such release will result in an increase of the void volume of a rock sample and thus perturb bulk density measurements and, if drilled with a drilling fluid, also the water content because some drilling fluid might enter this newly created void volume. Also, in rocks with such low water contents the measurements might simply not be accurate enough to resolve the effects of stress release. While a fully quantitative argumentation is difficult with the data at hand, several semi-quantitative arguments can be considered.

It is not well known if stress release in crystalline rocks occurs instantaneously (i.e. during drilling in the borehole) or more slowly over days, weeks, and/or even months. Stress could have occurred (or still can occur) continuously and slowly from the time of drillcore recovery to the end of the experiments in the laboratory and/or it could have occurred instantaneously during drilling in the borehole. In the first case this would result in a desaturation of the rock samples which, as mentioned above, is not observed. In the second case, the newly created pore space would, if connected with the core surface, become filled with the surrounding fluid used for drilling the borehole. This effect would not be detected by gravimetric water content measurements. However, if significant, it should have been detected in the water content determined by the isotope diffusive-exchange method, which seems not to be the case. Similarly, one would expect to see systematic perturbations in the chemical and isotopic composition of the out-diffusion experiments performed on the same rock type as a function of the sampling depth. This is because deep seated samples would suffer the strongest stress release, would therefore be in contact with the drilling fluid for the longest duration of time, and may also be more influenced by ruptured fluid inclusion effects. The chemical stratification obtained for the experimental solution as a function of

depth and transmissivity, and their strongly varying chloride and O-, H, Cl-, and Sr-isotopic compositions (cf Section 6.1) argue against a significant influence on the in situ pore water by mixing with drilling fluid in the borehole and the influence of ruptured fluid inclusions, both potentially induced by stress release.

Another argument against significant stress release is given by the behaviour of the samples and experimental solutions during the out-diffusion experiments. Initial model calculations show that the out-diffusion of chloride from the pore water of the rock into the experimental solution can be described by diffusion as the dominant transport mechanism (cf Section 6.2.4). Because the contact time between the drillcore and the drilling fluid was on average in the order of 1–2 hours, this suggests that the effect of possible dilution of the pore water by the less mineralised drilling fluid is very limited. Furthermore, any input from ruptured fluid inclusions would also be very limited, for example potential flushing out by the drilling water during drilling. Finally, to conclude, to detect either of these effects probably lies outside the resolution of the presently applied methods.

From this combination of semi-quantitative arguments it appears that measurable effects of stress release are minimal. Nevertheless, possible effects of stress release shall be further explored. The most important consequence is that instantaneous stress release in the borehole would result in an increase of the connected porosity followed by a dilution of the in situ pore water if the drilling water itself is dilute. Following the mass balance relationship, both effects would result in an underestimation of the in situ pore water chloride concentration when determined with out-diffusion experiments and water content measurements. Possible dilution of the in situ pore water cannot be easily assessed in a quantitative way because of the unknown in situ chloride concentration. In contrast, estimates can be calculated for lower in situ water contents. From the inverse proportionality of the water content to the pore water chloride concentration it follows that an increase in the in situ water content due to stress release by 30% and 50% would result in an increase of the calculated pore water chloride concentration by a factor of about 1.3 and 2, respectively, as shown in Figure 6-9.

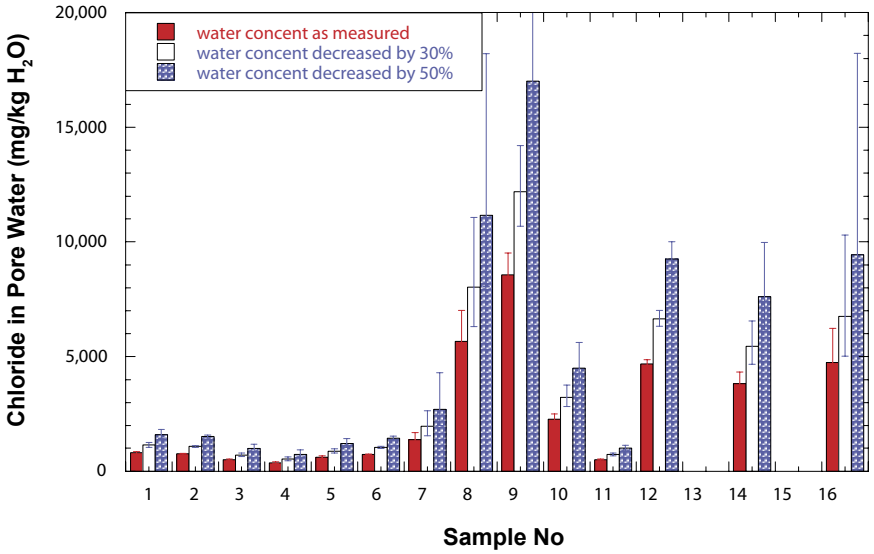

Figure 6-9. *Borehole KLX03: Sensitivity of calculated pore-water chloride concentrations with increasing sample number (i.e. depth). Two hypothetical scenarios are shown with water contents decreased by 30% and 50% to that measured due to possible stress release effects. Error bars indicate the cumulated error.*

6.3 Preliminary modelling of chloride breakthrough

The preliminary modelling of the chloride breakthrough curve obtained for sample KLX03-7 (Ävrö granite) is shown in Figure 6-10. The calculation was performed using an analytical solution of radial diffusion out of cylinder into a well-mixed solution reservoir /Crank 1975/. In this initial modelling the removal of small-sized samples of experimental solution was neglected in the transient phase, but incorporated in the mass balance for the steady state condition. In future calculations incorporation of this removal will lead to an improvement of the fit to the measured data.

For the granitic sample KLX03-7 the best fit of the measured data is obtained for a pore diffusion coefficient, D_P, for chloride of about 8.1×10^{-11} m^2/s at a water-content porosity of 0.77 ± 0.14 Vol.% and at a temperature of 45°C. This converts to an effective diffusion coefficient, D_e, at 20°C of about 3.1×10^{-13} m^2/s. This value is in good agreement with effective diffusion coefficients for dioritic rocks from the Laxemar area obtained from through-diffusion and through-electromigration experiments ($D_e = 3.9\times10^{-13}$ m^2/s; /Löfgren 2004/). It should be noted that these experiments have been performed on samples of 15 mm to 50 mm in thickness compared to the cylinders of about 50×190 mm used for the present out-diffusion experiments. Also, the samples used for through-diffusion and through-electromigration have been stored at the surface for variably long time periods (weeks to months) before the commencement of the experiments.

/Löfgren 2004/ further states that the formation factor derived by electromigration experiments in situ and in the laboratory compare well in the Simpevarp borehole KSH01A down to a depth of about 700 m below surface. This can be interpreted that down to this depth effects of stress release are small compared to the analytical errors. Sample KLX03-7 comes from a more shallow depth of about 463 m below surface. In addition to the arguments given in the previous section, this can be taken as a further (semi-quantitative) argument that stress release did not significantly alter the obtained water content and thus the chloride concentration of the pore water of this sample.

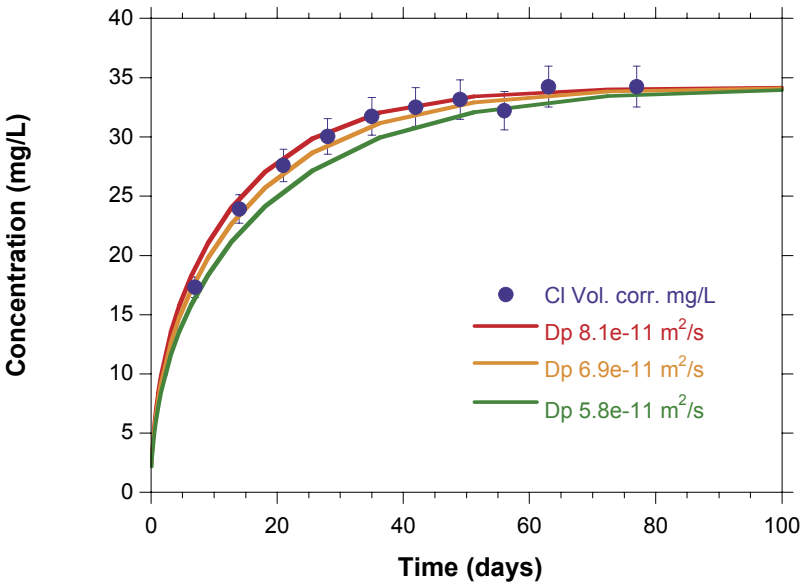

Figure 6-10. *Sample KLX03-7: Modelling of chloride out-diffusion at 45°C. The best fit is achieved for a diffusion coefficient D_P of 8.1×10^{-11} m^2/s. The average porosity of the sample is 0.77 ± 0.14 Vol.%.*

The agreement between diffusion coefficients derived by different techniques and on samples stored over different durations of time argues against significant stress release after the retrieval of the drillcore from the borehole. Similarly, the different mass of the rock samples used in the different experiments suggests also that instantaneous stress release in the borehole had no effect that can be resolved by the applied techniques because one would expect more erratic results from the different methods applied.

7 Comparison of pore water and groundwater composition

7.1 Chloride content

Chloride concentrations in pore water and fracture groundwater in the Ävrö granite are similar down to about 500 m depth suggesting steady state conditions between pore water and groundwater (Figure 7-1, left). This situation would slightly change in the shallow levels when taking an arbitrarily decreased water content due to stress release into account, in that in the most shallow levels the pore water would have higher chloride concentrations than the groundwater sampled at the same depth (Figure 7-1, right). Unfortunately, no groundwater could be sampled from the interval at the bottom of the Ävrö granite where the pore water chloride concentrations are highest in the entire profile.

At the top of the quartz monzodiorite the pore water is more dilute than groundwaters in the fractures. Assuming minimal stress release effects, this suggests that the pore water retains an older, more dilute signature. Interestingly, this dilute pore water is not associated with an isotopic component of glacial melt water (i.e. absence of lighter $\delta^{18}O$ values), which might initially be expected bearing in mind the palaeoevolution of the area. At least for $\delta^{18}O$, a meteoric signature similar to that prevailing at present seems to be indicated (see below).

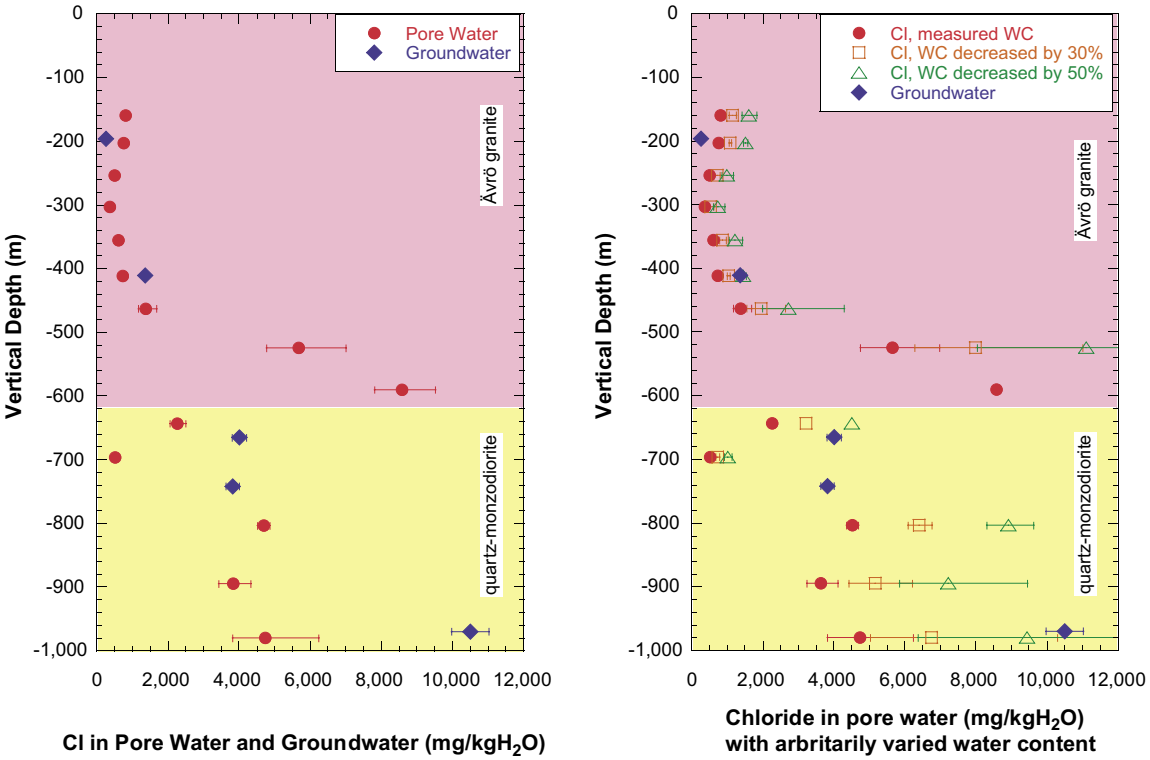

Figure 7-1. *Chloride concentrations of rock pore water from borehole KLX03 compared with groundwaters sampled from adjacent fractures as a function of sampling depth (left) and the same comparison with pore water chloride concentration calculated with arbitrarily decreased water contents to evaluate stress release effects (right; WC = water content).*

Below about 800 m of depth the chloride concentration of the pore water becomes similar to that of the fracture groundwater above and so does the general chemical type. The pore water differs, however, significantly in chloride content and chemical type from the deepest formation groundwater sampled from fractures. Chloride concentrations similar to that deep fracture groundwater would be roughly reached if the already very low measured water content of the samples would be arbitrarily decreased by 50% due to stress release (Figure 7-1, right).

The comparison of chloride concentrations derived for the pore water with those of the fracture groundwater is consistent with the results of the $\delta^{18}O$ and $\delta^{2}H$ values obtained (cf Section 5.2). For all three parameters steady-state conditions seem to have been established in the shallower bedrock levels within the Ävrö granite, while deeper down in the quartz monzodiorite the pore water and fracture groundwater are of different composition. Because of the higher diffusivity of water compared to that of solutes, steady-state conditions would be achieved earlier for the water isotopes than for chloride. Therefore, the isotope data support the differences observed for the chloride concentrations between pore water and fracture groundwater when calculated using the measured water contents. The spatial distribution of the stable water isotopes is thus an additional argument against significantly higher chloride concentrations in the pore water due to stress release.

7.2 Chlorine and strontium isotope composition

Compared to total chloride the chlorine isotopes differ in their behaviour with depth between pore water and groundwater sampled from fractures (Figure 7-2). In the Ävrö granite the $\delta^{37}Cl$ values of the pore water are strongly enriched in ^{37}Cl and far from being equal to those of the fracture groundwater. This is in contrast to the steady-state conditions between pore and groundwater as indicated by total chloride. Exactly the contrary is observed in the levels of the quartz monzodiorite. Here the chlorine isotopes suggest steady-state conditions while total chloride is different in pore water and fracture groundwater (Figure 7-2).

At present, these relationships are difficult to explain. In advection dominated systems chlorine isotopes do not fractionate and a correlation with total chloride will be immediately established. Chloride isotope fractionation, however, takes place during diffusion of chloride /Desaulniers et al. 1986, Eggenkamp et al. 1994/. Therefore in a diffusion-dominated system a correlation between chlorine isotopes and total chloride as a function of distance will only be established if the chemical and isotopic gradients between the two reservoirs (i.e. pore water and fracture groundwater) along this distance remained constant long enough until steady-state conditions are achieved. Thus the observed differences suggest that the present system represents a transitional state for chloride dissolved in the pore water and in the fracture groundwater. However, to what degree the observed patterns can be really related to such processes needs to be further investigated.

Total strontium concentrations in the experimental solutions are generally low and they are only weakly correlated with chloride (cf Figure 6-4) indicating that strontium in the experimental solutions is mainly controlled by mineral dissolution reactions. This is reflected in the strontium isotope ratio, $^{87}Sr/^{86}Sr$, which is characteristic for the experimental solutions of Ävrö granite and quartz monzodiorite (Figure7-3).

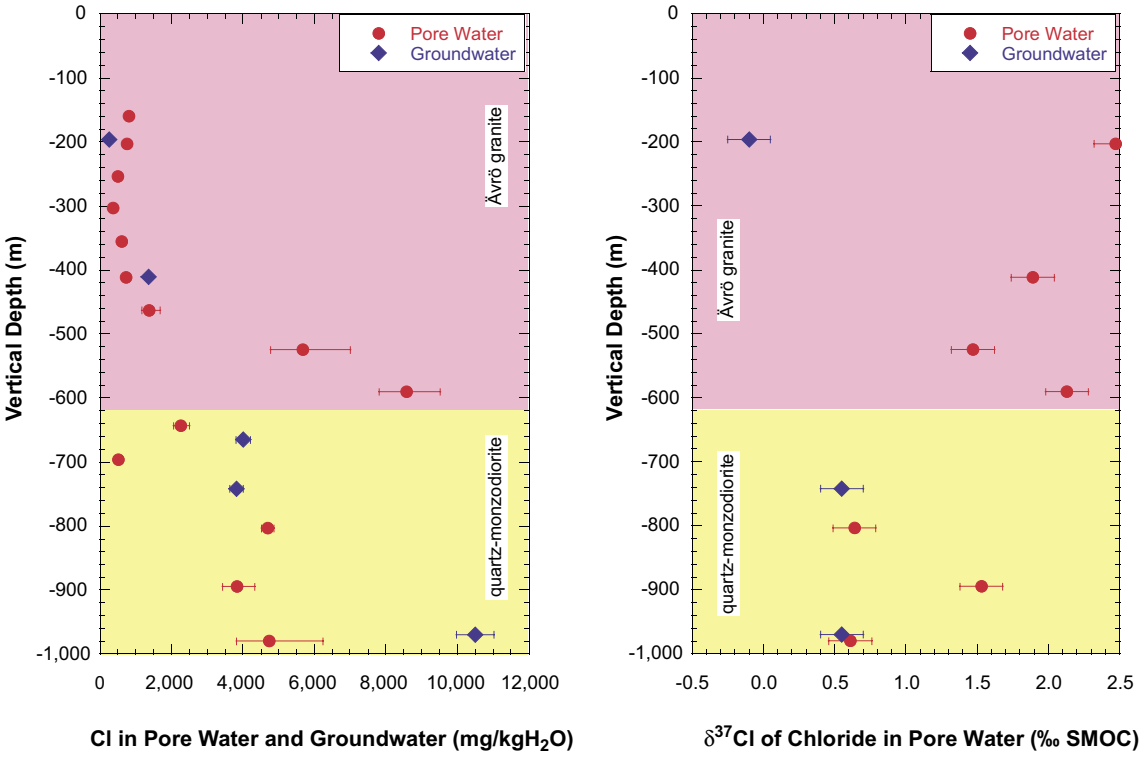

Figure 7-2. *Borehole KLX03: Chloride (left) and chlorine isotope ratio (right) of pore water compared with those of groundwater sampled from fractures as a function of sampling depth.*

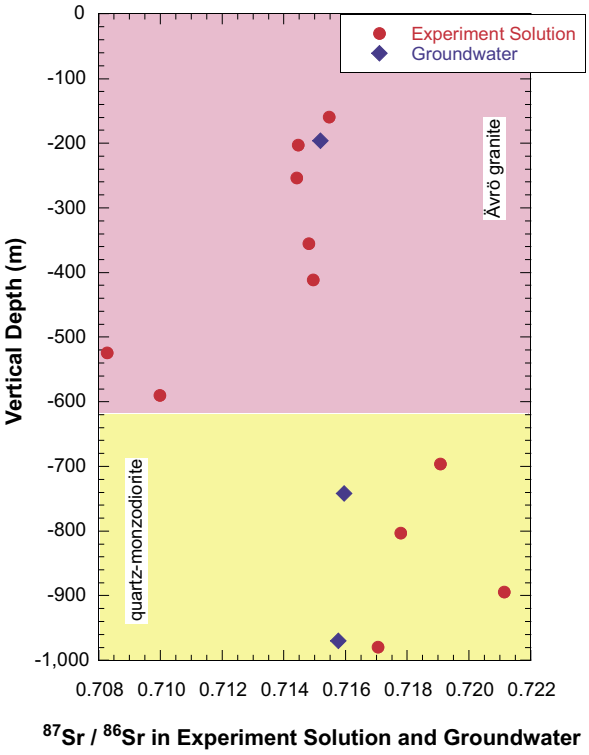

Figure 7-3. *Borehole KLX03: Strontium isotope ratio of pore water compared with those of fracture groundwater as a function of sampling depth.*

In the Ävrö granite uniform $^{87}Sr/^{86}Sr$ ratios are obtained for the experimental solution of samples down to about 450 m of depth. These solutions have also identical $^{87}Sr/^{86}Sr$ ratios to that of the groundwater. This can be interpreted that weathering is the dominant process in the fracture groundwater and the experimental solution and it is consistent with the steady state between the fracture groundwater and the pore water as indicated by the chloride contents and the stable isotopes. Of interest are the two pore water samples from the deepest levels in the Ävrö granite. These samples have by far the highest total strontium concentrations associated with the lowest $^{87}Sr/^{86}Sr$ ratios in the experimental solution (cf Figure 6-3). This suggests a substantial contribution from the pore water to the experimental solution which is different from that in the more shallow levels of the Ävrö granite. This supports the differences in total chloride and the general chemical type (cf Figure 6-1) observed for these pore waters.

In the quartz monzodiorite the $^{87}Sr/^{86}Sr$ ratios of the experimental solution are more radiogenic than those of the groundwater. Since the time for weathering reactions in the experiments is much shorter than the residence time of the groundwater in fractures at these depth levels, it appears that the more radiogenic $^{87}Sr/^{86}Sr$ ratio must be due to the contribution of the pore water. At these depths a difference between pore water and groundwater and a longer residence time of the pore water compared to the groundwater are consistent with the other parameters investigated.

8 Summary and conclusions

Pore water that resides in the pore space between minerals and along grain boundaries in crystalline rocks of low permeability has been extracted successfully by laboratory out-diffusion methods using drillcore samples from borehole KLX03 located in the Laxemar subarea. The obtained extracted experimental solutions could be characterised chemically and isotopically and related to the in situ pore water composition of the rock, which in turn was related to the present and past groundwater evolution of the site. In addition, the method of extraction, together with interfaced measurements of interconnected porosity, provides the opportunity to derive diffusion coefficient values of potential use in predicting future rates of solute transport. Because of the very small volumes of pore water extracted, and the possibility of rock stress release occurring during drilling which might: a) lead to contamination by drilling fluid, b) affect the derivation of rock porosity values, and c) result in input of fluids from ruptured fluid inclusions, great care was taken to avoid such problems or, at least further understand the repercussions.

Interpretation of the extracted pore waters are supported by investigations of the rock mineralogy, mineral chemistry, whole rock chemistry, mineral fluid inclusions, and crush-leach experiments.

The characterisation of rock properties and the pore water in rocks from the Laxemar borehole KLX03 resulted in the following main conclusions:

- The rocks encountered in borehole KLX03 are of similar mineralogical and chemical composition as rocks from the rest of the Laxemar subarea and the Simpevarp area as a whole.
- In the quartz monzodiorite rock type plagioclase shows a chemical zonation from centre to rim, while K-feldspar, hornblende, diopside and biotite are fairly homogeneous
- Fluid inclusions occur mainly in quartz were they constitute 2–3 Vol% of the total quartz volume; the inclusions show a bimodal distribution of salinity with 60% of the total inclusions having a salinity between about 2–8 eq-wt.% NaCl and about 40% having a salinity between about 16–18 eq-wt.% NaCl; in the highly saline inclusions $CaCl_2$ appears to be present in considerable amounts
- Aqueous leaching experiments of different grain-size fractions of the quartz monzodiorite reveal that the concentrations of Cl, but also that of Na, K and possibly SO_4, contain significant contributions from crushed fluid inclusions.
- Independent derivation of water content (to calculate water content porosity) by drying and isotope diffusive exchange methods gave consistent results excluding artefacts such as desaturation of the samples
- There is multiple evidence that no significant stress release and its potential effect on water content porosity values and related drilling water contamination has affected the rock samples; although quantitative proof cannot be given with the present data at hand, several qualitative arguments against such events happening have been discussed
- The uncertainties surrounding the possibility of stress release effects were addressed by calculating the hypothetical variation in water content using a change of 50% by stress release; this would essentially increase the pore water chloride by a factor of 2; it is shown that such an increase would be inconsistent with determined parameters independent from water content measurements

- Diffusion between rock pore water and adjacent water-conducting fractures and fracture zones, and *vice versa*, is identified as the dominant transport process; calculated diffusion coefficients agree well with present-day knowledge from the Laxemar subarea
- Chemical and isotopic pore water signatures are characteristic and show a variation of composition with rock type and depth; in the Ävrö granite a shallow (< 450 m) and intermediate (450–600 m) zone can be distinguished; the pore water in the quartz monzodiorite is divided into three zones (600–750 m, 750–850 m, and 850–1,000 m) ; this is in close agreement with the general trends in hydrochemistry of the adjacent formation groundwaters.
- Steady state between pore water and groundwaters in the fracture is essentially only developed in the shallow zone of the Ävrö granite, while at depths > 450 m the chemical and isotopic composition of the pore water differs markedly from those of the groundwater in fractures.

9 Acknowledgements

Much appreciation is given to Thomas Kisiel (SKB) for the on-site selection and packaging and rapid dispatching of the drillcore samples to the University of Bern. The support and patience of Liselotte Ekström (SKB) throughout the study was much appreciated. We are grateful for the analytical support by Dr. Y. Krüger and Prof. L.W. Diamond (fluid inclusions), PD Dr.E. Gnos (mineral chemical analysis), Prof. J. Kramers (Sr-isotope analysis) and R. Maeder (aqueous extraction chemistry), all at the Institute of Geological Sciences, University of Bern.

10 References

Crank J, 1975. The mathematics of diffusion. Oxford University Press, 2nd edition.

Desaulniers D E, Kaufmann R S, Cherry J A, Bentley H W, 1986. ^{37}Cl-^{35}Cl variations in a diffusion-controlled groundwater system. Geochim. Cosmochim. Acta 50, 1757–1764.

Edmunds W M, Andres J N, Burgess W G, Kay R L F, Lee D J, 1984. The evolution of saline and thermal groundwaters in the Carnmenellis granite. Min. Mag., 48, 407–428.

Edmunds W M, Kay R L F, McCartney R A, 1985. Origin of saline groundwaters in the Carnmenellis granite (Cornwall, Engalnd): Natural processes and reaction during hot dry rock reservoir circulation. Chem. Geol. 49, 287–301.

Eggenkamp H G M, Middelbourg J J, Kreulen R, 1994. Preferential diffusion of ^{35}Cl relative to ^{37}Cl in sediments of Kau Bay, Halmahera, Indonesia. Chem. Geol. 116, 317–325.

Eliasson T, 1993. Mineralogy, geochemistry and petrophysics of red coloured granite adjacent to fractures. SKB TR-93-06. Svensk Kärnbränslehantering AB.

Frape S K, Fritz P, 1987. Geochemical Trends for Groundwaters from the Canadian Shield. *In: P. Fritz and S.K. Frape (Eds.),* Saline water and gases in crystalline rocks. Geological Association of Canada Special Papers, 19–38.

Gimmi T, Waber H N, 2004. Modelling of Tracer Profiles in Pore Water of Argillaceous Rocks in the Benken Borehole: Stable Water Isotopes, Chloride, and Chlorine Isotopes. Nagra Tech. Rep. (NTB 04-05), Wettingen, Switzerland.

Horita J, Wesolowski D J, Cole D R, 1993. The activity-composition relationship of oxygen and hydrogen isotopes in aqueous salt solutions: I. Vapor-liquid water equilibration of single salt solutions from 50 to 100°C. Geochim. Cosmochim. Acta 57**,** 2797–2817.

Laaksoharju M, Tullborg E-L, Wikberg P, Wallin B, Smellie J A T, 1999. Hydrogeochemical conditions and evolution of the Äspö HRL, Sweden. Appl. Geochem., 14, 819–834.

Löfgren M, **2004.** Diffusive properties of granitic rocks as measured by in situ electrical methods. PhD Thesis, KTH Royal Insititute of Technology, Department of Chemical Engineering and Technology, Stockholm, Sweden.

Pearson F J, 1999. What is the porosity of a mudrock? *In: Aplin, A.C., Fleet, A.J., and Macquaker, J.H.S., (Eds.)*, Muds and Mudstones: Physical and Fluid Flow Properties. London, Geol. Soc. Spec. Publ. 158, 9–21.

Pearson F J, Arcos D, Bath A, Boisson J-Y, Fernández A M, Gäbler H-E, Gaucher E, Gautschi A, Griffault L, Hernán P, Waber H N, 2003. Mont Terri Project – Geochemistry of Water in the Opalinus Clay Formation at the Mont Terri Laboratory. Reports of the Federal Office of Water and Geology (FOWG), Geology Series No. 5, Bern, Switzerland.

Rogge T, 1997. Eine molekular-diffusive Methode zur Bestimmung des Porenwassergehaltes und der Zusammensetzung von stabilen Isotopen im Porenwasser von Gestein. Unpubl. Diploma Thesis, Institut für Umweltphysik, Unversity of Heidelberg.

Rübel A P, 2000. Stofftransport in undruchlässigen Gesteinsschichten – Isotopenuntersuchungen im Grund- und Porenwasser. PhD Thesis, Institut für Umweltphysik, Unversity of Heidelberg, Der Andere Verlag, Osnabrück, Germany.

Rübel A P, Sonntag Ch, Lippmann J, Pearson F J, Gautschi A, 2002. Solute transport in formations of very low permeability: Profiles of stable isotope and dissolved noble gas contents of pore water in the Opalinus Clay, Mont Terri, Switzerland. Geochim. Cosmochim. Acta, 1311–1321.

Sacchi E, Michelot J-L, 2000. Pore water Extraction from Argillaceous Rocks for Geochemical Characterisation. Methods and Interpretation. Paris, OECD Nuclear Energy Agency.

Sacchi E, Michelot J-L, Pitsch H, Lalieux P, Aranyossy F-J, 2001. Extraction of water and solutes from argillaceous rocks for geochemical characterisation: Methods, processes, and current understanding. Hydrogeol. J., 9, 17–33.

Smellie J A T, Waber H N, Frape S K, 2003. Matrix fluid chemistry experiment, Final Report. SKB TR-03-18, Svensk Kärnbränslehantering AB.

Waber H N, Nordstrom D K, 1992. Geochemical modeling of granitic groundwaters at the Stripa site (Sweden) using a mass balance approach. 7th Int. Symp. on Water-Rock Interaction WRI-7, Kharaka Y.K. and Maest A.S. (eds), Balkema, Rotterdam, 243–246.

Waber H N, Smellie J A T, 2004. Oskarshamn site investigations Borehole KSH02: Characterisation of matrix pore water (Feasibility Study). SKB P-04-249, Svensk Kärnbränslehantering AB.

Waber H N, Smellie J, 2005. Forsmark site investigation. Borehole KFM06: Characterisation of pore water. Part I: Diffusion experiments. SKB P-05-196, Svensk Kärnbränslehantering AB.

Waber H N, Smellie J, 2006. Oskarshamn site investigation. Borehole KLX03: Characterisation of pore water. Part I: Diffusion experiments. SKB P-06-xx, Svensk Kärnbränslehantering AB.

Appendix

Table A1. Mineral chemistry data of sample KLX03-11: Plagioclase I (normalised to 32 charges and 8 cations).

	KLX03-11 plg3	KLX03-11 plg4	KLX03-11 plg5	KLX03-11 plg6	KLX03-11 plg7	KLX03-11 plg8	KLX03-11 plg1
Weight %							
SiO_2	60.93	60.79	59.81	60.10	59.37	59.35	59.017
TiO_2	0.00	0.00	0.00	0.00	0.00	0.00	0.000
Cr_2O_3	0.00	0.00	0.00	0.00	0.00	0.00	0.000
Al_2O_3	25.48	25.56	25.93	25.98	25.47	25.65	26.578
Fe_2O_3	0.00	0.00	0.00	0.00	0.00	0.00	0.000
FeO	0.05	0.14	0.00	0.05	0.13	0.14	0.057
MnO	0.01	0.00	0.00	0.00	0.00	0.00	0.020
MgO	0.00	0.00	0.00	0.00	0.00	0.00	0.000
CaO	6.77	6.72	7.54	7.47	7.42	7.53	8.010
Na_2O	7.41	7.52	7.12	7.13	7.23	7.20	6.751
K_2O	0.24	0.19	0.22	0.20	0.12	0.20	0.078
Total	100.89	100.93	100.61	100.93	99.73	100.08	100.511
Cations (Fe^{2+}/Fe^{3+} charge balance)							
Si	2.697	2.689	2.658	2.663	2.660	2.650	2.63
Ti	0.000	0.000	0.000	0.000	0.000	0.000	0.00
Cr	0.000	0.000	0.000	0.000	0.000	0.000	0.00
Al	1.330	1.332	1.358	1.357	1.345	1.350	1.40
Fe^{3+}	0.000	0.000	0.000	0.000	0.000	0.000	0.00
Fe^{2+}	0.002	0.005	0.000	0.002	0.005	0.005	0.00
Mn	0.000	0.000	0.000	0.000	0.000	0.000	0.00
Mg	0.000	0.000	0.000	0.000	0.000	0.000	0.00
Ca	0.321	0.318	0.359	0.355	0.356	0.360	0.38
Na	0.636	0.645	0.613	0.612	0.628	0.623	0.58
K	0.013	0.011	0.012	0.011	0.007	0.011	0.00
Total	5.000	5.000	5.000	5.000	5.000	5.000	5.00
End members							
$CaAl_2Si_2O_8$ (An)	0.331	0.327	0.365	0.362	0.359	0.362	0.394
$NaAlSi_3O_8$ (Alb)	0.655	0.662	0.623	0.626	0.634	0.626	0.601
$KAlSi_3O_8$	0.014	0.011	0.013	0.012	0.007	0.011	0.005
Total End members	1.000	1.000	1.000	1.000	1.000	1.000	1.000
Residuals and Ratios							
Al_Fe3_deficite	–0.001	0.005	–0.007	–0.006	–0.015	–0.012	0.002
Si Deficite	0.028	0.016	0.022	0.026	0.019	0.012	0.025
An/An+Ab	0.335	0.331	0.369	0.367	0.362	0.366	0.396
Fe3/Fetot	0.000	0.000	–	0.000	0.000	0.000	0.000
Charge deficite	–0.075	–0.054	–0.048	–0.059	–0.030	–0.015	–0.070
Sum Feldspar	0.971	0.974	0.984	0.978	0.990	0.995	0.970

Table A1 (cont.). Plagioclase II (normalised to 32 charges and 8 cations).

	KLX 03-11 plgc3	KLX 03-11 plgc4	KLX 03-11 plgr6	KLX 03-11 plgr7	KLX 03-11 plgr8	KLX 03-11 plgc9	KLX 03-11 plgc10	KLX 03-11 plgc11	KLX 03-11 plgr12	KLX 03-11 plgr13	KLX 03-11 plgr14
Weight %											
SiO_2	58.72	60.33	61.00	61.59	60.57	58.21	58.64	58.08	59.08	61.60	58.03
TiO_2	0.01	0.02	0.01	0.01	0.00	0.02	0.00	0.43	0.02	0.00	0.01
Cr_2O_3	0.04	0.04	0.00	0.01	0.00	0.00	0.03	0.00	0.02	0.00	0.06
Al_2O_3	27.02	25.88	25.72	25.38	26.10	27.21	27.10	26.56	26.40	23.19	27.21
Fe_2O_3	0.00	0.00	0.00	0.00	0.00	0.00	0.00	0.00	0.00	0.00	0.00
FeO	0.08	0.14	0.21	0.15	0.03	0.11	0.13	0.06	0.20	0.07	0.19
MnO	0.00	0.00	0.00	0.01	0.00	0.03	0.02	0.04	0.00	0.01	0.02
MgO	0.00	0.00	0.00	0.00	0.00	0.00	0.00	0.00	0.00	0.00	0.00
CaO	8.34	7.08	6.71	6.32	7.12	8.68	8.44	8.39	7.36	4.71	8.62
Na_2O	6.68	7.35	7.61	7.46	7.38	6.32	6.56	6.51	7.26	4.87	6.45
K_2O	0.23	0.20	0.30	0.15	0.09	0.26	0.21	0.26	0.08	5.88	0.26
Total	101.11	101.04	101.54	101.07	101.29	100.82	101.14	100.33	100.41	100.34	100.84
Cations (Fe^{2+}/Fe^{3+} charge balance)											
Si	2.602	2.667	2.680	2.723	2.670	2.592	2.600	2.599	2.627	2.775	2.581
Ti	0.000	0.001	0.000	0.000	0.000	0.001	0.000	0.015	0.001	0.000	0.000
Cr	0.001	0.001	0.000	0.000	0.000	0.000	0.001	0.000	0.001	0.000	0.002
Al	1.411	1.349	1.332	1.323	1.356	1.428	1.416	1.401	1.383	1.232	1.426
Fe^{3+}	0.000	0.000	0.000	0.000	0.000	0.000	0.000	0.000	0.000	0.000	0.000
Fe^{2+}	0.003	0.005	0.008	0.006	0.001	0.004	0.005	0.002	0.007	0.003	0.007
Mn	0.000	0.000	0.000	0.000	0.000	0.001	0.001	0.002	0.000	0.000	0.001
Mg	0.000	0.000	0.000	0.000	0.000	0.000	0.000	0.000	0.000	0.000	0.000
Ca	0.396	0.336	0.316	0.299	0.336	0.414	0.401	0.402	0.351	0.227	0.411
Na	0.574	0.630	0.648	0.640	0.631	0.545	0.564	0.565	0.626	0.425	0.557
K	0.013	0.011	0.017	0.008	0.005	0.015	0.012	0.015	0.005	0.338	0.015
Total	5.000	5.000	5.000	5.000	5.000	5.000	5.000	5.000	5.000	5.000	5.000
End members											
$CaAl_2Si_2O_8$ (An)	0.403	0.344	0.322	0.316	0.346	0.425	0.411	0.410	0.357	0.230	0.418
$NaAlSi_3O_8$ (Alb)	0.584	0.645	0.661	0.675	0.649	0.560	0.577	0.575	0.638	0.429	0.567
$KAlSi_3O_8$	0.013	0.011	0.017	0.009	0.005	0.015	0.012	0.015	0.005	0.341	0.015
Total End memb.	1.000	1.000	1.000	1.000	1.000	1.000	1.000	1.000	1.000	1.000	1.000
Residuals and Ratios											
Al_Fe3_deficite	0.008	0.005	0.010	0.007	0.010	0.003	0.006	–0.009	0.026	0.002	0.008
Si Deficite	0.005	0.011	0.002	0.039	0.016	0.017	0.011	0.008	–0.016	0.004	–0.001
An/An+Ab	0.408	0.347	0.328	0.319	0.348	0.431	0.416	0.416	0.359	0.349	0.425
Fe3/Fetot	0.000	0.000	0.000	0.000	0.000	0.000	0.000	0.000	0.000	0.000	0.000
Charge deficite	–0.029	–0.045	–0.028	–0.123	–0.061	–0.053	–0.042	–0.048	–0.009	–0.018	–0.020
Sum Feldspar	0.983	0.977	0.980	0.947	0.972	0.974	0.977	0.982	0.981	0.990	0.982

plgc : centre of plagioclase crystal.

plgr : rim of plagioclase crystal.

Table A1 (cont.). K-feldspar I (normalised to 32 charges and 8 cations)

	KLX03-11 kf1	KLX03-11 kf2	KLX03-11 kf3	KLX03-11 kf4
Weight %				
SiO_2	64.85	64.46	64.28	64.22
TiO_2	0.00	0.00	0.00	0.00
Cr_2O_3	0.00	0.00	0.00	0.00
Al_2O_3	18.84	18.75	18.86	19.98
Fe_2O_3	0.00	0.00	0.00	0.00
FeO	0.00	0.00	0.00	0.02
MnO	0.05	0.04	0.01	0.00
MgO	0.00	0.00	0.00	0.00
CaO	0.00	0.00	0.13	1.33
Na_2O	0.64	0.68	0.81	1.90
K_2O	16.04	15.89	15.65	12.89
Total	100.41	99.83	99.75	100.34
Cations (Fe^{2+}/Fe^{3+} charge balance)				
Si	2.980	2.979	2.970	2.937
Ti	0.000	0.000	0.000	0.000
Cr	0.000	0.000	0.000	0.000
Al	1.020	1.022	1.027	1.077
Fe^{3+}	0.000	0.000	0.000	0.000
Fe^{2+}	0.000	0.000	0.000	0.001
Mn	0.002	0.002	0.000	0.000
Mg	0.000	0.000	0.000	0.000
Ca	0.000	0.000	0.006	0.065
Na	0.057	0.061	0.073	0.168
K	0.940	0.937	0.923	0.752
Total	5.000	5.000	5.000	5.000
End members				
$CaAl_2Si_2O_8$ (An)	0.000	0.000	0.006	0.066
$NaAlSi_3O_8$ (Alb)	0.057	0.061	0.073	0.171
$KAlSi_3O_8$	0.943	0.939	0.921	0.763
Total End members	1.000	1.000	1.000	1.000
Residuals and Ratios				
Al_Fe3_deficite	0.020	0.022	0.021	0.011
Si Deficite	–0.020	–0.021	–0.023	0.003
An/An+Ab	0.000	0.000	0.081	0.279
Fe3/Fetot	–	–	1.000	0.000
Charge deficite	0.017	0.017	0.028	–0.030
Sum Feldspar	0.998	0.998	1.002	0.986

Table A1 (cont.). K-feldspar II (normalised to 32 charges and 8 cations).

	KLX03-11 kfc5	KLX03-11 kfc6	KLX03-11 kfc7	KLX03-11 kfr8	KLX03-11 kfr9	KLX03-11 kfr10
Weight %						
SiO_2	66.09	64.72	64.37	65.12	65.09	64.52
TiO_2	0.01	0.02	0.02	0.01	0.00	0.01
Cr_2O_3	0.00	0.00	0.05	0.01	0.03	0.00
Al_2O_3	19.68	18.83	20.06	19.00	18.83	18.89
Fe_2O_3	0.00	0.00	0.00	0.00	0.07	0.00
FeO	0.08	0.06	0.00	0.00	0.00	0.00
MnO	0.00	0.04	0.11	0.00	0.00	0.09
MgO	0.00	0.00	0.00	0.00	0.00	0.01
CaO	1.59	0.02	1.06	0.00	0.00	0.00
Na_2O	2.48	0.89	2.13	0.86	0.76	0.63
K_2O	11.15	15.37	12.37	15.68	15.85	16.09
Total	101.08	99.94	100.17	100.67	100.63	100.24
Cations (Fe^{2+}/Fe^{3+} charge balance)						
Si	3.002	2.986	2.947	2.982	2.984	2.970
Ti	0.000	0.001	0.001	0.000	0.000	0.000
Cr	0.000	0.000	0.002	0.000	0.001	0.000
Al	1.053	1.024	1.083	1.026	1.018	1.025
Fe^{3+}	0.000	0.000	0.000	0.000	0.002	0.000
Fe^{2+}	0.003	0.002	0.000	0.000	0.000	0.000
Mn	0.000	0.001	0.004	0.000	0.000	0.003
Mg	0.000	0.000	0.000	0.000	0.000	0.000
Ca	0.077	0.001	0.052	0.000	0.000	0.000
Na	0.218	0.079	0.189	0.076	0.068	0.056
K	0.646	0.905	0.723	0.916	0.927	0.945
Total	5.000	5.000	5.000	5.000	5.000	5.000
End members						
$CaAl_2Si_2O_8$ (An)	0.082	0.001	0.054	0.000	0.000	0.000
$NaAlSi_3O_8$ (Alb)	0.232	0.080	0.196	0.077	0.068	0.056
$KAlSi_3O_8$	0.686	0.919	0.750	0.923	0.932	0.944
Total End members	1.000	1.000	1.000	1.000	1.000	1.000
Residuals and Ratios						
Al_Fe3_deficite	–0.029	0.023	0.029	0.026	0.020	0.025
Si Deficite	0.084	–0.013	0.001	–0.018	–0.016	–0.030
An/An+Ab	0.262	0.010	0.216	0.000	0.000	0.000
Fe3/Fetot	0.000	0.000	–	–	1.000	–
Charge deficite	–0.194	–0.015	–0.069	0.001	0.007	0.035
Sum Feldspar	0.941	0.985	0.963	0.992	0.994	1.001

kfc : centre of K-feldspar crystal.

kfr : rim of K-feldspar crystal.

Table A1 (cont.). Diopside (normalised to 12 charges).

	KLX03-11 cpx6	KLX03-11 cpx7	KLX03-11 cpx10	KLX03-11 cpx1	KLX03-11 cpx2	KLX03-11 cpx3
Weight %						
SiO_2	52.84	53.24	53.05	52.07	51.48	52.36
TiO_2	0.18	0.15	0.11	0.14	0.14	0.14
Cr_2O_3	0.02	0.07	0.03	0.02	0.14	0.18
Al_2O_3	1.16	0.93	0.94	0.95	1.11	0.93
Fe_2O_3	0.15	0.00	0.00	0.99	1.31	0.77
FeO	9.03	8.97	9.35	10.35	9.55	10.16
MnO	0.43	0.50	0.71	0.79	0.88	0.77
MgO	12.93	13.11	12.89	11.88	11.75	11.72
CaO	23.02	22.88	22.56	22.38	22.55	22.90
Na_2O	0.31	0.31	0.33	0.40	0.41	0.41
K_2O	0.00	0.01	0.01	0.00	0.03	0.01
Total	100.06	100.17	99.99	99.97	99.34	100.35
Cations (according to Lindsley, with AFe3+)						
Si	1.978	1.988	1.988	1.975	1.966	1.977
Ti	0.005	0.004	0.003	0.004	0.004	0.004
Cr	0.000	0.002	0.001	0.001	0.004	0.005
Al	0.051	0.041	0.041	0.042	0.050	0.041
Fe^{3+}	0.004	0.000	0.000	0.028	0.038	0.022
Fe^{2+}	0.283	0.280	0.293	0.328	0.305	0.321
Mn	0.014	0.016	0.023	0.026	0.028	0.025
Mg	0.721	0.729	0.720	0.672	0.669	0.659
Ca	0.923	0.915	0.906	0.909	0.923	0.926
Na	0.022	0.023	0.024	0.029	0.031	0.030
K	0.000	0.000	0.001	0.000	0.002	0.000
Total	4.002	3.998	4.000	4.014	4.019	4.011
Ratios and Site activities						
Al4	0.022	0.012	0.012	0.025	0.034	0.023
Al6	0.029	0.029	0.030	0.017	0.016	0.018
xMg(Fe^{2+})	0.718	0.723	0.711	0.672	0.687	0.673
xMg(Fetot)	0.715	0.723	0.711	0.653	0.661	0.658
Fe^{3+}/Fe(tot)	0.015	0.000	0.000	0.079	0.110	0.064
End members						
$NaFeSi2O_6$ (acm)	0.004	0.000	0.000	0.028	0.032	0.022
$NaAlSi2O_6$ (jad)	0.018	0.023	0.024	0.001	0.000	0.008
$CaTiAl2O_6$	0.005	0.004	0.003	0.004	0.004	0.004
$CaCrAlSiO_6$	0.000	0.002	0.001	0.001	0.004	0.005
$CaFeAlSiO_6$	0.000	0.000	0.000	0.000	0.006	0.000
$CaAl2SiO_6$ (CaTs)	0.011	0.002	0.005	0.016	0.016	0.010
$Ca_{0.5}AlSi_2O_6$ (esc)	0.000	0.004	0.000	0.000	0.000	0.000
$Mg_2Si_2O_6$ (enst)	0.361	0.365	0.360	0.336	0.334	0.330
$Fe_2Si_2O_6$	0.141	0.140	0.147	0.164	0.152	0.160
$Mn_2Si_2O_6$	0.007	0.008	0.011	0.013	0.014	0.012
$Ca_2Si_2O_6$	0.453	0.453	0.449	0.444	0.446	0.454
Total End members	1.001	1.000	1.000	1.007	1.009	1.005
Total Diopside	0.643	0.644	0.624	0.582	0.596	0.595

Table A1 (cont.). Amphibole (normalised to 46 charges and 2OH).

	KLX03-11 amp4	KLX03-11 amp5	KLX03-11 amp8	KLX03-11 amp9	KLX03-11amp11	KLX03-11 amp12
Weight %						
SiO_2	59.90	54.76	50.15	57.57	54.30	51.31
TiO_2	0.01	0.10	0.78	0.11	0.15	0.69
Cr_2O_3	0.00	0.00	0.00	0.00	0.01	0.15
Al_2O_3	0.95	1.45	5.15	1.92	2.16	4.42
Fe_2O_3	0.00	0.00	0.00	0.00	0.00	0.00
FeO	11.85	13.26	15.37	11.45	13.08	14.87
MnO	0.47	0.52	0.55	0.42	0.44	0.34
MgO	12.93	14.36	12.68	14.11	15.01	13.49
CaO	11.13	12.48	11.90	11.62	12.51	12.21
Na_2O	0.14	0.15	0.68	0.22	0.24	0.53
K_2O	0.03	0.04	0.45	0.09	0.11	0.29
H_2O	2.05	2.06	2.03	2.07	2.08	2.06
Total	99.45	99.17	99.73	99.57	100.09	100.34
Cations (Fe^{2+}/Fe^{3+} charge balance)						
Si	8.764	7.987	7.392	8.359	7.828	7.469
Ti	0.001	0.011	0.086	0.011	0.017	0.076
Cr	0.000	0.000	0.000	0.000	0.001	0.017
Al	0.164	0.249	0.894	0.328	0.367	0.758
Fe^{3+}	0.000	0.000	0.000	0.000	0.000	0.000
Fe^{2+}	1.449	1.617	1.895	1.391	1.576	1.810
Mn	0.058	0.064	0.068	0.052	0.054	0.041
Mg	2.819	3.122	2.785	3.052	3.225	2.926
Ca	1.745	1.950	1.879	1.807	1.932	1.904
Na	0.039	0.041	0.195	0.061	0.066	0.149
K	0.005	0.008	0.085	0.017	0.021	0.053
H	2.000	2.000	2.000	2.000	2.000	2.000
Total	15.044	15.049	15.279	15.078	15.087	15.202
Ratios and Site activities						
Al4	0.000	0.013	0.608	0.000	0.172	0.531
Al6	0.164	0.236	0.287	0.328	0.195	0.227
xMg(Fe^{2+})	0.660	0.659	0.595	0.687	0.672	0.618
xMg(Fetot)	0.660	0.659	0.595	0.687	0.672	0.618
xFe^{3+}	0.000	0.000	0.000	0.000	0.000	0.000
NaM4	0.000	0.000	0.000	0.000	0.000	0.000
NaA	0.039	0.041	0.195	0.061	0.066	0.149
NaK (A)	0.044	0.049	0.279	0.078	0.087	0.202

Table A1 (cont.). Biotite (normalised to 44 charges, 16 cations and 4OH).

	KLX 03-11 bt1	KLX 03-11 bt2	KLX 03-11 bt3	KLX 03-11 bt4	KLX 03-11 bt5	KLX 03-11 bt6	KLX 03-11 bt7	KLX 03-11 bt8	KLX 03-11 bt9	KLX 03-11 bt10
Weight %										
SiO_2	36.88	37.02	37.00	37.00	37.11	37.05	36.85	37.25	36.92	37.04
TiO_2	2.69	2.61	3.22	3.01	3.01	2.80	3.10	2.90	3.59	3.53
Cr_2O_3	0.01	0.06	0.02	0.00	0.00	0.00	0.00	0.12	0.05	0.02
Al_2O_3	14.81	14.92	14.57	14.70	15.31	15.40	15.08	14.91	14.79	14.75
Fe_2O_3	0.00	0.00	0.00	0.00	0.00	0.00	0.00	0.00	0.00	0.00
FeO	19.78	20.31	21.01	20.75	19.39	19.83	19.15	19.70	19.56	19.41
MnO	0.25	0.24	0.25	0.16	0.12	0.25	0.22	0.22	0.18	0.20
MgO	10.94	11.05	10.71	10.78	10.93	11.08	10.77	11.03	11.03	11.23
CaO	0.00	0.00	0.02	0.02	0.00	0.01	0.05	0.00	0.02	0.00
Na_2O	0.09	0.08	0.11	0.09	0.08	0.10	0.09	0.12	0.10	0.09
K_2O	9.89	9.79	9.86	9.81	10.00	10.01	9.86	9.99	9.83	9.89
H_2O	3.83	3.86	3.87	3.85	3.86	3.88	3.82	3.87	3.85	3.86
F	0.00	0.00	0.00	0.00	0.00	0.00	0.00	0.00	0.00	0.00
Cl	0.00	0.00	0.00	0.00	0.00	0.00	0.00	0.00	0.00	0.00
Total	99.17	99.94	100.63	100.17	99.79	100.38	98.99	100.10	99.92	100.01
F,Cl = O	0.00	0.00	0.00	0.00	0.00	0.00	0.00	0.00	0.00	0.00
Total	99.17	99.94	100.63	100.17	99.79	100.38	98.99	100.10	99.92	100.01
General Cations										
Cations (Fe^{2+}/Fe^{3+} charge balance)										
Si	5.773	5.755	5.739	5.756	5.769	5.724	5.780	5.777	5.747	5.753
Ti	0.317	0.305	0.375	0.353	0.351	0.325	0.366	0.338	0.421	0.412
Cr	0.001	0.007	0.002	0.000	0.000	0.000	0.000	0.014	0.006	0.002
Al	2.733	2.734	2.665	2.695	2.806	2.804	2.789	2.725	2.713	2.700
Fe^{3+}	0.000	0.000	0.000	0.000	0.000	0.000	0.000	0.000	0.000	0.000
Fe^{2+}	2.590	2.640	2.725	2.699	2.520	2.562	2.512	2.555	2.546	2.521
Mn	0.033	0.032	0.033	0.021	0.016	0.032	0.029	0.029	0.024	0.026
Mg	2.553	2.561	2.476	2.499	2.532	2.550	2.517	2.550	2.558	2.601
Ca	0.000	0.000	0.003	0.004	0.000	0.001	0.008	0.000	0.004	0.000
Na	0.027	0.024	0.033	0.028	0.023	0.029	0.027	0.037	0.031	0.026
K	1.974	1.942	1.950	1.946	1.983	1.972	1.972	1.976	1.951	1.960
H	4.000	4.000	4.000	4.000	4.000	4.000	4.000	4.000	4.000	4.000
F	0.000	0.000	0.000	0.000	0.000	0.000	0.000	0.000	0.000	0.000
Cl	0.000	0.000	0.000	0.000	0.000	0.000	0.000	0.000	0.000	0.000
Total	16.000	16.000	16.000	16.000	16.000	16.000	16.000	16.000	16.000	16.000
Ratios and Site activities										
xMg(Fe2+)	0.496	0.492	0.476	0.481	0.501	0.499	0.501	0.499	0.501	0.508
xMg(Fetot)	0.496	0.492	0.476	0.481	0.501	0.499	0.501	0.499	0.501	0.508
xFe^{3+}	0.000	0.000	0.000	0.000	0.000	0.000	0.000	0.000	0.000	0.000

Table A1 (cont.). Prehnite (normalised to 22 charges, 7 cations and 2OH).

	KLX03-11 prh5	KLX03-11 prh6	KLX03-11 prh7	KLX03-11 prh8	KLX03-11 prh9	KLX03-11 prh19
Weight %						
SiO_2	43.16	43.36	43.24	43.14	42.83	43.17
TiO_2	0.31	0.25	0.36	0.10	0.32	1.24
Cr_2O_3	0.02	0.00	0.00	0.00	0.02	0.04
Al_2O_3	21.76	22.14	21.41	22.37	21.51	20.72
Fe_2O_3	0.00	0.00	0.00	0.00	0.00	0.00
FeO	3.35	2.94	3.97	2.90	4.53	3.57
MnO	0.11	0.00	0.03	0.00	0.00	0.09
MgO	0.00	0.00	0.00	0.00	0.33	0.00
CaO	26.18	26.53	26.41	26.56	25.70	26.07
Na_2O	0.03	0.01	0.01	0.02	0.00	0.01
K_2O	0.01	0.02	0.02	0.01	0.01	0.01
H_2O	4.29	4.31	4.30	4.31	4.29	4.27
Total	99.22	99.55	99.74	99.40	99.52	99.20
General Cations Cations (Fe^{2+}/Fe^{3+} charge balance)						
Si	3.019	3.018	3.014	3.004	2.991	3.034
Ti	0.016	0.013	0.019	0.005	0.017	0.065
Cr	0.001	0.000	0.000	0.000	0.001	0.002
Al	1.794	1.817	1.759	1.837	1.770	1.717
Fe^{3+}	0.000	0.000	0.000	0.000	0.000	0.000
Fe^{2+}	0.196	0.171	0.232	0.169	0.264	0.210
Mn	0.006	0.000	0.002	0.000	0.000	0.005
Mg	0.000	0.000	0.000	0.000	0.034	0.000
Ca	1.962	1.978	1.972	1.981	1.922	1.963
Na	0.004	0.001	0.001	0.002	0.000	0.002
K	0.001	0.001	0.002	0.001	0.001	0.001
H	2.000	2.000	2.000	2.000	2.000	2.000
Total	7.000	7.000	7.000	7.000	7.000	7.000
Ratios and Site activities						
xMg(Fe^{2+})	0.000	0.000	0.000	0.000	0.114	0.000
xMg(Fetot)	0.000	0.000	0.000	0.000	0.114	0.000
xFe^{3+}	0.000	0.000	0.000	0.000	0.000	0.000

Table A1 (cont.). Vesuvianite (normalised to Ca + Na + K + Ba + Sr = 19).

Comment	KLX03-11prh14	KLX03-11prh16	KLX03-11prh17	KLX03-11pre5	KLX03-11pre6	KLX03-11pre7	KLX03-11pre8
Weight %							
SiO_2	34.63	34.54	35.07	34.81	35.52	35.42	34.84
TiO_2	1.18	3.32	0.24	1.92	1.70	1.62	1.77
Cr_2O_3	0.00	0.04	0.04	0.00	0.02	0.00	0.00
Al_2O_3	9.22	8.90	10.71	11.36	10.87	10.55	11.35
FeO	15.96	14.11	15.04	12.95	13.47	13.86	12.64
MnO	0.01	0.01	0.00	0.03	0.01	0.00	0.03
MgO	0.00	0.00	0.00	0.00	0.00	0.00	0.00
CaO	36.08	36.05	35.76	35.96	36.16	36.37	35.68
Na_2O	0.00	0.01	0.01	0.00	0.00	0.01	0.00
K_2O	0.01	0.00	0.01	0.02	0.00	0.01	0.02
H_2O	2.73	2.75	2.73	2.76	2.78	2.78	2.74
Total	99.81	99.73	99.61	99.81	100.53	100.62	99.06
Normalised to Ca+K+Na+Ba+Sr = 19							
Si	17.019	16.983	17.380	17.157	17.419	17.256	17.309
Ti	0.435	1.228	0.090	0.713	0.626	0.593	0.661
Cr	0.000	0.015	0.015	0.000	0.006	0.000	0.000
Al	5.337	5.159	6.253	6.600	6.284	6.058	6.647
Fe^{2+}	6.559	5.800	6.232	5.337	5.521	5.649	5.250
Mn	0.003	0.002	0.000	0.013	0.003	0.001	0.011
Mg	0.000	0.000	0.000	0.000	0.000	0.000	0.000
Ca	18.994	18.991	18.984	18.987	18.996	18.987	18.989
Na	0.000	0.009	0.012	0.000	0.004	0.009	0.000
K	0.006	0.000	0.004	0.013	0.001	0.005	0.011

Table A1 (cont.). Magnetite (mgt, normalised to 8 charges) and Sphene (tit, normalised to 10 charges).

Comment	KLX03-11 mgt1	KLX03-11 mgt2	KLX03-11 tit3
Weight %			
SiO_2	0.02	0.02	27.76
TiO_2	0.04	0.04	37.90
Cr_2O_3	0.11	0.16	0.00
Al_2O_3	0.02	0.02	1.53
Fe_2O_3	0.00	0.00	0.00
FeO	93.21	92.95	7.02
MnO	0.04	0.00	1.19
MgO	0.00	0.01	0.00
CaO	0.03	0.05	24.69
Na_2O	0.03	0.02	0.01
K_2O	0.00	0.00	0.01
Total	93.51	93.28	100.11
General Oxygen Cations (Fe^{2+}/Fe^{3+} Input)			
Si	0.001	0.001	0.934
Ti	0.002	0.002	0.959
Cr	0.004	0.007	0.000
Al	0.001	0.001	0.061
Fe^{3+}	0.000	0.000	0.000
Fe^{2+}	3.981	3.978	0.198
Mn	0.002	0.000	0.034
Mg	0.000	0.001	0.000
Ca	0.002	0.003	0.890
Na	0.003	0.002	0.001
K	0.000	0.000	0.000
Total Cations	3.996	3.994	3.077
Ratios and Site activities			
xMg(Fe^{2+})	0.000	0.000	0.000
xMg(Fetot)	0.000	0.000	0.000
xFe^{3+}	0.000	0.000	0.000

Table A2. Fluid inclusion data of quartz.

Abbreviations:

Sample KLX03-11 FI-x:	thick section with several quartz grains
FI-No:	number of inclusion in thick section
T_nIce:	nucleation temperature of ice
T_mIce:	melting of ice
T_nCla:	nucleation temperature of clathrate
T_mCla:	melting temperature of clathrate
T_hCO_2:	homogenisation temperature of clathrate.

Sample KLX03-11 FI-1

FI-No[1)]	$T_n$ice (°C)	$T_m$ice (°C)	T_nCla (°C)	T_mCla (°C)	T_hCO_2 (°C)	NaCl eq-wt%	Comments
1			–37	+1.2	+27.7 →L	14.2	3-phase: pure CO_2 (L+V), salt solution
2			–37	+1.4	+29.5 →L	14.0	3-phase: CO_2 with little N_2 (L+V), salt solution; calcite inclusion
3	–41	–1.9				3.2	
4	–40	–1.8				3.1	
5	–72	–23.6		+ 0.7		> 24	CO_2 calcite and rutile inclusions
6	–43	–2.5				4.2	
7	–55	–18.8		Cla?		21.8	CO_2
8			–35	+3.0	+ 26.3 →L	11.9	3-phase: CO_2 (L+V), salt solution; calcite inclusion
9	–61	–12.6				16.6	
10	–61	–12.7				16.7	T_m hydrohalite = –27.0°C
11	–71	–22.2				> 24	
12	–59	–12.4				16.4	
13	–60	–11.9				16.0	
14	–86	–44.3				> 24	$T_n$ice prograde, calcite and biotite inclusions
15	–60	–12.2				16.2	
16	–44	–3.8				6.1	
17	–59	–21.8				> 24	T_mCla = –14.8°C, CO_2
18	–70	–18.1				21.3	
19	–39	–0.7				1.2	
20	–40	–1.3				2.2	
21	–41	–1.4				2.4	

[1)] FI No 1 to 15 are fluid inclusions in quartz with solid inclusions of rutile and biotite, FI No 16 to 20 are fluid inclusions in quartz free of solid inclusions

Table A2 (continued).

Sample KLX03-11 FI-2				
FI-No	**$T_n$ice (°C)**	**$T_m$ice (°C)**	**NaCl eq-wt%**	**Comments**
1	–62	–14.1	18.0	Quartz free of solid inclusions
2	–61	–14.0	17.9	Quartz free of solid inclusions
3	–64	–14.7	18.5	Quartz free of solid inclusions
4	–42	–3.2	5.3	Quartz free of solid inclusions
5	–43	–3.3	5.4	Quartz free of solid inclusions
6	–41	–2.4	4.0	Quartz free of solid inclusions
7	–42	–2.5	4.2	Quartz free of solid inclusions
8	–66	–16.2	19.8	Quartz free of solid inclusions
9	–64	–15.0	18.8	Quartz free of solid inclusions
10	–50	–6.7	10.1	Quartz free of solid inclusions
11	–49	–6.3	9.6	Quartz free of solid inclusions
12	–33	–4.0	6.4	Quartz free of solid inclusions
13	–65	–16.2	19.8	Quartz free of solid inclusions
14	–40	–1.9	3.2	Quartz free of solid inclusions
15	–46	–4.6	7.3	Quartz free of solid inclusions
16	–42	–2.6	4.3	Quartz free of solid inclusions
17	–47	–5.1	8.0	Quartz free of solid inclusions
18	–42	–2.4	4.0	Quartz free of solid inclusions
19	–46	–4.6	7.3	Quartz free of solid inclusions
20	–41	–1.8	3.1	Quartz free of solid inclusions

Sample KLX03-11 FI-3				
FI-No	**$T_n$ice (°C)**	**$T_m$ice (°C)**	**NaCl eq-wt%**	**Comments**
1	–45	–4.3	6.9	Quartz free of solid inclusions
2	–40	–0.9	1.6	Quartz free of solid inclusions
3	–35	–4.6	7.3	N_2 detected, no CO_2, quartz free of solid inclusions
4	–46	–4.2	6.7	Quartz free of solid inclusions
5	–59	–11.7	15.8	Quartz free of solid inclusions
6	–59	–12.0	16.0	Quartz free of solid inclusions
7	–43	–2.8	4.6	Quartz free of solid inclusions
8	–47	–4.6	7.3	Quartz free of solid inclusions
9	–45	–4.2	6.7	Quartz free of solid inclusions
10	–50	–10.9	14.9	N_2 detected, no CO_2, quartz free of solid inclusions
11	–60	–12.4	16.4	Quartz free of solid inclusions
12	–41	–1.4	2.4	Quartz free of solid inclusions
13	–31	–1.1	1.9	Quartz free of solid inclusions
14	–40	–1.2	2.1	Quartz free of solid inclusions
15	–62	–13.0	17.0	Quartz free of solid inclusions
16	–42	–2.8	4.6	Quartz free of solid inclusions
17	–47	–4.8	7.6	Quartz free of solid inclusions
18	–48	–5.6	8.7	Quartz free of solid inclusions
19	–54	–12.1	16.1	N_2 detected, no CO_2, quartz free of solid inclusions
20	–51	–12.2	16.2	Quartz free of solid inclusions
21	–40	–1.7	2.9	Quartz free of solid inclusions
22	–40	–1.2	2.1	Quartz free of solid inclusions
23	–61	–12.8	16.8	Quartz free of solid inclusions
24	–42	–2.5	4.2	Quartz free of solid inclusions
25	–42	–2.6	4.3	Quartz free of solid inclusions
26	–60	–14.3	18.2	Quartz free of solid inclusions
27	–43	–2.3	3.9	Quartz free of solid inclusions
28	–33	–1.6	2.7	Quartz free of solid inclusions
29	–40	–1.1	1.9	Quartz free of solid inclusions

Table A2. (continued).

Sample KLX03-11 FI-4				
FI-No	$T_n$ice (°C)	$T_m$ice (°C)	NaCl eq-wt%	Comments
1	–44	–3.3	5.4	Quartz with solid inclusions
2	–49	–6.0	9.2	Quartz with solid inclusions
3	–49	–5.7	8.8	Quartz with solid inclusions
4	–44	–3.4	5.6	Quartz with solid inclusions
5	–48	–10.0	14.0	Quartz with solid inclusions
6	–55	–10.3	14.3	Quartz with solid inclusions
7	–66	–15.4	19.1	Quartz with solid inclusions
8	–60	–12.2	16.2	Quartz with solid inclusions
9	–71	–18.8	21.8	Quartz with solid inclusions
10	–57	–10.7	14.7	Quartz with solid inclusions
11	–42	–2.0	3.4	Quartz with solid inclusions
12	–54	–9.0	12.9	Quartz with solid inclusions
13	–45	–3.3	5.4	Quartz with solid inclusions
14	–44	–3.0	4.9	Quartz with solid inclusions
15	–70	–18.0	21.2	Quartz with solid inclusions
16	–43	–3.0	4.9	Quartz with solid inclusions
17	–27	–0.4	0.7	Quartz with solid inclusions
18	–34	–0.4	0.7	Quartz with solid inclusions
19	–43	–2.8	4.6	Quartz free of solid inclusions
20	–45	–4.3	6.9	Quartz free of solid inclusions
21	–44	–3.9	6.3	Quartz free of solid inclusions
22	–63	–14.7	18.5	Quartz free of solid inclusions
23	–62	–13.8	17.7	Quartz free of solid inclusions
24	–64	–16.3	19.9	Quartz free of solid inclusions
25	–67	–16.9	20.4	Quartz free of solid inclusions
26	–45	–3.8	6.1	Quartz free of solid inclusions
27	–45	–3.7	6.0	Quartz free of solid inclusions
28	–41	–1.8	3.1	Quartz free of solid inclusions
29	–62	–13.5	17.5	Quartz free of solid inclusions
30	–62	–13.1	17.1	Quartz free of solid inclusions

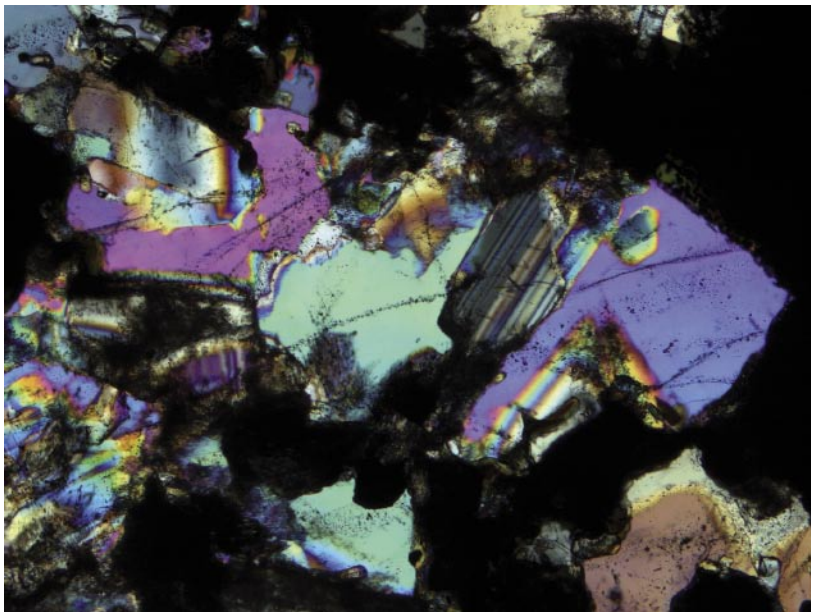

Figure A1. *Sample KLX03-11: Typical occurrence of quartz in the rock matrix.*

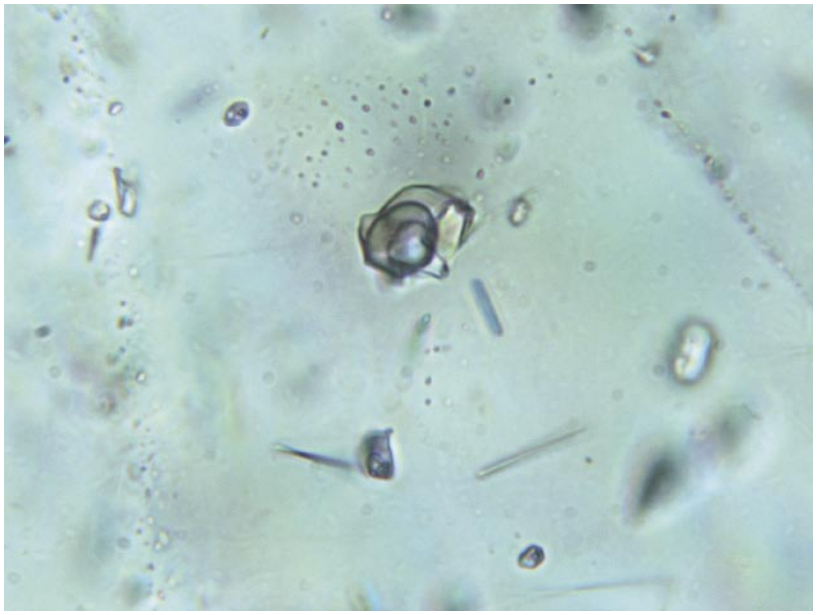

Figure A2. *3-phase CO_2-gas, CO_2-liquid and salt solution (14.0 eq-wt% NaCl) fluid inclusion with a solid calcite and biotite inclusion (sample KLX03-11 FI1 No 2).*

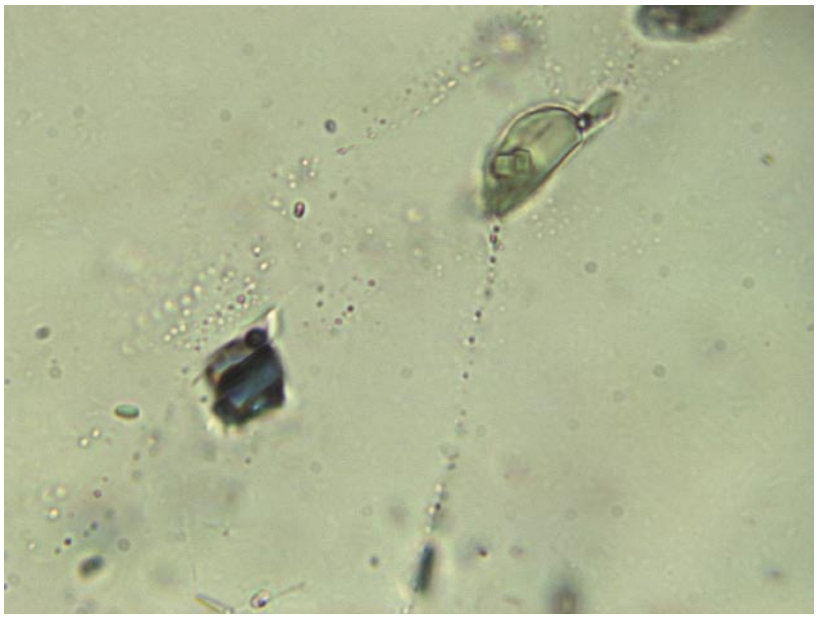

Figure A3. *2-phase CO_2-gas and salt solution (< 24.0 eq-wt% NaCl) fluid inclusion with a solid calcite and biotite inclusion (sample KLX03-11 FI1 No 14).*

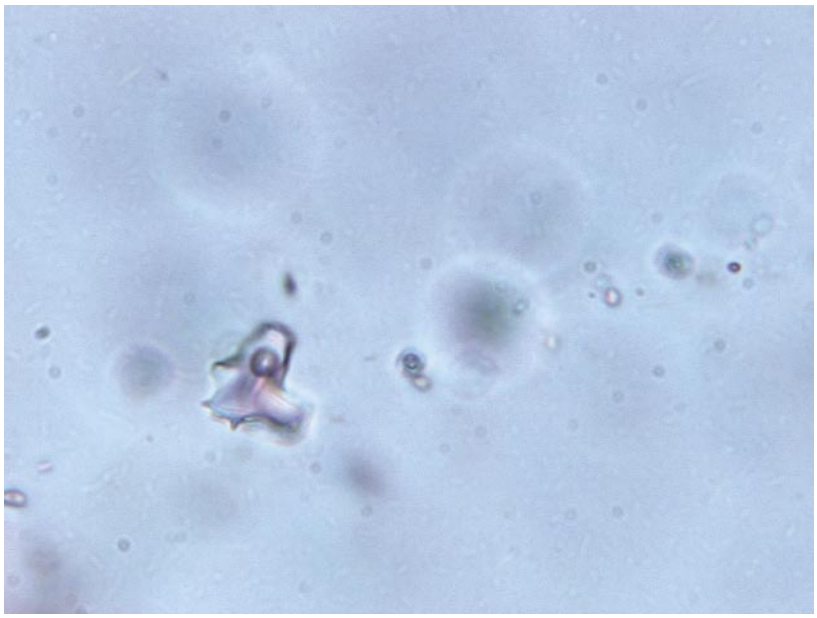

Figure A4. *2-phase CO_2-gas and salt solution (19.8 eq-wt% NaCl) fluid inclusion in quartz free of solid inclusions (sample KLX03-11 FI2 No 8).*

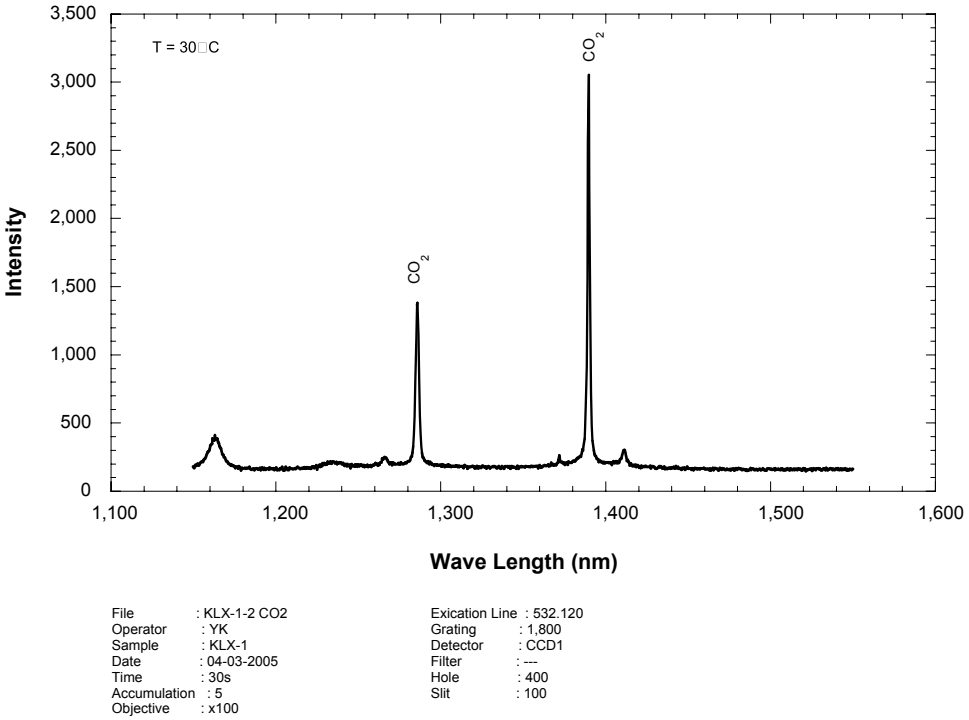

File : KLX-1-2 CO2
Operator : YK
Sample : KLX-1
Date : 04-03-2005
Time : 30s
Accumulation : 5
Objective : x100

Exication Line : 532.120
Grating : 1,800
Detector : CCD1
Filter : ---
Hole : 400
Slit : 100

Figure A5. *Raman Spectra of fluid inclusion KLX03-11 FI-1 No 2 showing the occurrence of CO_2.*

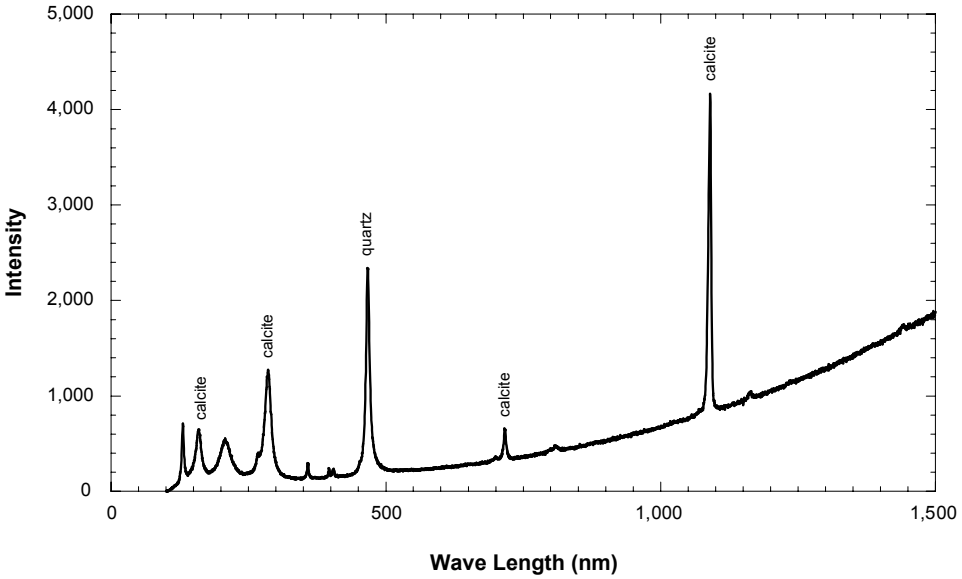

File : KLX-1-2 Calcite
Operator : YK
Sample : KLX-1
Date : 04-03-2005
Time : 30s
Accumulation : 6
Objective : x100

Exication Line : 532.120
Grating : 1,800
Detector : CCD1
Filter : ---
Hole : 400
Slit : 100

Figure A6. *Raman Spectra of fluid inclusion KLX03-11 FI-1 No 2 showing the occurrence of calcite solid inclusion.*

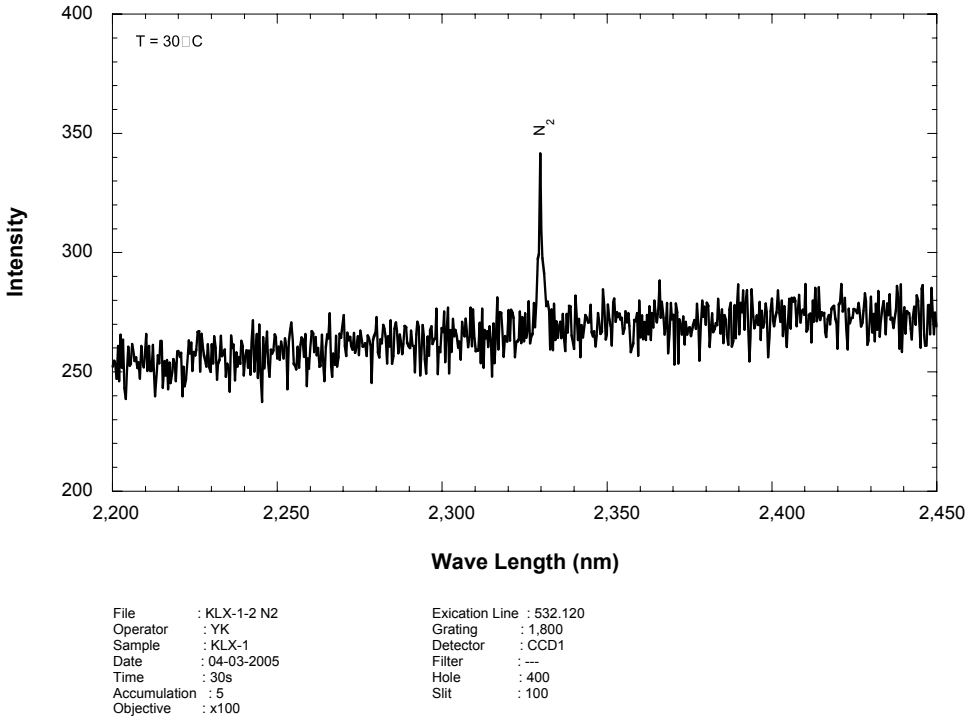

File : KLX-1-2 N2
Operator : YK
Sample : KLX-1
Date : 04-03-2005
Time : 30s
Accumulation : 5
Objective : x100

Exication Line : 532.120
Grating : 1,800
Detector : CCD1
Filter : ---
Hole : 400
Slit : 100

Figure A7. *Raman Spectra of fluid inclusion KLX03-11 FI-1 No 2 showing the occurrence of N_2.*

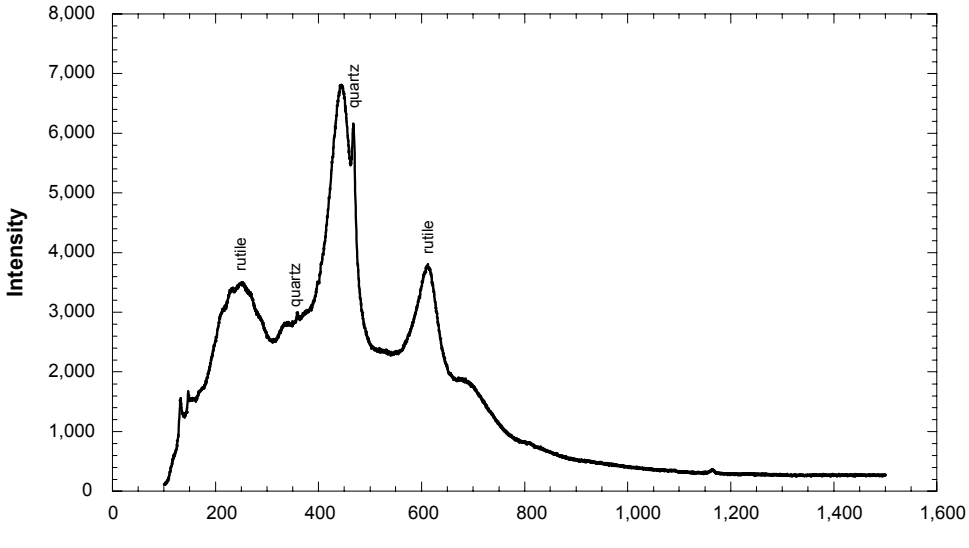

File : KLX-1-5 Rutile
Operator : YK
Sample : KLX-1
Date : 04-03-2005
Time : 10s
Accumulation : 6
Objective : x100

Exication Line : 532.120
Grating : 1,800
Detector : CCD1
Filter : ---
Hole : 400
Slit : 100

Figure A8. *Raman Spectra of fluid inclusion KLX03-11 FI-1 No 5 showing the occurrence of rutile.*

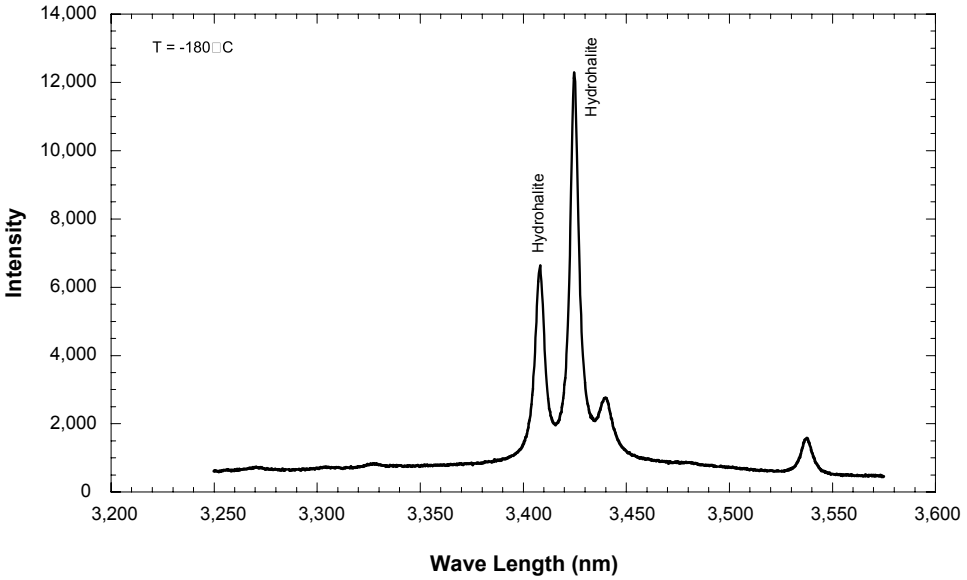

File : KLX-1-10 HH
Operator : YK
Sample : KLX-1
Date : 04-03-2005
Time : 30s
Accumulation : 6
Objective : x100

Exication Line : 532.120
Grating : 1,800
Detector : CCD1
Filter : ---
Hole : 400
Slit : 100

Figure A9. *Raman Spectra of fluid inclusion KLX03-11 FI-1 No 10 showing the occurrence of hydrohalite.*

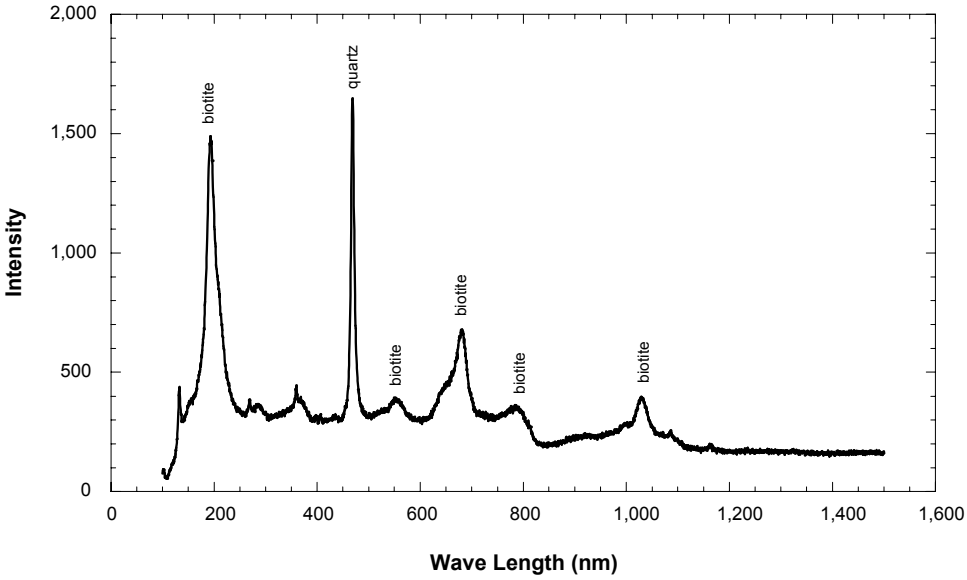

File : KLX-1-14 Biotite
Operator : YK
Sample : KLX-1
Date : 04-03-2005
Time : 10s
Accumulation : 6
Objective : x100

Exication Line : 532.120
Grating : 1,800
Detector : CCD1
Filter : ---
Hole : 400
Slit : 100

Figure A10. *Raman Spectra of fluid inclusion KLX03-11 FI-1 No 14 showing the occurrence of biotite.*

Table A3. Chemical data and modelling results of aqueous leaching experiments.

Sample description						
Borehole		KLX03	KLX03	KLX03	KLX03	KLX03
Sample		KLX03-11A	KLX03-11B	KLX03-11C	KLX03-11D	KLX03-11E
Type of Sample		Aq. Extract	Aq. Extract	Aq. Extract	Aq. Extract	Aq. Extract
Laboratory Extract		RWI, UniBe	RWI, UniBe	RWI, UniBe	RWI, UniBe	RWI, UniBe
Extraction Date		May 05	May 05	May 05	May 05	May 05
Conditions Extraction		ambient	ambient	ambient	ambient	ambient
Extraction Time		24 hours	24 hours	24 hours	24 hours	24 hours
S:L ratio		1:1	1:1	1:1	2:1	2:1
Grain Size		> 63 µm	0.14–0.8 mm	0.8–2 mm	2–4 mm	> 4 mm
Miscellaneous properties						
pH (lab)	-log(H+)	9.56	9.58	9.49	9.31	9.55
Sample Temperature	°C	20	20	20	20	20
Dissolved constituents						
Cations						
Sodium (Na^+)	mg/L	50.9	24.6	18.9	26.5	15.5
Potassium (K^+)	mg/L	65.8	10.8	4.6	4.7	3.8
Magnesium (Mg^{+2})	mg/L	0.2	< 0.1	< 0.1	< 0.1	< 0.1
Calcium (Ca^{+2})	mg/L	3.3	1.5	2.1	2	1.4
Strontium (Sr^{+2})	mg/L	< 0.1	< 0.1	< 0.1	< 0.1	< 0.1
Anions						
Fluoride (F^-)	mg/L	2.1	0.4	0.2	0.3	0.2
Chloride (Cl^-)	mg/L	38.8	9.2	5	8.2	3.6
Bromide (Br^-)	mg/L	0.3	0.1	0.1	0.1	< 0.1
Sulphate (SO_4^{-2})	mg/L	14.5	3.9	4.9	9	1.6
Nitrate (NO_3^-)	mg/L	0.9	0.4	0.2	0.3	0.3
Total Alkalinity	meq/L	2.21	1.03	0.69	0.92	0.66
Tot. Alkal. as HCO_3	mg/L	134.8	62.8	42.1	56.1	40.3
Parameters calculated from analytical data						
Sum of Anal. Constit.	mg/L	312	114	78	107	67
Charge Balance:	%	4.39	0.77	4.84	0.44	1.88
Ion-ion ratios						
Br/Cl molal	molar	3.431	4.823	8.874	5.411	–
Na/Cl molal	molar	2.023	4.124	5.829	4.984	6.640
K/Na molal	molar	0.760	0.258	0.143	0.104	0.144
SO_4/Cl molal	molar	0.138	0.156	0.362	0.405	0.164
Carbonate system						
Calculated using measured values						
TIC from alkalinity	mol/kg	1.869e–03	8.647e–04	5.895e–04	8.284e–04	5.537e–03
Calcite saturation index		0.48	–0.07	–0.13	–0.17	–0.27
log $p(CO_2)$		–4.61	–4.95	–5.01	–4.67	–5.10
Isotopes						
$\delta^{37}Cl$ (‰ V-SMOC)						
^{87}Sr / ^{86}Sr						
87^{Sr} / ^{86}Sr error						

Table A4. $\delta^{18}O$ and $\delta^{2}H$ of standard solutions used for the isotope diffusive exchange method and the out-diffusion experiments.

Standard no	Date	$\delta^{18}O$ ‰ V-SMOW	$\delta^{2}H$ ‰ V-SMOW	Sample KLX03-isotope diffusive exchange	Sample KLX03-out-diffusion
STD-LAB 1	16.06.2004	–11.13	–78.2	1–6	
STD-LAB 2	24.06.2004	–11.20	–80.6	7	
STD-LAB 3	21.07.2004	–11.05	–78.1		
STD-LAB 4	04.09.2004	–11.94	–84.2	8–12	
STD-LAB 5	25.09.2004	–11.32	–80.0	13–16	
STD-LAB 6	25.09.2004	–11.14	–79.2		
STD-TEW 1	16.06.2004	–109.76	425.5	1–6	1–6
STD-TEW 2	24.06.2004	–109.79	425.7	7	7
STD-TEW 3	21.07.2004	–109.86	425.5		
STD-TEW 4	04.09.2004	–109.85	425.8	8–12	8–12
STD-TEW 5	25.09.2004	–109.84	425.3	13–16	13–16
STD-TEW 6	25.09.2004	–109.68	426.9		

Table A5. Chemical composition of solutions from out-diffusion experiments at steady state conditions.

Out-Diffusion experiment solution	Units	KLX03-1	KLX03-2	KLX03-3	KLX03-4	KLX03-5	KLX03-6	KLX03-7	KLX03-8
Sample description									
Vertical Depth	m	159.22	202.66	253.72	303.10	355.66	411.70	462.76	524.63
Rock Type									
Water-Rock Ratio		0.118	0.106	0.091	0.105	0.111	0.086	0.108	0.110
Experiment Temperature	°C	20	45	45	45	45	45	45	45
Experiment Time	days	190	100	100	100	100	100	99	90
Misc. properties									
Chemical Type	Na-HCO_3-(F)-(Cl)	Na-HCO_3-(Cl)	Na-HCO_3	Na-HCO_3-(F)-(Cl)	Na-HCO_3	Na-HCO_3-(Cl)	Ca-Na-SO_4-(HCO_3)	Na-Ca-Cl-HCO_3-SO_4	Na-Ca-Cl-HCO_3-SO_4
pH (lab)	-log(H+)	8.02	7.89	8.15	7.55	7.85	7.88	7.27	7.34
Electrical Conductivity	µS/cm	390	475	637	353	625	446	1,303	
Sample Temperature	°C	20	20	20	20	20	20	20	20
Cations									
Sodium (Na^+)	mg/L	93.3	116	166	87.2	145	101	145	173
Potassium (K^+)	mg/L	1.8	2.2	1.5	1.3	5.5	4.1	12.6	7.3
Magnesium (Mg^{+2})	mg/L	< 0.5	< 0.5	< 0.5	< 0.5	< 0.5	< 0.5	1.2	0.8
Calcium (Ca^{+2})	mg/L	3.2	3.6	3.4	2.4	9.3	6.7	149	140
Strontium (Sr^{+2})	mg/L	0.012	0.053	0.047	0.097	0.13	0.1	1.7	1.8
Anions									
Fluoride (F^-)	mg/L	11.7	6.6	7.4	10.4	5.2	2.8	2.4	2.1
Chloride (Cl^-)	mg/L	16	16.2	14.3	13.8	12.9	15.5	35.8	198
Bromide (Br^-)	mg/L	< 0.1	< 0.1	< 0.1	< 0.1	< 0.1	< 0.1	< 0.1	1.3
Sulphate (SO_4^{-2})	mg/L	7.8	8.1	16.4	11.8	21.7	9.3	506	347
Nitrate (NO_3^-)	mg/L	< 0.5	< 0.5	< 0.5	< 0.5	< 0.5	< 0.5	< 0.5	1.4
Total Alkalinity as HCO_3^-	mg/L	171.5	213.6	307.5	123.9	309.4	211.7	100.1	98.8
Calc. parameters									
Total dissolved solids	mg/L	305	366	517	251	509	351	954	969
Charge Balance	%	2.71	8.30	9.23	10.28	5.78	6.46	3.24	3.32

Table A5. (continued).

Out-Diffusion experiment solution	Units	KLX03-9	KLX03-10	KLX03-11	KLX03-12	KLX03-13	KLX03-14	KLX03-15	KLX03-16	Standard solution
Sample description										
Vertical Depth	m	590.12	643.14	695.95	803.21	841.15	894.53	942.47	979.78	
Rock Type										
Water-Rock Ratio		0.116	0.109	0.109	0.101	0.106	0.107	0.110	0.111	
Experiment Temperature	°C	45	45	45	45	20	45	45	45	
Experiment Time	days	90	90	90	90	149	89	89	89	
Misc. properties										
Chemical Type	Na-HCO_3-(F)-(Cl)	Na-HCO_3-(F)-(Cl)	Na-Ca-HCO_3-Cl	Na-Ca-HCO_3	Na-(Ca)-HCO_3-Cl		Na-Ca-HCO_3-Cl		Na-Ca-HCO_3-Cl	
pH (lab)	-log(H+)	7.36	7.43	7.4	7.32	7.45	7.26	7.32	7.27	
Electrical Conductivity	µS/cm	983		328	830		486		400	14
Sample Temperature	°C	20	20	20	20		20		20	20
Cations										
Sodium (Na^+)	mg/L	167	57.3	40.1	158		70.3		69.9	0.2
Potassium (K^+)	mg/L	4.8	5	8.4	8.6		8.9		6.3	< 0.1
Magnesium (Mg^{+2})	mg/L	< 0.5	0.5	< 0.5	0.8		0.8		< 0.5	0.3
Calcium (Ca^{+2})	mg/L	42.5	15.6	28.3	23.6		37		19.2	0.1
Strontium (Sr^{+2})	mg/L	0.68	0.081	0.16	0.19		0.25		0.12	
Anions										
Fluoride (F^-)	mg/L	4.7	0.4	0.9	3.9		1.1		1	< 0.1
Chloride (Cl^-)	mg/L	142	15.9	6.8	120		30.3		41.4	1.1
Bromide (Br^-)	mg/L	0.58	0.23	< 0.1	0.59		< 0.1		0.18	< 0.1
Sulphate (SO_4^{-2})	mg/L	100	9.8	4.9	16.2		10.9		9.5	< 0.1
Nitrate (NO_3^-)	mg/L	< 0.5	0.7	4	6.3		< 0.5		< 0.5	
Total Alkalinity as HCO_3^-	mg/L	137.3	138.5	172.7	220.3	159.9	189.2	160.5	136.7	< 0.1
Calc. parameters										
Total dissolved solids	mg/L	599	243	262	552		349		284	< 2
Charge Balance	%	5.14	7.16	2.11	3.95		10.21		6.42	2.57